SURFACE-ENHANCED RAMAN SPECTROSCOPY FOR DETECTING AGRICULTURAL VOLATILE ORGANIC COMPOUNDS COLLECTED WITH ADSORBENTS

A Dissertation

by

JINHYUK PARK

Submitted to the Office of Graduate and Professional Studies of
Texas A&M University
in partial fulfillment of the requirements for the degree of

DOCTOR OF PHILOSOPHY

Chair of Committee,	J. Alex Thomasson
Committee Members,	Girish Agarwal
	Michael J. Brewer
	Sandun D. Fernando
	William L. Rooney
Head of Department,	Stephen W Searcy

December 2019

Major Subject: Biological and Agricultural Engineering

ABSTRACT

Volatile organic compounds (VOCs) emitted from any crop contain useful information that can tell its physiological status, and especially, herbivore-induced plant VOCs can be considered as an important phenome that can alert the infestation at the early stage. Therefore, main objective for this dissertation was to develop a reliable sensor to detect agricultural VOCs, and it consisted of total four research items: (1) fundamental analysis of VOCs induced from the interaction between major crop and major insect pest by adsorbent-gas chromatography/mass spectrometry (GC/MS) (2) development of adsorbent coupled Raman spectroscopy for detecting agricultural VOCs (3) phase transfer of Ag-nanospheres (AgNSs) from aqueous to non-aqueous for fabricating surface-enhanced Raman spectroscopy (SERS) substrate (4) Development of adsorbent-SERS substrate for collecting and detecting agricultural VOCs and its application.

The VOCs from two major crops of sorghum and cotton were analyzed by adsorbent-GC/MS in response to major insect pests of sugarcane aphid (*Melanaphis sacchari*) and beet armyworm (*Spodoptera exigua*) respectively, and they showed that the pattern of VOCs induction was totally different depending on the feeding habit by the insect.

However, GC/MS technique always required an hour to perform one analysis, so new detection system of adsorbent-Raman spectroscopy was finally developed to overcome that shortcoming. Based on the fundamental analyses, four different VOCs

were selected for proof of concept study with the developed system, and they were successfully tested by the system, showing high sensitivity down to ppm level and high selectivity from simultaneous detection of four different VOCs.

To improve the functionality of the detection system, especially sensitivity, SERS technique needed to be employed rather than standard Raman, so phase transfer of AgNSs was investigated, and electrostatic interaction by surfactants made successful transferred AgNSs with good interfacial compatibility with any organic chemicals.

Based on the transferred AgNSs, adsorbent-coated SERS substrate was finally developed for detecting agricultural VOCs, and much enhanced interfacial compatibility between the AgNSs and the adsorbent polymer made it possible to detect the VOCs produced from different VOCs sources: aromas from three teas and caterpillar-induced cotton VOCs.

DEDICATION

To my family who supported me throughout the life

ACKNOWLEDGEMENTS

I would like to thank my committee chair, Dr. J. Alex Thomasson, for his continuous support and encouragement throughout the course of this dissertation research. Without his true guidance during the degree, I could not successfully finalize this long journey. I would also like to thank my committee members, Dr. Girish Agarwal, Dr. Michael J. Brewer, Dr. William L. Rooney, and Dr. Sandun Fernando, for their advice and support, making me go right direction for the research.

Thanks also go to Dr. Kyung-Min Lee, Dr. Tim Herrman, Dr. Charles P Suh, Jose Perez, Zachary Gorman, and Dr. Michael V. Kolomiets for their continuous assistances to make me to design and develop experimental set-up. I would also thank Cody Gale and Dr. Gregory Sword for their support of experimental materials which were very essential for the dissertation.

Thanks also go to my friends and colleagues and the department faculty and staff for making my time at Texas A&M University a great experience.

My heartfelt thanks to my parents (Inkeun Park and Moungsook Lee) and parents-in-law (Soonheon Hong, Youngkyung Ha), for their unconditional support and encouragement.

Finally, I would like to express deepest thanks to my wife, Sangeun Hong, and my daughter, Erin Sobin Park, for their patience and continuous love, trust in me. Especially, without my lovely two women, Sangeun and Erin, I could not survive my new life at Texas A&M.

CONTRIBUTORS AND FUNDING SOURCES

Contributors

This work was supervised by a dissertation committee consisting of Professor J. Alex Thomasson, Professor Girish Agarwal, Professor Michael J. Brewer, and Professor William L. Rooney.

The analysis depicted in Figure 5.5 were conducted by Cody Gale of the Department of Entomology.

All other work conducted for the dissertation was completed by the student independently.

Funding Sources

Graduate study was supported by a graduate fellowship from Texas A&M Energy Institute and an excellence fellowship from Texas A&M University.

TABLE OF CONTENTS

Page

LIST OF FIGURES

Page

LIST OF TABLES

Page

1. INTRODUCTION

1.1. Background

Sorghum is considered an important source of food and feed and is the third-ranked cereal produced in the U.S. Sorghum is also an important potential crop for the production of renewable bioenergy. However, various pests can cause major losses to the crop. In recent years, sugarcane aphids (SCAs) have spread throughout Texas and are now a major pest that can cause major damage to sorghum fields. Other insect pests have been reported to cause about 30% damage to other major crops including cotton, soybean, wheat and maize [1]. Therefore, it is urgent to develop methods to reliably detect insect infestations and alert growers at the early infestation stage so some mitigating action can be taken.

1.2. Literature Review

Insect scouting is an important technique in integrated pest management (IPM) and is the common strategy for control of pest populations in farm fields. This technique is based on periodic monitoring of field conditions such as presence of various pest species and populations, as well as crop physiological condition, in order to predict severe infestation problems. Many different monitoring techniques have been proposed, and common methods include visual insect counting, leaf brushing and the use of sweeping nets or beating trays. As an example of scouting SCAs in sorghum fields, Texas A&M Agrilife Research recommends checking at least four locations within a

field and examining the underside of leaves on 20 plants per location[2]. Then, the average number of SCAs per leaf is calculated, and if the average number is above an estimated range of 50 to 125 aphids per leaf, an insecticide will be applied to the field to minimize the damage.

Sensors can detect changes in light reflectance when plants are damaged by insect infestations, and imaging sensors can potentially detect unique features associated with an infestation. Remote sensing can be an effective way to detect crop conditions from aerial or satellite-based sensors, and it can potentially be combined with ground-based sensing to detect insect infestations. Several studies have been conducted on the ability of ground-based sensors to discriminate between healthy and insect-infested plants. Wheat aphid density was estimated based on partial least squares regression (PLSR) of reflectance data from a spectroradiometer coupled with a leaf clip [3-4], and a spectrometer equipped with an integrating sphere was proposed to discriminate plants infested with powdery mildew, yellow rust, or aphids by developing new spectral indices (NSI) [5]. A spectroradiometer was also applied to detect mealybug infestation in cotton and aphid infestation in Mustard by analyzing canopy reflectance changes and considering different spectral indices [6-7]. Aerial-based remote sensing has also been utilized for insect detection. A hyperspectral airborne imaging spectrometer was used to quantify Russian wheat aphid damage with the constrained energy minimization (CEM) method [8], and images from a an airborne multispectral camera were analyzed by considering spatial-pattern metrics to discriminate field infestation of Russian wheat aphid and greenbug [9]. Multispectral image analysis was used to detect SCA infestation

with normalized differenced vegetation index (NDVI) calculated from light reflectance [10].

Other detection methods can possibly be based on the concept that emission of volatile organic compounds (VOCs) from plants is a common defense mechanism caused by insect attacks. These herbivore-induced plant volatiles (HIPVs) can be collected with an adsorbent, and pre-concentrated volatiles can be analyzed with analytical systems. Therefore, they require the specific step for the pre-concentration of the VOCs prior to the analysis of them.

Methods for VOC extraction can be divided into two groups, dynamic and static. Dynamic uses air circulation by pump for VOC pre-concentration with the adsorbent inside the chamber where plant VOCs are present, and static uses natural diffusion to collect VOCs on the adsorbent.

The air circulation in dynamic VOCs extraction onto an adsorbent makes the method more efficient [11]. Common adsorbents for dynamic sampling include certain kinds of porous polymer, SuperQ (ethylvinylbenzene-divinylbenzene) and Tenax (2,6-diphenyl-p-phenylene oxide), which have a high affinity to a wide range of plant VOCs [12-13]. Generally, the dynamic method is more useful for large chambers and longer collection times.

However, the static method does not use air circulation, so only specific adsorbents are used inside the chamber [11]. An important static sampling adsorbent type is solid phase microextraction (SPME), which involves different commercially available fibers such as polydimethylsiloxane (PDMS), polydimethylsiloxane-divinylbenzene

(PDMS-DVB) and polyacrylate (PA), which are selected depending on the polarity of plant VOCs [14]. Even though it is very simple to set-up and efficient for VOC collection over a short time, the static method of collection can be affected by environmental conditions and may not be useful for VOC collection in a large chamber.

In addition to the VOC extraction methods, there are two different representative techniques for analyzing the VOCs. First, a GC/MS consists of two parts: a gas chromatograph that can separate volatile mixtures in a column, and a mass spectrometer that can identify each separated volatile by analyzing its mass to charge ratio from ionized fragments. The GC/MS has been widely used for analysis of HIPVs that are pre-concentrated with static or dynamic sampling. Certain investigators have reported on analysis of HIPVs produced by green peach aphids, *Myzus persicae*. The volatiles emitted from Turnip plants infested with green peach aphids were collected with SuperQ for 120 hours [15], and the VOCs from Salix alba infested with aphids were pre-concentrated onto Tenax [16]. All the VOCs collected were identified with GC/MS. In addition to dynamic sampling, the VOCs from green peach aphid-infested Capsicum annuum L. were enriched with SPME of PDMS/DVB 65μm [17], and other types of SPME, PDMS and Carboxen-PDMS 75 μm were used to collect VOCs from cotton plants and soybean plants infested by cotton aphids, *Aphis gossypii*, and soybean aphids, *Aphis glycines* Matsumura, respectively [18-19].

Second, an E-nose (electronic nose) is composed of several sensors having conductive material to enable conductivity measurement, each coupled with an insulating polymer in which gas molecules can react and the mixture can be coated on

the electrode structure. When the molecule is absorbed on the surface of the polymer, the polymer swells, resulting in a reduction in conductivity of the mixture. Different fingerprints can be observed based on conductivity changes related to the degree of reaction with different gas molecules on the coated mixture. Therefore, if any VOCs profile can be changed in response to the insect infestation, the sensors consisting of the E-nose can potentially detect the changes.

Several commercial E-nose products have been developed and tested with plant samples to distinguish between healthy and infested ones. The Cyranose 320 (C-320) is composed of an array of 32 sensors, and it was used to detect basal stem rot (BSR) disease with artificial neural network (ANN) analysis [20], and the Bloodhound model ST214 was used to discriminate between healthy and Tobacco-Hornworm-Infested Tomato leaves [21]. In addition to commercial products, the literature includes references about new E-nose designs for HIPV determination. Different polymer films were deposited on 25 pairs of interdigitated electrodes, and several plant volatiles were tested for volatile discrimination [22]. More sophisticated E-noses have been developed, including a sampler that was tested in a cotton field to distinguish VOCs between healthy and infested cotton bolls [23].

1.3. Objectives

Based on different detection methods that have been reviewed so far, we can identify current problems of the methods for on-field insect detection.

Scouting is time-consuming and expensive, and at best it allows for sparse sampling in the field.

Remote sensing would be an attractive alternative and could be performed with UAVs (Unmanned Aerial Vehicles), making it suitable for exhaustive sampling on large fields. However, there is generally no visual or spectral sign available from the plant to downward-looking sensors in the early infestation stage. The insects are commonly under the leaves and are small, so it is likely impossible to detect the infestation from above before major damage has occurred.

The sensitivity of GC/MS is generally superior to other methods of measuring VOCs as an indicator of insect infestation, but it is not applicable for field detection due to its cost and lack of its portability.

E-noses may be useful for field application, but the price is relatively high and sensitivity not good enough to detect many kinds of gas molecules at low concentrations.

In addition to the problems of the present methods, we can also identify the research area that has not been investigated yet. Studies have been conducted on VOC emission from healthy and infested sorghum by insects other than any phloem feeder including aphids [24-25], but no work has been reported on VOC analysis from SCA infested sorghum.

From those possible research gaps, a new, reliable and field-deployable method for detecting insect infestations in major crops is needed and can be specified as follows.

First, a study to identify specific VOCs associated with interactions between important crops and major insect pests could potentially lead to sensors capable of detecting infestations at stages in which symptoms. However, it would be challenging to discriminate VOCs induced by herbivorous insects from those caused by mechanical

damage. Any herbivorous attack can eventually result in mechanical injury to a plant, and the damage might not be different from that induced by factors other than herbivory. Actually, previous studies have shown that damage from instant mechanical stimulus can affect the plant VOC emissions, but the effect was small when compared to plant VOC emissions due to insect herbivory [26-28]. However, if mechanical wounding were intensified by continuous artificial stimulus to simulate insect herbivory, the VOC profile might be similar to herbivore-induced VOCs [29]. On the other hand, many terpenes and aromatic compounds were not found when insect herbivory was not involved in the injury, meaning that mechanical damage other than by herbivorous insects apparently did not induce those specific VOCs [30]. Thus, finding specific VOCs relevant to insect herbivory could potentially provide an alert to insect infestation at an early stage, and the problems of other methods like low specificity and lack of ability for early detection might be solved.

Second, the resolution of field measurements could be improved greatly over scouting if the sensing of VOCs from infested crops were integrated with an autonomous vehicle for in-field sampling. Furthermore, the sensitivity of field-based VOC measurement could be enhanced by pre-concentration on an adsorbent.

Third, a reliable VOC detector could potentially be developed as a bio-photonic sensor that detects light absorption, emission and scattering associated with VOC molecules. Such a sensor would need high sensitivity and fast response and to be relatively inexpensive.

Fourth, several references have discussed detecting analytes pre-concentrated by an adsorbent with another type of bio-photonic sensing technology, Raman spectroscopy. Organic contaminants such as toluene and benzene were detected in water by combining PDMS as an SPME technique with a Raman spectrometer [31]. Organic vapors of benzene and toluene were also detected with solid phase extraction (SPE) involving C-18 adsorbent rather than PDMS [32]. Surface-enhanced Raman spectroscopy (SERS) has also been combined with the use of an adsorbent. The SERS technique uses an applied laser field that is intensified when it interacts with metal-based nanoparticles, so if the sample can be located on the surface of or near the nanoparticles , an intensified Raman signal from the sample can be obtained by the electromagnetic field enhancement associated with the nanoparticles near the sample. Microextraction with packed sorbents (MEPS) for pre-concentration of musk ketone in water, combined with SERS with Ag-nanoparticles, was proposed for improving detection sensitivity [33]. Other methods were mainly based on SERS with Au-nanoparticles deposited in a substrate in which hydrophobic molecules and PDMS were applied in an adsorbent coating to sense aromatic vapor [34]. While several concepts in these studies appear to be potentially useful for detecting a few VOCs associated with insect infestation in plants, none of the approaches was directly suitable for plant VOC detection in that the adsorbents used cannot be used for a wide range of plant VOCs, and all nanoparticles cannot function well in any sample compatible with non-aqueous solution.

Therefore, the system proposed for this research includes pre-concentrating VOCs on the adsorbent to improve plant VOC collection efficiency. Also proposed is

bio-photonic sensing immediately after sampling of VOCs from the plant. Specifically, Raman spectroscopy is proposed as the bio-photonic sensing method, with a specific adsorbent and a unique nanoparticle application to enhance the sensitivity of the system.

The overall objective is to develop a system for the detection of VOCs relevant to insect infestations in plants. Four objectives must be accomplished. Hypotheses for these research objectives are explained below.

The first objective is to develop and test a method to differentiate healthy from SCA-infested sorghum plants. The null hypothesis is that the VOC profile (absolute or relative amount of constitutive VOCs) emitted by an SCA-infested sorghum plant will not be significantly different from the profile emitted by a healthy sorghum plant. In order to determine whether or not this is true, the adsorbent-GC/MS method is used to find induced specific VOC profiles from both healthy sorghum and SCA-infested sorghum so that they can be distinguished from each other.

The second objective was to use Raman spectroscopy with an adsorbent to detect VOCs. The null hypothesis is that a new VOC detection system combining VOCs pre-concentration by the adsorbent and a Raman measurement of the VOCs eluate from the adsorbent cannot identify four different kinds of HIPVs at the same time.

The third objective was to develop a method to transfer Ag-nanospheres from aqueous to non-aqueous phase. The null hypothesis is that Ag-nanospheres dissolved in aqueous solution cannot be effectively phase transferred to non-aqueous solution by surfactant-induced electrostatic interaction for their unique SERS application.

The fourth objective was to measure naturally occurring plant VOCs with SERS with an adsorbent. A unique SERS substrate will be prepared based on the complex between adsorbent polymer and the transferred Ag-nanospheres to test whether it can directly collect the VOCs and thus significantly enhance the Raman signal from the collected VOCs, so the null hypothesis is that the Raman signal from the SERS substrate will not be significantly enhanced than that from standard Raman. It will be also applied to two agriculture-related samples (cotton plant and teas): (1) to identify caterpillar infestation on cotton based on the detection of cotton emitting VOCs, and (2) to classify different tea variety based on the detection of tea aromas.

2. MULTIVARIATE ANALYSIS OF SORGHUM VOLATILES FOR THE FAST SCREENING OF SUGARCANE APHID INFESTATION

2.1. Abstract

The sugarcane aphid, *Melanaphis sacchari*, has been a severe pest throughout the sorghum field in Texas, which can worse the sorghum yield economically. For this purpose of early detection, the mechanism of herbivore-induced plant volatiles (HIPVs) needs to be utilized in the detection method. In this study, the HayeSep Q adsorbent combined gas chromatography mass spectrometry (GC/MS) was tested to analyze the volatile organic compounds (VOCs) that sorghum can emit when they are in good shape as well as they are infested by the sugarcane aphids and multivariate techniques were performed for the fast screening of the infestation. Several VOCs identified from analysis of variance (ANOVA) with $p<0.05$ were finally chosen as variables for multivariate analysis, and both unsupervised learning of principle component analysis (PCA) and clustering analysis (CA) and supervised learning of linear discriminant analysis (LDA) were done, showing good performance on discrimination between healthy and infested sorghum.

2.2. Introduction

Plants have two defensive tactics for coping with herbivore attacks [35]. One is to use a constitutive plant defense via physical barriers of their body such as leaf hair, glandular trichomes, and the other is to use an induced plant defense composed of direct defense and indirect defense. The direct defense is related to the production of many

antifeedants, and the indirect defense is to attract natural enemies of the attacking herbivore by emitting informative semiochemicals called volatile organic compounds (VOCs) [36]. Information about the VOCs should be helpful to control the population of a pest insect if it can be used in integrated pest management (IPM) [37]. In recent years, sugarcane aphid (SCA), *Melanaphis sacchari*, has spread throughout Texas as well as other states and is now a major pest that can catastrophically damage sorghum fields. Therefore, it is urgent to develop methods to reliably detect field infestations to alert growers at the early infestation stage so some mitigating action can be taken. Exploitation of semiochemicals has the potential to be a key component of a new method.

Much previous research has focused on VOCs produced by plants having been attacked by aphids, and the most accurate method for analysis is headspace VOC collection followed by gas chromatography/mass spectrometry (GC/MS). Common collection methods involve using solid phase microextraction (SPME) fiber in static sampling [11, 14], or using various adsorbents in dynamic sampling with a pump [11]. The SPME technique is easy to use and can be effective inside small chambers, so many have used that set-up to collect VOCs from leaf extract or from a few leaves within a short time. An aphid that has been often reported in relation to VOCs collected with this technique is the green peach aphid, *Myzus persicae*. The VOCs analyzed were from the interaction between the aphid and many plants such as potato, tomato, *Achillea collina*, Arabidopsis, *Pisum sativum*, *Prunus persica* and chilli [17, 28, 38-43]. Five other aphids have also been shown to induce VOCs in plants [19, 44-46], and the common VOCs emitted from

all kinds of aphid feeding were various terpenes and methyl salicylate. In contrast to static sampling, dynamic sampling with certain adsorbents has been applied when VOCs must be collected from whole plant leaves over a prolonged time period. Green peach aphid induced plant VOCs from sweet peppers [47] and turnip plants [15] have been analyzed with this technique. Moreover, soybean VOCs caused by the soybean aphid, *Aphis glycines* Matsumura, have been collected on SPME [48], and the interaction between the cotton aphid, *Aphis gossypii*, and various plants has also been widely studied [18, 49-50]. Three additional kinds of aphid have been investigated with regard to herbivore-induced plant volatiles (HIPVs) [51-53], and the most mentioned VOCs from the literature were various terpenes, methyl salicylate and green leaf volatiles (GLVs). While multiple articles have reported on aphid herbivory in plants other than cereal grasses, studies related to cereal VOCs have not been widely reported. Specifically, VOCs from piercing-sucking herbivory in cereal grasses have been rarely studied. Among cereal grasses, maize has been widely studied, and the VOC profile from healthy maize plants was compared with that from maize plants with chewing herbivores having different kinds of larvae [54-57]. In addition, induced maize VOCs from the piercing-sucking of the China leafhopper or southern green stink bug have been also investigated [58-59]. Various terpenes were emitted from infested maize, similar to results with the plants mentioned previously.

In contrast to research in which plant VOCs were induced by herbivory, other research has focused on the opposite effect, that the plant VOCs were not induced or were reduced by herbivorous insects. First, silverleaf whitefly, *Bemisia tabaci*, did not

induce VOCs when infesting cotton [60], and it also interfered with the Lima bean plant's indirect defense signal pathway induced by the herbivore spider mite, *Tetranychus urticae* [61]. Second, *Tetranychus urticae* or *Tetranychus evansi*, suppressed the induction of tomato plant VOCs depending on intraspecific genetic variation of the mites [62-63]. Lastly, it has been reported that some VOC components decreased in cotton-aphid infested weeds compared with healthy weeds [49], and the VOC profile from healthy Broad Bean was not significantly different from that of Broad Bean infested with the pea aphid, *Acyrthosiphon pisum* [64]. For cereals, it was first reported that the induction of maize VOCs could not be clearly shown even after heavy infestation with the corn leaf aphid, *Rhopalosiphum maidis* [65].

While many kinds of plants have been studied to uncover the VOCs induced or repressed by insect herbivores, few studies have been focused on the emission of VOCs by sorghum plants. One fundamental study reported on sorghum VOCs from seedlings of the Serena cultivar [66] and two other cultivars having different susceptibility to Sorghum Shoot Fly, *Atherigona soccata*. Observations were made on differences in the VOC profile between the cultivars [24]. A few studies have also focused on herbivore induced sorghum VOCs. The VOCs emitted from sorghum damaged by the larvae of Fall armyworm (FAW), *Spodoptera frugiperda*, have been analyzed to characterize the genetic pathway related to sesquiterpene emission [25]. VOCs emitted by sorghum roots (rather than leaves) damaged by arbuscular mycorrhizal (AM) fungi have also been investigated [67]. However, apparently no literature shows the VOC profile from the interaction between sorghum and any phloem-feeder.

The goal of the current study was to investigate the effects that SCA feeding on sorghum seedlings can have on VOCs emission. Specific objectives were (1) to identify the VOCs emitted by healthy and SCA-infested sorghum seedlings, (2) to measure the identified VOCs in absolute and relative concentrations, and (3) to compare them for the discrimination between healthy and infested sorghum seedlings.

2.3. Material and methods

2.3.1. Material description

Seed of the sorghum genotype SC 748-5, a line susceptible to SCA, were planted in pots filled with Fafard 52 soil mix. The plants were grown in a controlled chamber in which the temperature was maintained at 77°F, and daylight lamps were operated on a 16 h light and 8 h dark cycle for about 3 weeks. SCAs were obtained from an established colony maintained on a grain sorghum hybrid known to be susceptible to SCAs [68]. The colony was established and periodically supplemented with field-collected SCAs taken from sorghum growing at the Texas A&M AgriLife Research and Extension Center in Corpus Christi, TX.

2.3.2. Experimental procedure

2.3.2.1. Experimental design

Eighty healthy sorghum seedlings were selected for the experiment. Half were purposefully infested with SCAs. Eight experimental blocks, four infested and four non-infested, were formed in a randomized block design, each block with ten randomly chosen seedlings assigned to it. Ten seedlings per block were used because preliminary data suggested the concentration of VOCs needed for detection cannot be collected from

a single seedling. Therefore, the number of experimental replications was somewhat limited by the number of seedlings needed per replication.

One infested block and one non-infested block were randomly assigned as a pair to form one replication. As a result, a total of four experimental replications were completed for both healthy and aphid-infested seedling groups.

2.3.2.2. Aphid feeding on sorghum

The seedlings assigned to the infested group were moved to a separate growing chamber from those in the healthy group. A set of infested sorghum leaves that had been collected in the field were placed in the chamber with the seedlings in the infested treatment group for about 24 hours to ensure transfer of the infestation. As the collected leaves dry out quickly, the aphids on those surfaces move to the new healthy surfaces of the seedlings' leaves. Most of the aphids moved to the seedlings, resulting in heavy infestation.

2.3.2.3. Air entrainment

Each seedling was placed in a 6 L jar, and the headspace air was drawn through a SuperQ filter trap containing adsorbent resin (HayeSep Q, 80-100 mesh, Supelco). Air collection was conducted for 5 hours, with the air entering the system filtered through activated charcoal. Airflow was approximately 0.1 to 0.2 L/min, and volatiles trapped on the resin were eluted with 300uL dichloromethane containing 100µM octane as an internal standard.

2.3.2.4. GC/MS analysis

GC/MS analysis was carried out with a Shimadzu GCMS-QP2010 Ultra (Shimadzu Scientific Instruments (Oceania) Pty Ltd, Henderson, New Zealand). The column employed for the separation of plant volatile components was a Zebron ZB-WAX plus (30 m length × 0.25 mm I.D. × 0.25 μm film thickness) supplied by Phenomenex (Torrence CA, USA). The carrier gas used was helium at a flow rate of 1.5 mL min^{-1}. The temperature of the injection port was 250°C, and a 1μL sample was injected with a split ratio of 1:1. The column temperature program was as follows: (A) initial temperature of 40°C, (B) temperature held for 3 min, (C) temperature increased at a rate of 5 °C/min up to 240°C, (D) temperature held for 3 min, (E) temperature increased at a rate of 40°C/min up to final temperature of 250°C. Mass spectrometry conditions involved electron impact ionization with an interface temperature of 250 °C and an ion source temperature of 200°C. Initial identification of volatile compounds was made by comparing the mass spectra of experimental samples to those stored in the National Institute of Standards and Technology (NIST) and Wiley Registry (10th edition) libraries. Compound identification was made by confirmed chromatograms that contained a peak at identical retention times with greater than 85% similarity to the mass spectrum of libraries and available authentic standards.

2.3.3. **Statistical analysis**

JMP software (SAS Institute, Cary, NC) was used to perform an analysis of variance (ANOVA) test and several multivariate techniques such as principal component analysis (PCA), clustering analysis (CA) and linear discriminant analysis (LDA) with

the GC/MS data sets. The GC/MS data were expected to include peaks with amplitudes related to the concentration for each identified VOC. Additionally, custom code written in R software was applied to the GC/MS data to validate the LDA model classification accuracy through k-fold cross-validation.

2.3.3.1. Data consolidation

To calculate the absolute concentration of the VOCs, the areas of peaks associated with identified VOCs were exported from the built-in GC/MS software, Shimadzu GCMSsolution (version 2.7) package and divided by the areas of peaks of the internal standard at the same spectral position (Equation 1). In addition, each individual absolute concentration associated with a peak was divided by the total absolute concentration across the measured spectrum to determine the relative proportion of each compound (Equation 2). Both absolute and relative values were utilized as input for statistical analysis. Moreover, all identified VOCs were again classified into seven representative molecular groups – terpene, hydrocarbon, ketone, aldehyde, ester, alcohol, and aromatic – so that all the values could be summarized for each molecular group.

$$\mathrm{A}_{absolute} = \frac{PA_A}{PA_{IS}} \quad \text{(Equation 1)}$$

$$\mathrm{A}_{relative} = \frac{\mathrm{A}_{absolute}}{\mathrm{Total}_{absolute}} \quad \text{(Equation 2)}$$

(A: any identified VOCs, PA: peak area, IS: internal standard)

2.3.3.2. ANOVA

The aim of the ANOVA test was to identify VOCs or representative molecular groups that had a significant difference ($\alpha = 0.05$) between healthy and infested groups of plants, considering either absolute or relative concentrations.

2.3.3.3. PCA

An important step related to PCA is to optimize variable selection to include those that can produce differentiable clusters between two groups. In this study, a limited set of variables was selected for each of the absolute and relative cases, and two main principle components produced from the selected variables were plotted.

2.3.3.4. CA

The selected variable sets were also used for hierarchical clustering analysis, and a dendrogram was created to see how well the healthy and infested groups could be clustered.

2.3.3.5. LDA

LDA was used to include a supervised learning analysis method to classify the same data sets into healthy and infested. However, the number of replications is small to validate model accuracy. Therefore, the performance of the LDA model was evaluated with modified k-fold cross-validation (where k=4, number of replications). The two data (from one healthy plant and one infested plant) were randomly sampled and assigned as the validation set, and the remaining data were assigned as the training set. The model was created based only on the training set, and then the validation set was evaluated by the model for the classification accuracy. This step was repeated four times until all data

were used as part of a training set, and the whole procedure was repeated ten times to arrive at an average classification accuracy. Because the problem included two classes (healthy vs. infested), the threshold value was set to 0.5 by default, meaning that if the posterior probability of classifying a plant from the validation set as infested was greater than 0.5, that plant was classified into the infested group, but the threshold parameter were fine-tuned in the range from 0 to 0.5 at 0.01 intervals. Finally, the classification accuracy was plotted according to the threshold parameters.

2.4. Results and discussion

For the qualitative evaluation of VOCs from healthy and SCA-infested seedlings, a total of 54 VOCs were identified (Table 2-1), and there was no qualitative difference between two treatments.

Quantitative evaluation based on absolute and relative concentrations was also calculated (Table 2-1) for each identified VOC. Only one VOC, methyl laurate, was significantly different between healthy and infested sorghum plants (Table 2-1) when comparing both absolute ($df = 7$, $P=0.0059$) and relative concentrations ($df = 7$, $P=0.0133$). The aphids feeding on the sorghum leaves apparently reduced the emitted concentration of methyl laurate by a ratio of roughly 4 compared to healthy sorghum seedlings. Moreover, several other compounds were identified as significantly changed ($\alpha=0.05$) in the relative comparison. Among those compounds were alkanes of dodecane ($df = 7$, $P=0.0059$) and phytane ($df = 7$, $P=0.0414$), aromatics of naphthalene ($df = 7$, $P=0.0111$) and 1-methylnaphthalene ($df = 7$, $P=0.0135$), a ketone of acetophenone ($df = 7$, $P=0.0205$), and an alcohol of 2-phenoxyethanol ($df = 7$, $P=0.029$).

In addition to individual VOCs, seven chemical classes were considered to determine whether differences between treatments could be identified. In absolute concentrations, no chemical class was significantly different between healthy and infested sorghum, but when relative changes were considered, insect infestation increased the ratio of terpene by about 9% (df = 7, P=0.0376) and decreased the ratios of alcohol and aromatics by about 6% (df = 7, P=0.043) and 2.4% (df = 7, P=0.0134), respectively.

When PCA was applied to the available variables (Table 2-1) and the first two principal components were plotted for absolute and relative comparisons (Figure 2.1), clear discrimination between the healthy and infested groups was observed only in the relative case. A group of 15 variables were then selected as a more focused data set based on their contributions to the principle components, improving discrimination for the absolute case (Figure 2.2). Discrimination for the relative case was improved to the point that all plotted points from the infested plants were negative on the first principal component axis and the points from healthy plants were positive.

The dendrograms from CA (Figure 2.3) show three clusters for the absolute case, not a good classification result. However, two clusters representing infested and non-infested plants were clearly observable for the relative case.

With LDA (Figure 2.4), the classification rate for the absolute case was below 80% for all the threshold parameters, but for the relative case converged to 100% when the threshold approached 0.5, meaning that the model based on relative values could accurately estimate whether plants were infested or not. From all results by multivariate

techniques, the relative-based case had much better performance in discrimination than the absolute-based case, which corresponds to the fact that many compounds with significant differences were identified only in the relative case.

Our first key finding here were that there was no qualitative difference between healthy and infested sorghum, and the absolute concentration from the infested group was not statistically different from the control for most VOCs. One possibility to result in the finding might be feeding habits by specific herbivorous insects which already explained earlier section, suggesting that the VOCs could not be induced by two specific feeding habits: mesophyll-feeding by spider mite and phloem-feeding by aphid and whitefly [60, 63-64]. Especially, our another finding that the total concentration from the infested group was also not statistically different from the control (df = 7, P=0.4947), which corresponded to the example of cotton plants infested with the silverleaf whitefly [60].

The sorghum genotype used in our experiment was susceptible to SCAs, so it might be expected that more damage would induce a higher concentration of emitted VOCs. This expectation is supported by previous research comparing VOCs between insect-resistant and non-resistant maize [69]. Significantly more larvae-induced VOCs were produced from non-resistant maize than from resistant maize due to altered feeding behavior, in which the non-resistant maize was damaged much more severely than resistant maize. However, in our research no statistical difference was found for most VOCs between healthy and infested plants, and the feeding habit by aphid that was not totally different from larvae feeding would be the answer for this result. Concerning the

larvae herbivore on a sorghum, FAW larvae feeding on a sorghum seedlings induced significant VOC emissions, especially sesquiterpenes and other compounds not found with healthy sorghum [25]. Although the experimental conditions for this study, overnight feeding and 4 hours of VOC collection, were pretty similar to our study, the feeding habits of FAW were different from our feeding habits by SCA.

Another possibility might be the sorghum genotype we tested. This idea could be supported by a finding from recently published work in which SCA-resistant and younger sorghum plants (2 weeks post-emergence) can make the transcriptional molecular response relevant to plant defenses more easily than SCA-susceptible and older sorghum like in our case. Therefore, the emission of the VOCs in susceptible and older seedlings might not be effectively induced due to the delayed activation [70]. We did not test genotypes resistant to the SCA, so VOCs comparison to them are important for future research.

Our second key finding was that good discrimination between healthy and infested sorghum seedlings could be possible from the data in relative concentrations, but poor discrimination was observed with the data in absolute concentrations. The possible reason why the data in absolute concentrations were not predictable would be high variability in experimental condition, which was mainly caused by uncontrollable levels of the aphid herbivory such as the number of the aphids. However, this variation could be eliminated by taking the relative ratio of each individuals in absolute concentration, and much more consistent data could be generated across the replicates for relative aspect. From this point, the relative concentration comparison of the

chemical classes instead of the individuals could be alternative way for the discrimination between healthy and infested group. For example, no individual terpene compound had a significant difference in relative concentration, but the relative concentration of the entire terpene class was significantly different between infested plants and the control. The analysis of the chemical classes in the relative concentration could be found in other cereal grass of maize plants with different genotypes, and there was substantial variation in relative percent for five molecular groups such as monoterpene, homoterpene, sesquiterpene, ester and aromatic [71-73], which was pretty similar to our finding of terpene and aromatic with significant difference in the relative concentration.

2.5. Conclusions

According to GC/MS data, SCA herbivory on sorghum seedlings did not affect plant VOC emissions qualitatively, but it did seem to affect them quantitatively. Even though the absolute concentration of the VOCs was not significantly different between healthy and unhealthy seedlings, the relative concentration was significantly different even after a short collection time. This finding is important in that it is apparently the first report of sorghum VOC response to phloem-feeder herbivory, and the use of relative concentration rather than absolute will be very effectively used as a parameter to identify the infestation by any phloem-feeder.

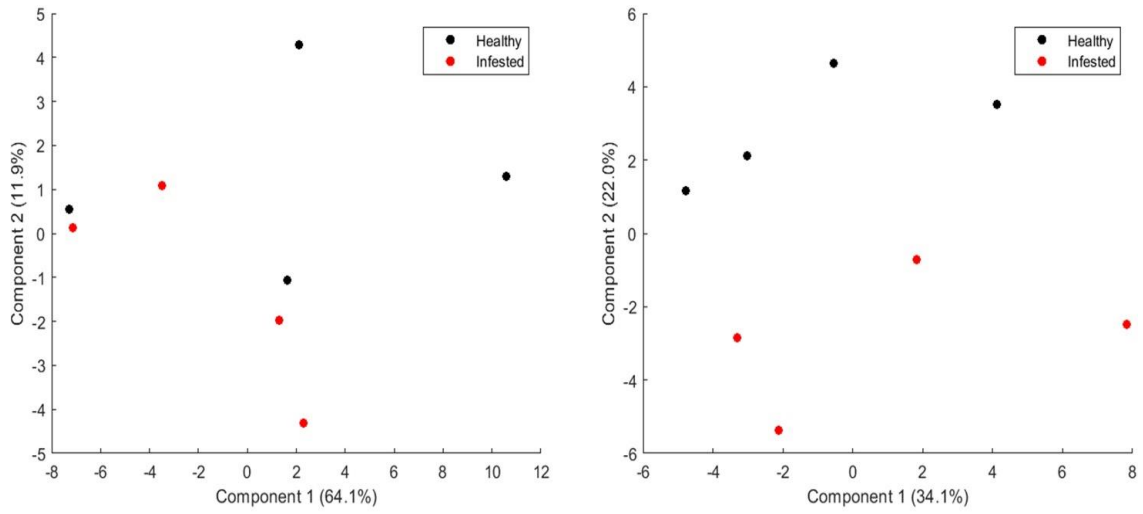

Figure 2.1 PCA plot based on all variables
(Left: absolute amount, Right: relative amount)

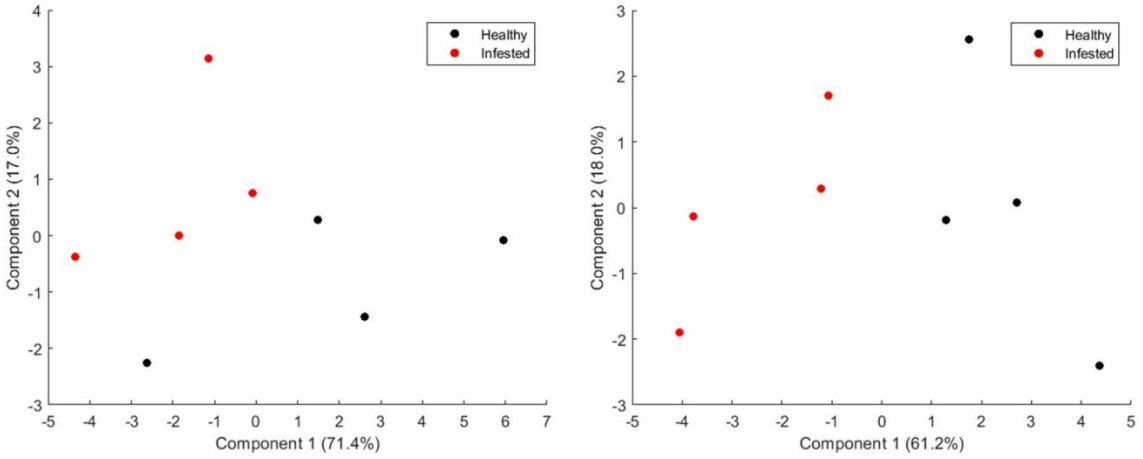

Figure 2.2 PCA plot based on optimized variables
(Left: absolute amount, Right: relative amount)

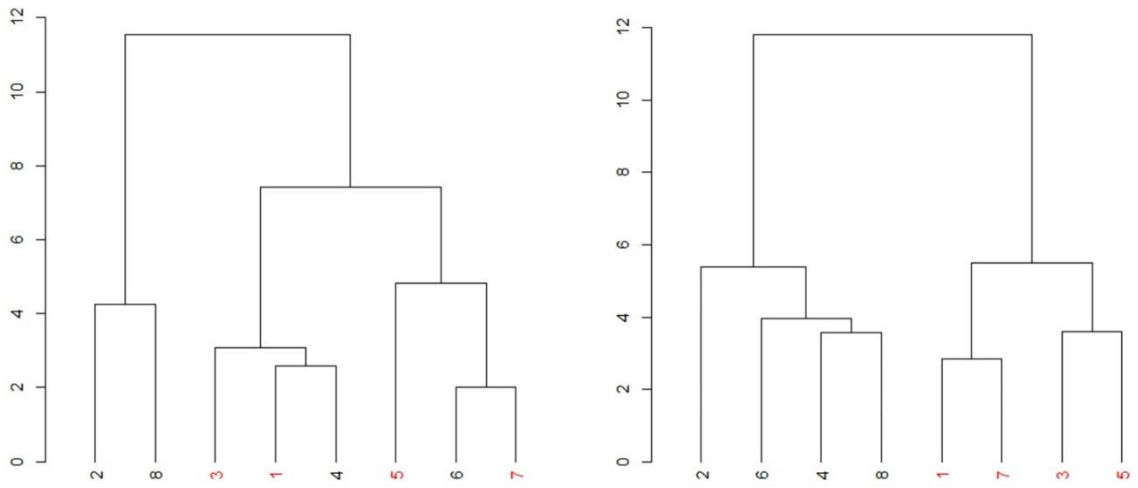

Figure 2.3 Hierarchical dendrogram based on optimized variables
(Left: absolute amount, Right: relative amount)
(Black: healthy, Red: infested)

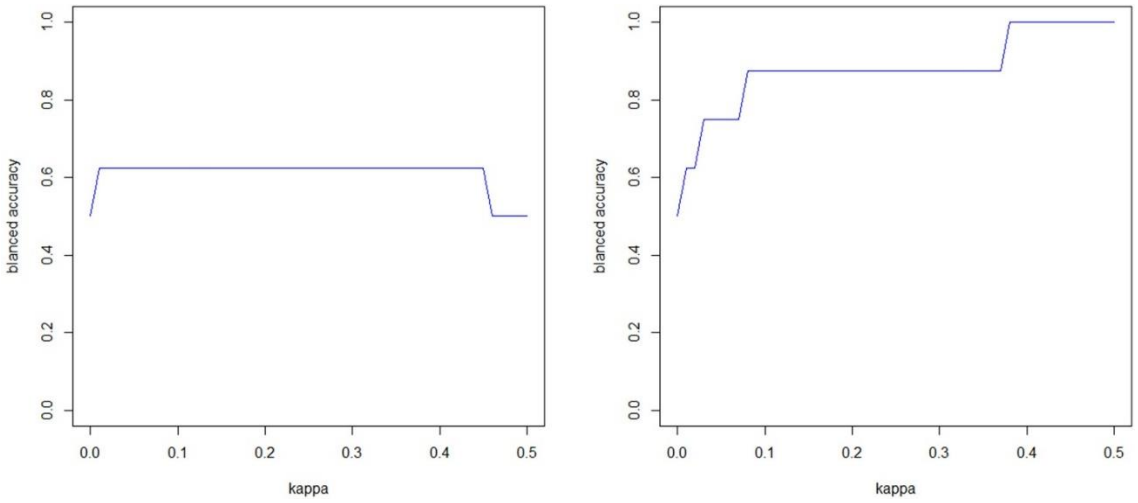

Figure 2.4 LDA classification accuracy according to the kappa statistic
(Left: absolute amount, Right: relative amount)

Table 2-1 Volatile organic compounds released from sorghum seedlings with or without sugarcane aphids for 5 hours collection.
Data show means of absolute amount ±SE of four replicates
(Bold: significantly different compound with $\alpha = 0.05$)

RT (min)	Compound	Absolute (nmole/5hours)	
		Control	Infested
8.30	β-myrcene	27.62±13.30	24.76±11.44
9.16	Limonene	1170.80±579.58	1215.23±519.59
10.41	γ-Terpinene	16.26±6.47	17.60±2.56
10.72	3,3-Dimethylhexane	60.09±9.84	48.55±2.96
11.04	m-Cymene	23.82±3.45	22.66±2.06
11.45	Cyclohexanone	16.98±1.19	14.31±5.28
11.62	Octanal	63.22±13.81	54.50±10.92
12.13	Undecane	74.83±21.09	40.94±3.86
12.90	5-Hepten-2-one, 6-methyl-	59.16±20.55	56.90±16.10
14.42	Nonanal	262.70±61.69	207.57±34.88
14.68	2-butoxy-ethanol	266.20±50.82	231.53±25.79
14.78	Dodecane	95.39±24.64	50.22±8.25
15.64	Tetrahydrolinalool	60.67±17.49	57.77±5.73
15.84	Tridecane	37.55±9.00	24.23±3.50
16.01	Tetradecane	45.26±7.09	35.50±0.61
16.55	Dihydromyrcenol	92.89±30.05	80.04±14.03
17.04	1-Hexanol, 2-ethyl-	530.78±127.42	289.99±24.89
17.14	Decanal	171.95±35.66	135.54±20.52
17.48	Benzaldehyde	104.41±13.40	82.91±9.65
18.45	Linalool	48.82±11.36	30.14±3.07
19.30	Ethanol, 2-(2-methoxyethoxy)-	38.79±7.14	27.22±3.99
19.78	Hexadecane	101.59±21.10	73.93±13.50
20.10	Ethanol, 2-(2-ethoxyethoxy)-	198.86±32.94	159.31±19.05
20.57	Acetophenone	50.32±11.36	27.39±5.68
20.62	Menthol	97.05±14.29	93.70±10.61
22.10	Heptadecane	44.72±8.37	52.11±10.43
22.19	Cyclodecanol	15.12±5.35	12.46±4.40
22.54	Naphthalene	469.44±94.75	252.81±31.35
22.87	(S)-(+)-1,3-Butanediol	18.20±3.09	19.31±2.95
23.40	Methyl salicylate	34.15±15.12	32.13±4.97
23.46	1-Decanol	9.77±6.60	11.81±4.49
24.06	Ethanol, 2-(2-butoxyethoxy)-	20.42±8.42	17.72±6.67
24.28	Methyl laurate	**37.37±3.80**	**9.08±5.64**
24.32	Phytane	15.43±8.97	34.13±9.36
24.97	Naphthalene, 1-methyl-	26.03±6.99	10.00±3.36
25.13	1-dodecanol	39.65±11.24	17.92±6.10
25.62	Propanoic acid, 2-methyl-, 3-hydroxy-2,4,4-trimethylpentyl ester	9.30±9.30	17.76±6.25

Table 2.1 Continued

RT (min)	Compound	Absolute (nmole/5hours)	
		Control	Infested
25.66	Benzenemethanol	99.28±19.59	81.18±16.49
26.07	1-Propanol, 2-(2-hydroxypropoxy)-	15.11±6.06	17.11±2.01
26.9	Neophytadiene	456.94±37.23	509.66±44.56
27.25	Naphthalene, 1,5-dimethyl-	7.12±4.42	12.26±4.63
27.53	Neophytadiene isomer	87.51±34.23	102.14±18.35
27.76	1-dodecanol	986.88±244.24	574.40±101.43
28.07	Phytol	147.78±9.27	161.92±13.70
28.25	Phenol	93.11±22.12	65.72±6.35
28.56	Methyl tridecanoate	40.66±7.87	20.33±7.83
29.74	Triacetin	22.46±3.80	29.86±6.67
30.89	Ethanol, 2-phenoxy-	21.04±3.23	22.84±3.04
31.56	2-Octanol, benzoate	170.80±35.40	135.58±23.11
31.80	Nonanoic acid	15.29±5.53	14.45±5.28
32.48	Methyl myristate	67.09±13.26	34.83±15.58
33.90	1,2,3-Propanetriol	232.82±61.82	213.61±104.97
34.95	Diethyl phthalate	92.90±2.87	93.89±3.08
39.14	Phytol isomer	58.39±10.95	69.34±14.33

7 chemical classes	Absolute (nmole/5hours)	
	Control	Infested
Terpene	2288.55±631.04	2384.97±509.21
Alkane	474.86±87.97	359.62±49.48
Ketone	126.46±31.88	98.60±25.04
Aldehyde	602.28±123.31	480.52±74.54
Ester	474.73±73.93	373.46±54.17
Alcohol	2492.92±491.27	1696.41±276.91
Aromatic	595.70±125.59	340.78±44.28
Acid	15.29±5.53	14.45±5.28

Table 2.1 Continued

Data show means of relative amount ±SE of four replicates (Bold: significantly different compound with $\alpha = 0.05$)

RT (min)	Compound	Relative (%)	
		Control	Infested
8.30	β-myrcene	0.32±0.12	0.36±0.15
9.16	Limonene	13.94±4.82	18.20±6.07
10.41	γ-Terpinene	0.20±0.07	0.31±0.02
10.72	3,3-Dimethylhexane	0.88±0.08	0.91±0.13
11.04	m-Cymene	0.36±0.04	0.42±0.04
11.45	Cyclohexanone	0.27±0.05	0.25±0.10
11.62	Octanal	0.90±0.03	0.94±0.03
12.13	Undecane	1.05±0.20	0.75±0.07
12.90	5-Hepten-2-one, 6-methyl-	0.77±0.11	0.94±0.13
14.42	Nonanal	3.66±0.21	3.62±0.07
14.68	2-butoxy-ethanol	3.84±0.16	4.19±0.31
14.78	Dodecane	**1.30±0.11**	**0.88±0.02**
15.64	Tetrahydrolinalool	0.82±0.14	1.07±0.13
15.84	Tridecane	0.53±0.05	0.43±0.03
16.01	Tetradecane	0.67±0.04	0.68±0.13
16.55	Dihydromyrcenol	1.21±0.18	1.39±0.01
17.04	1-Hexanol, 2-ethyl-	7.48±0.83	5.35±0.62
17.14	Decanal	2.43±0.07	2.39±0.08
17.48	Benzaldehyde	1.57±0.14	1.52±0.17
18.45	Linalool	0.70±0.11	0.56±0.07
19.30	Ethanol, 2-(2-methoxyethoxy)-	0.56±0.03	0.49±0.07
19.78	Hexadecane	1.54±0.31	1.28±0.05
20.10	Ethanol, 2-(2-ethoxyethoxy)-	2.91±0.19	2.89±0.29
20.57	Acetophenone	**0.70±0.05**	**0.48±0.05**
20.62	Menthol	1.43±0.11	1.69±0.13
22.10	Heptadecane	0.67±0.11	0.89±0.04
22.19	Cyclodecanol	0.19±0.06	0.19±0.06
22.54	Naphthalene	**6.74±0.54**	**4.54±0.28**
22.87	(S)-(+)-1,3-Butanediol	0.28±0.05	0.37±0.08
23.40	Methyl salicylate	0.42±0.19	0.57±0.04
23.46	1-Decanol	0.10±0.06	0.18±0.06
24.06	Ethanol, 2-(2-butoxyethoxy)-	0.24±0.08	0.27±0.09
24.28	Methyl laurate	**0.58±0.09**	**0.15±0.09**
24.32	Phytane	**0.19±0.12**	**0.59±0.10**
24.97	Naphthalene, 1-methyl-	**0.36±0.02**	**0.16±0.05**
25.13	1-dodecanol	0.53±0.07	0.28±0.10
25.62	Propanoic acid, 2-methyl-, 3-hydroxy-2,4,4-trimethylpentyl ester	0.14±0.14	0.37±0.13
25.66	Benzenemethanol	1.44±0.11	1.41±0.09
26.07	1-Propanol, 2-(2-hydroxypropoxy)-	0.18±0.06	0.32±0.05

Table 2.1 Continued

	Compound	Relative (%)	
		Control	Infested
26.9	Neophytadiene	7.83±2.33	10.17±2.54
27.25	Naphthalene, 1,5-dimethyl-	0.08±0.05	0.19±0.07
27.53	Neophytadiene isomer	1.37±0.57	1.93±0.39
27.76	1-dodecanol	13.56±1.34	10.02±0.74
28.07	Phytol	2.50±0.72	3.22±0.79
28.25	Phenol	1.32±0.13	1.20±0.12
28.56	Methyl tridecanoate	0.58±0.06	0.33±0.14
29.74	Triacetin	0.33±0.05	0.53±0.06
30.89	Ethanol, 2-phenoxy-	**0.31±0.02**	**0.41±0.02**
31.56	2-Octanol, benzoate	2.40±0.15	2.37±0.03
31.80	Nonanoic acid	0.19±0.06	0.22±0.07
32.48	Methyl myristate	0.96±0.12	0.54±0.23
33.90	1,2,3-Propanetriol	3.94±1.33	3.42±1.28
34.95	Diethyl phthalate	1.55±0.41	1.79±0.32
39.14	Phytol isomer	1.02±0.33	1.42±0.45

7 chemical classes	Relative (%)	
	Control	Infested
Terpene	**31.69±2.59**	**40.73±2.21**
Alkane	6.82±0.39	6.41±0.30
Ketone	1.74±0.08	1.68±0.23
Aldehyde	8.56±0.19	8.46±0.24
Ester	6.97±0.53	6.64±0.43
Alcohol	**35.54±1.39**	**29.78±1.78**
Aromatic	**8.49±0.61**	**6.09±0.33**
Acid	0.19±0.06	0.22±0.07

3. VOCS DETERMINATION BY ADSORBENT-RAMAN SYSTEM IN FOOD AND BOTANICALS

3.1. Abstract

Volatile organic compounds (VOCs) emitted from foods and plants are typically analyzed by gas chromatography/mass spectrometry (GC/MS) or electronic-nose (E-nose) analysis. GC/MS is highly sensitive but lacks portability, while E-nose equipment is portable but has a narrow range of analysis. In this study, a Raman-based VOC detection system was developed along with multivariate analysis for spectral differentiation of VOCs. A 5 µL droplet each of four representative VOCs (linalool, cis-3-hexenyl acetate, cis-3-hexen-1-ol, methyl salicylate) was pre-concentrated with Hayesep Q adsorbent in a sealed chamber. After a given collection time (20 and 60 mins), Raman spectroscopy was used to measure the VOC eluates from each adsorbent. Two collection times were tested, and single VOCs versus VOC mixtures were compared. Finally, Raman spectral data were processed with baseline correction and normalization and analyzed with unsupervised and supervised learning techniques. After 20 minutes of collection, individual and mixed volatiles showed unique spectral features, and the multivariate techniques produced good discrimination among the VOCs. Raman spectroscopy was also used to measure mixtures containing three VOCs at five different concentrations, and when principle component regression was applied, a concentration-estimation curve with a high R^2 of 0.953 was generated. This system developed on VOC standards was tested on two types of tea (black and earl grey) to determine the

differentiability of tea aromas, and several unique Raman spectra were observed from the tea samples. Therefore, the proposed Raman technique has proven to be effective at fast screening of multiple VOCs given off from foods and plants and is a good candidate for fast and portable applications.

3.2. Introduction

Volatile organic compounds (VOCs) have been considered as non-invasive markers for plant stress detection and phenotyping as well as for estimating food quality [74-75]. Several different techniques have been used to analyze VOCs for these purposes, and a sensing system to determine VOCs quickly and accurately would be advantageous.

A standard method used for analyzing VOCs emitted from foods and plants is gas-chromatography/mass spectrometry (GC/MS), which is highly sensitive and selective. Most cases involving GC/MS require an additional step to pre-concentrate the VOCs on an adsorbent polymer or solid phase microextraction (SPME) fiber. Many different kinds of herbivore induced plant volatiles (HIPVs) and VOCs from different food sources have been analyzed by this method [15, 76-78]. However, analysis of each sample takes significant time to complete, and the method lacks portability for field application. Another popular, and commercial, method for the analysis of VOCs is by the using an electronic-nose (E-nose) [79]. E-nose systems have been utilized to analyze the VOCs from infested plants [20-21] and damaged food [80-81]. Recently developed E-nose systems have incorporated different types of sensors. For example, composites of carbon black and conducting polymer (CP) coated sensors were evaluated for their ability to detect VOCs associated with stink bug infestation on cotton bolls [23] as well as six relevant phytochemicals [22].

Other E-nose systems developed from metal oxide semiconductor (MOS) sensors or surface acoustic wave (SAW) resonators were designed to differentiate quality levels in food and plant products [82-83] as well as VOCs relevant to food contamination [84]. While each of these E-nose systems offers potential for portability, they require significant sampling time to produce a measurable signal and can analyze only a narrow range of VOCs.

Raman spectroscopy may be an alternative method to overcome the above stated limitations for VOC analysis. Raman has been applied widely for determining analytes of all material phases, but gases are more challenging to detect than liquids and solids. Two methods can be used to enhance Raman sensitivity for detecting VOCs at low concentrations.

First, metal-based nano-particles or nano-structures can be combined with Raman spectroscopy, a technique called surface-enhanced Raman spectroscopy (SERS). The most commonly used substrates are based on Au or Ag metal, and the surface of the substrate can be modified with specific linkers that can absorb specifically targeted VOCs. For example, cyanide on an Au substrate was used to detect the biogenic VOC, farnesol, down to 76 parts per million (ppm) [85]. CCl_4 vapor was detected down to 6.5 ppm, with the use of 2,6-DMPI adsorbed on Au substrate [86]. Moreover, an Ag-nanoparticle layer modified with p-aminobenzenethiol (PABT) or 1-propanethiol was used to detect 1.4 ppm trinitrotoluene (TNT) VOC [87] or toluene and 1,2-dichlorobenzene (ODCB) vapors (0.6 to 10.0 ppm) [88]. Other approaches have been attempted without any linker on the substrate. Polyvinyl alcohol (PVA) nanofibers on which Ag nanoparticles

were deposited were investigated to detect the biogenic VOC, ethylendiamine (EDA), and 100 ppm EDA as well as VOC from fresh shrimp meat was successfully detected [89]. Furthermore, the multiplex VOC detection of acetone and ethanol was demonstrated with a silicon-based nanopillar structure [90], and improved detection of acetone vapor at about 6400 ppm was reported with an Au-Ag based nanogap structure [91].

Second, the added step of pre-concentrating the VOCs before measuring them with Raman spectroscopy has been researched. SPME with polydimethylsiloxane (PDMS) has been used to pre-concentrate trace levels of benzene, toluene, ethyl benzene and xylene from contaminated water, and the PDMS was subsequently analyzed with Raman spectroscopy [31]. PDMS was also coated on a 1-propanethiol-modified Au@Ag nanoparticle monolayer film, and the aromatic vapor of toluene was ultimately detected with the SERS technique via a vapor-flow system [92]. This type of pre-concentration has also been integrated into the internal optical components of a Raman spectroscope. VOCs were successfully detected by coating the optical lens with a thin polymer film to enrich the VOCs of isovaleric acid, 2-aminoacetophenone, and indole [93]. Limitations of these techniques have been evident in the literature. Most SERS substrates have been designed to detect only a narrow range of VOCs, and the limit of detection was only around the ppm level, even though the SERS technique, not standard Raman, was employed. Moreover, the adsorbent layer coupled with the Raman system has not been very effective for collecting many VOCs from foods or plants.

A few studies have been conducted regarding detection of VOCs common to food and plants. Linalool has been detected with Raman spectroscopy in various

vegetable oils [94] and essential oils [94-96]. Cis-3-hexenyl acetate was used to verify the functionality of an e-nose sensor [22], but the detection limit was not mentioned. Methyl salicylate was successfully detected with an electrochemical sensor at the parts per billion (ppb) level [97]. However, the sensor was designed only to detect methyl salicylate and required two very specific enzymes to induce electrochemical reduction. Additionally, the study only included methyl salicylate in solution at well-controlled pH, so this sensing system would likely not be well-suited to detecting methyl salicylate in vapor phase.

The goal of this study was to evaluate the concept of detecting multiplex VOCs from foods and plants with Raman spectroscopy. Specific objectives were (1) to use several VOC standards to develop a method involving Raman coupled with an adsorbent to detect multiplex VOCs at roughly the ppm level, and (2) to test the method on naturally occurring multiplex VOCs associated with tea aroma.

3.3. Material and methods

3.3.1. In-parallel VOC collection system

As shown in Figure 3.1a, the VOC collection system was composed of three main components. First, five 120-mL glass bottles capped with Teflon-lined lids (Qorpak, Bridgeville, PA,) were used as VOC collection chambers. Each lid was equipped with two stainless steel unions (6 mm O.D.; Swagelok, Solon, OH) which were used to hold glass columns (178 mm length x 6 mm O.D.; Supelco, Bellafonte, PA) containing adsorbent material. One column was used for purification of incoming air and the other for pre-concentration of the VOCs. Second was the adsorbent Hayesep Q resin

(80/100 Mesh; Hayes Separations, Inc., Bandera, TX), which has been widely used to collect plant VOCs. Each glass column was filled with a 5-cm bed of the resin and tightly packed with a thin layer of deactivated borosilicate glass wool (Restek, Bellafonte, PA). The third component involved a diaphragm pump (Thomas Scientific, USA) which was used to pull air through VOC collection system, and airflow was controlled by manual flow regulators. Each resin-packed column was connected to a flow regulator with Nalgene vacuum tubing, and the air was drawn through the collection column at 1.0 liter/min. The entire collection system was kept in a fume hood lined with foam insulation and maintained at 27 ± 2°C with a thermostatically-controlled electric heater for the isothermal volatilization of each standard.

3.3.2. **Experimental procedure**

3.3.2.1. Experimental design

Two different collection times (20 and 60 mins) were considered in order to vary the level of pre-concentrated VOCs on the adsorbent. Four VOC standards as well as a mixture of VOCs were tested for the selectivity of Raman VOC detection. In addition, a mixture of three different standards was prepared at five different concentrations to test the sensitivity of Raman VOC detection. All procedures were done in quadruplicate. Two different tea samples were also considered, and VOC collection for each tea sample was also replicated four times.

3.3.2.2. Preparation of VOCs samples

Four standards (Sigma Aldrich) were used as known VOCs: linalool as a terpene, cis-3-hexenyl acetate and cis-3-hexen-1-ol as green leaf volatiles (GLVs), and methyl salicylate as an aromatic. A 5µL sample of each standard was placed into a separate chamber for single VOC collection. To collect the mixed VOCs, a 5 µL sample of each standard was added into a fifth chamber. All five chambers were tightly sealed, and VOC collection carried out for 60 min. After VOC collection, each column was removed from its chamber, and the VOCs trapped on the adsorbent resin were eluted with GC-grade dichloromethane. The first 1-ml of eluate was directly sampled and sealed into a 1.5-ml GC vial until it was measured by Raman spectroscopy. The same procedure was repeated for a 20 min collection time. To prepare the mixed standard samples for Raman tests at various known concentrations, a 10 µL each of three standards (linalool, cis-3-hexen-1-ol, and methyl salicylate) was combined and then diluted with dichloromethane in 0.5 volume/volume percent (0.5 v/v %). It was repeated by four times until the final concentration reached 0.005 v/v %. Therefore, a total of five mixture samples of different concentrations (0.5, 0.1, 0.05, 0.01, 0.005 v/v %) were used for Raman measurement. To approximate the mixture concentrations, it was assumed that the mixture was an ideal gas, which means that the sum of each volume of the analyte would be the same as the total volume of the mixture. If the volume of each compound was same, the density of the mixture would be the average density of each compound, so the density of the concentration ranged from 4795 µg/ml to 47.95 µg/ml (Appendix A, S1b).

Aroma samples of black and earl grey teas (Upton Tea Imports) were used for the analysis of unknown VOCs. Samples (10g) of each tea were individually placed into two different chambers. After tightly sealing the chambers, VOC collection was carried out for 60 min, and pre-concentrated VOCs on the resin were eluted with dichloromethane. The first 1-ml of eluate was sampled and sealed into a 1.5-ml GC vial until it was measured by GC/MS and Raman spectroscopy.

3.3.2.3. GC/MS

Each collected tea VOC eluate was first analyzed for qualitative identification by injecting 1μL into a Shimadzu GCMS-QP 2010 Ultra (Shimadzu Scientific Instruments (Oceania) Pty Ltd, Henderson, New Zealand) equipped with a Zebron ZB-WAX plus column (30 m length x 0.25 mm I.D. × 0.25 μm film thickness; Phenomenex, Torrence CA, USA). The carrier gas was helium at a flow rate of 1.5 mL /min. The temperature of the injection port was 250 °C and a 1 μl sample was injected with a split ratio of 1:1. The initial column temperature was set at 40 °C and maintained at that temperature for 3 min. Thereafter, the temperature was increased to 240 °C at a rate of 5 °C/min and held at that temperature for 3 min. Finally, the temperature was increased to 250 °C at a rate of 40°C/min ramp. Mass spectrometry involved electron impact ionization at an interface temperature of 250 °C and an ion source temperature of 200 °C. Finally, the VOCs were identified based on data in the National Institute of Standards and Technology (NIST) Mass Spectral Library and the Wiley Registry of Mass Spectral Data (10th edition). The peak areas of identified VOCs were exported from Shimadzu GCMSsolution (version

2.7) package software and divided by the total peak areas to calculate the relative amount of the VOCs.

3.3.2.4. Raman spectroscopy

A volume of 30 µl of each VOC eluate was placed inside a quartz cuvette with a lid, to prevent evaporation during measurement. The cuvette was placed on the stage of the Raman spectroscopy device (RamanStation 400 F, Perkin-Elmer, Beaconsfield, Buckinghamshire, UK) with a 256 × 1024 pixel CCD detector and a 785 nm near-infrared laser with 175 mW power (Figure 3.1b). Each spectrum was collected in quadruplicate with 15s exposure time at the spectral resolution of 4 cm^{-1} in the Raman shift range of 200 to 2,000 cm^{-1}.

3.3.3. Statistical analysis

3.3.3.1. Data consolidation and pre-processing

All collected Raman spectra were exported from the built-in software called The Spectrum (v. 6.3) and processed using the bioinformatics toolbox in MATLAB with base-line correction and normalization. The pre-processed spectra were then used as inputs for statistical analysis.

3.3.3.2. Principal component analysis (PCA)

A range of wavenumbers was specified as a variable set from each VOC sample in which as many unique spectral features as possible could be clearly differentiated. For each VOC sample type and collection time replicate, principal component analysis (PCA) was then performed on the variable set with JMP 13 Pro software. The first two principal components (PCs) were plotted to give an indication as to whether each VOC

can be readily classified and whether individual VOCs can be readily separated from mixtures of VOCs. PCA was also performed for tea discrimination, and the first two PCs were plotted to determine whether each tea could be readily classified.

3.3.3.3. Linear discriminant analysis (LDA)

Data from the same set of wavenumbers used in PCA analysis was also employed to create two linear discriminant analysis (LDA) classification models. The first model was calculated based on the three single VOC data sets for discrimination among the three (terpene vs. GLV vs. aromatic), and the second model was based on two different data sets of any single VOC and the mixture, for discrimination between the two (VOC vs. mixture). Before the analysis, the four replicates of data from each of the two collection times were combined, so that a total of eight replications were used as the training set. To evaluate model performance, k-fold cross-validation (k = 8 replications) was applied with custom R-software code for generating randomly partitioned data set for two different models. The partitioned data set for the first model contained three individual data points randomly sampled from each single VOC (total 8 data sets with three each individuals (one terpene, one GLV, one aromatic) per set). The second model contained two data points randomly sampled from any single VOC and mixture (total 8 data sets with two each individuals (one VOC, one mixture) per set).

3.3.3.4. Principal component regression (PCR)

PCA analysis was also used on the Raman spectral data sets from the VOC mixture with five different concentrations, and five PCs were used as predictor variables for a principle component regression (PCR) quantification model. If it is assumed that an

unknown sample contains the tested three VOCs as major components, one specific wavenumber will not suffice for overall VOC quantification, because many characteristic peaks corresponding to the VOCs can be related to their concentrations in the sample. However, using multiple PCs rather than directly using the intensities at specific wavenumbers can be useful in conveying information about numerous characteristic peaks.

The Fit Model function in JMP 13 Pro was used to generate three models, each with the logarithm of each concentration term as a response variable. The first (equation 3) included only linear terms as predictor variables, the second (equation 4) included linear and quadratic terms as predictor variables, and the third (equation 5) included linear and interaction terms as predictor variables. Finally, the calibration curve which plotted estimated mixture concentration versus experimental (actual) concentration was calculated, and three different plots were finally compared with respect to the model selection criteria of R^2, adjusted R^2, and root mean square error (RMSE).

$$Y_1 = \text{Constant}_1 + \sum_{i=1}^{5} C_i PC_i \text{ for only linear (Equation 3)}$$

$$Y_2 = \text{Constant}_2 + \sum_{i=1}^{5} C_i PC_i + \sum_{i=1}^{5} C_i (PC_i)^2 \text{ for linear and quadratic (Equation 4)}$$

$$Y_3 = \text{Constant}_3 + \sum_{i=1}^{5} C_i PC_i + \sum_{i=1}^{5} \sum_{j=1}^{5} C_{ij} PC_i PC_j \ (i \neq j)$$

for linear and interaction (Equation 5)

(Y: response variable, C: coefficient, PC_i: principal component i)

3.4. Results and discussion

3.4.1. **VOCs collection**

Each spectrum from a VOC eluate contained unique features clearly visible throughout the range of wavenumbers considered (Figure 3.2 and Figure 3.3). Three main wavenumber regions where Raman spectra were important included 1700 – 1600 cm^{-1}, 1100 – 1000 cm^{-1} and 900 – 800 cm^{-1} (Table 3-1). During the 60 min collection period, each liquid of standard was completely evaporated by the pump-induced air flow and collected on the adsorbent. The standards from the 20 min collection period were not fully evaporated, but the VOC spectral features were still clearly visible. The maximum concentration limit for each VOC, corresponding to complete evaporation of each standard, could be approximated by the modified ideal gas law, and thus the approximate concentration was calculated for each VOC (Table A 1). The concept that VOC pre-concentration should be conducted prior to Raman spectroscopy has also been proposed by other research groups [92-93]. As explained earlier, Park et al. (2015) proposed a VOC detection system in which the First Contact® solution was coated on a ZnSe lens surface as the adsorbent layer, and the enriched surface was simultaneously measured with Raman [93]. However, the solution was not originally designed as an adsorbent, so the collection efficiency was poor and the collection time was around 120 min. Moreover, the layer of solution was coupled to an optical component, which may become an obstacle to making the device portable and applying the system in the field. Xia et al. (2016) developed a SERS substrate configuration in which PDMS polymer was coated as an adsorbent layer [92], but it was not attached to the Raman optical components and

could be used for field applications like field VOC collection. However, the polymer was not adept at collecting the wide range of VOCs relevant to food and plants. Our VOC collection system is also separate from the Raman components, and the specific adsorbent we used is known to be an effective polymer for pre-concentrating a wide range of VOCs.

3.4.2. **Selectivity performance**

Spectra from the four individual VOCs collected for 60 min were clearly discriminated from each other and from the VOC mixture (Figure 3.4). In addition, the 20 min collection time (Figure 3.5) gave similar results of good discrimination among individual VOCs. However, when the mixture was considered, discrimination among individual VOCs was not clear, possibly due to the reduced concentration of each component. An observation noted for both collection times was that all points from the two GLVs were closely clustered, while a clear separation was observed between terpenes, GLVs and aromatics. The main characteristic peaks from the two GLVs were observed at roughly the same wavenumber, around 1655 cm^{-1}, and the spectral regions of each VOC group were quite different.

PCA analysis of individual VOCs vs. a mixture (Figure 3.6) showed that the same clustering features appear regardless of the particular VOC, such that all replicates from a single VOC had a negative PC1, and those from the mixture had a positive PC1. This situation can be explained by the fact that all the signs of the first loading matrix component from the covariance matrix were positive, and the values in the first loading matrix were used as coefficients to calculate the PC (Table A 2). Therefore, the stronger

the intensity of the variable, the higher the PC value that was derived. Raman intensity from the mixture samples was higher than for any single compound in every variable, because the mixture had several spectral features associated with each VOC, resulting in a higher PC.

PCA analysis of terpene vs. aromatic vs. GLVs (Figure 3.7) showed clear discrimination, and it was clear that each VOC group stayed in its own typical location on the PC1 axis (GLVs at left, terpene at middle, and aromatic at right). Regardless of collection time, a unique set of wavenumbers was identified for each VOC, and the set of variables in any of the three groups pointed in the same PC direction, causing the replicates from the same groups to be in the same general locations.

LDA analysis of individual VOCs vs. a mixture (Table 3-2) resulted in a classification accuracy of 100%, and the classification among the three groups was over 90% accurate. Wong et al. (2014) also succeeded in multiplex SERS detection of two VOCs without any specific chemical linker [90], but the SERS substrate they used as the adsorbent layer and in signal enhancement was too expensive and complex to be fabricated on a large scale. The high-specificity performance in this study can be credited to the combination of the adsorbent system and Raman functionality. VOCs can easily be collected and then used to produce unique spectra. Even though the concentrations of the VOC samples used for verification was somewhat high, this system is a worthwhile method to successfully detect up to at least four multiplex VOCs without the SERS substrate.

3.4.3. **Sensitivity performance**

PCA analysis of Raman features of VOCs from the three different groups (linalool as a terpene, cis-3-hexen-1-ol as a GLV, and methyl salicylate as an aromatic) at different concentrations showed that Raman spectra accounted for about 90% of the variation with five PCs, and PC 1 alone accounted for about 40% (Table A 3). Similar to findings in the selectivity results, the PC 1 coefficients (Table A 4) were also all positive, and the coefficients induced at the wavenumbers identified in methyl salicylate were larger than those at the wavenumber associated with the other VOCs. This finding may have resulted from the fact that Raman intensity at a characteristic peak of one VOC will likely be different than the intensity at a characteristic peak of another VOC, even if they are at the same concentration, and methyl salicylate may have affected the overall mixture spectra more than the other compounds.

The regression curve containing only linear terms (Figure 3.8) did not effectively relate the PCs to the change in mixture concentration and resulted in a R^2 of 0.774. However, when the quadratic or interaction terms were included, the accuracy of estimation was improved (Table 3-3). The regression curve including the interaction effect was an especially good fit, with an R^2 of 0.953 and a low RMSE of 0.159 logarithmic units. Similar research has been done to investigate how PCR could be applied to complex environmental data with many variables (e.g., multiple trace of chemical pollutants in ambient air), and the addition of an interaction term between any PCs resulted in better model [98]. Each PC in the PCR analysis was determined by several coefficients at several wavenumbers, so the signs of the coefficients (Table A 4) were

very important. Although the signs of the coefficients for PC 1 were the same, those of the coefficients for PC2 were different. For example, the size of PC 2 coefficients at 1644 and 1656 cm^{-1} was similar, but the sign was opposite. Thus, the difference in peak intensity at 1656 cm^{-1} can affect PC 1 and PC 2 oppositely, indicating two PCs could be correlated. Although they were correlated, we could not confirm that they also interact significantly. If the effect of PC 1 on the response variable was not same as that of PC 2, we could say that the interaction effect existed, and the interaction effect was clearly shown in Figure A 1. The slope of the data (PC1 vs. concentration) was totally different according to the sign of PC 2, meaning that the change of PC 1 depended on the level of PC 2. This finding may explain why adding the interaction term was the best fit for estimating the concentration.

3.4.4. **Practical application**

The Raman spectra from the tea aromas enabled identification of multiple VOCs which were different in relative amount. Most compounds identified in the earl grey tea had higher concentrations than those in the black tea (Table 3-4). When the Raman spectra were compared, some wavenumber regions had clear differences that can be seen in the orange-shaded regions in Figure 3.9a. Two unique peaks were observed at around 800 cm^{-1} from only the earl grey tea, and the collected VOCs likely resulted in the differences between tea samples. Limonene has weak Raman bands at 799 and 789 cm^{-1} [99], so it likely directly contributed to those two peaks. A minor peak from black tea was observed around 788 cm^{-1}, probably because it has a relatively high percentage of limonene. The vibrational properties of three additional compounds may have also

created differences in the Raman spectra between the teas. These compounds include linalyl acetate, linalool and *p*-cymene, with Raman signatures around 800 cm^{-1} due to C-O stretching or ring deformation [100]. One clear peak was identified around 860 cm^{-1} from only the earl grey tea. This result may be explained by the presence of β-pinene. Commercial Raman libraries (KnowItAll Informatics System 2018, Bio-Rad Laboratories, Inc., USA) confirmed that the Raman spectra of β-pinene have a clear peak around 860 cm^{-1}. Finally, the two VOCs of phytol and phytol isomer were identified in the black tea samples, and KnowItAll software confirmed that the Raman peak around 950 cm^{-1} on the black tea could only be explained by these two compounds due to their spectra at the same wavenumber. Based on the identified wavenumbers, the differences between the teas were also confirmed by PCA analysis, in that all replicates from black tea were completely separated from those of earl grey (Figure 3.9b).

The VOCs tested in this study have been analyzed in previous studies to quantify their emissions from several plants, and we can relate those results with the concentrations we used. Depending on the collection time and herbivore type, the amount of emitted VOC varied, and it was reported that the total amount emitted ranged from 0.1 µg to 2 µg [15, 18, 48, 52, 54, 58, 64, 101]. If that amount was eluted with about 500µl dichloromethane, the final concentration would be between 0.2 µg/ml and 4 µg/ml. Although the minimum concentration tested in our experiment is higher than the reported concentration, the sensitivity of the proposed system would be still reasonable for any biological sample producing enough VOCs, like tea samples. However, if these methods are applied to plant samples emitting ppb level VOCs, the detection limit

should be improved. Therefore, future work will include sensitivity enhancement of our proposed system by use of nanoparticles or nanostructure with the VOC eluate for SERS application.

3.5. Conclusions

A relatively cost-effective and simple VOC detection system was developed based on Raman spectroscopy, and a proof of concept study was successfully completed with several common VOCs emitted from food and plants. The high specificity of the system was achieved by utilizing an adsorbent to collect the VOCs and Raman scattering to identify the adsorbed VOCs. The sensitivity of this Raman system was down to the ppm level of VOCs in a mixture. The system was tested to detect two different tea aromas, and 1.0 hr collection was adequate to produce spectra that clearly discriminated between them. Our collection system ultimately needs to be upgraded to be used as a portable VOC collector, but combining a portable collector with a portable Raman spectrometer could potentially have merit for screening VOCs in the field.

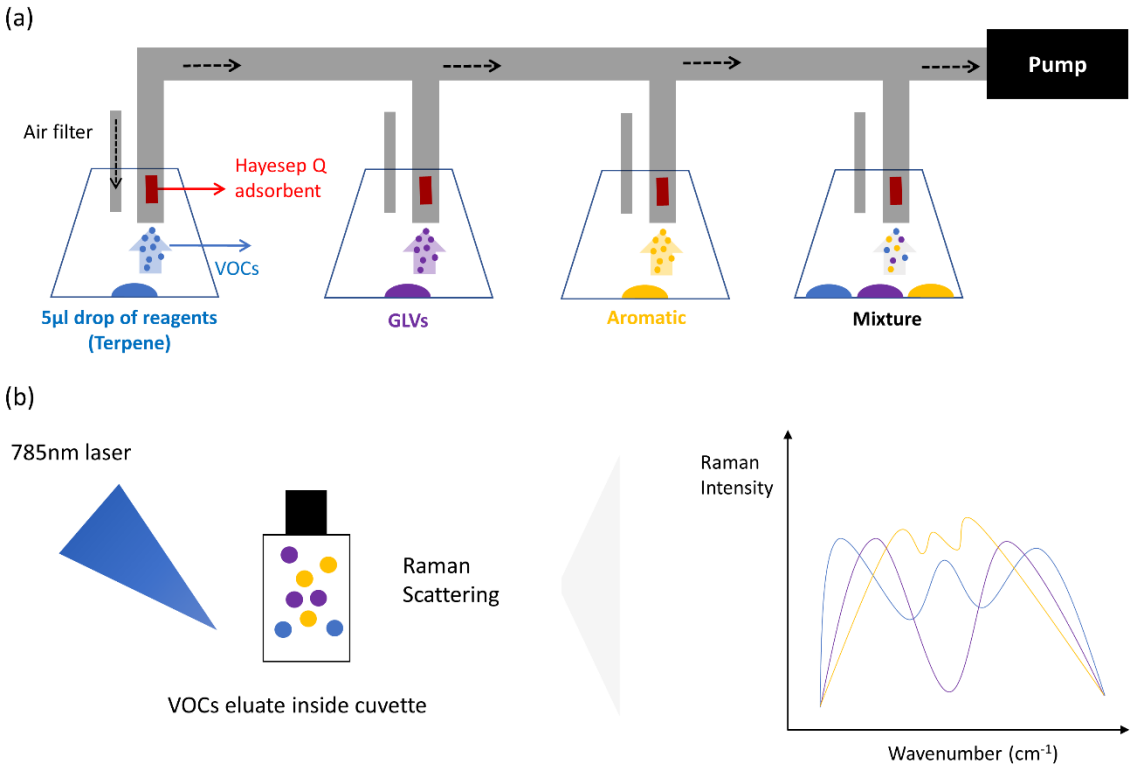

Figure 3.1 Scheme of experimental set-up (a) In-parallel VOCs collection system (b) Raman measurement from VOCs eluate

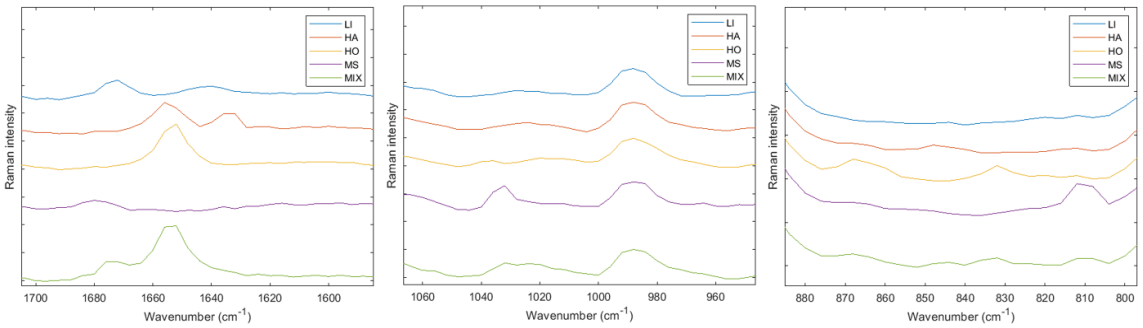

Figure 3.2 Raman spectral signatures according to the VOCs for 60 min collection (LI: Linalool, HA: Cis-3-hexenyl acetate, HO: Cis-3-hexen-1-ol, MS: Methyl salicylate, MIX: Mixture)

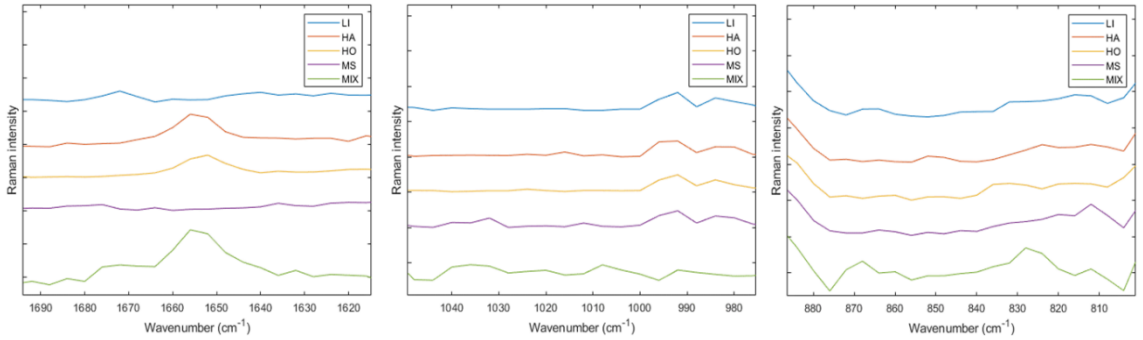

Figure 3.3 Raman spectral signatures according to the VOCs for 20 min collection (LI: Linalool, HA: Cis-3-hexenyl acetate, HO: Cis-3-hexen-1-ol, MS: Methyl salicylate, MIX: Mixture)

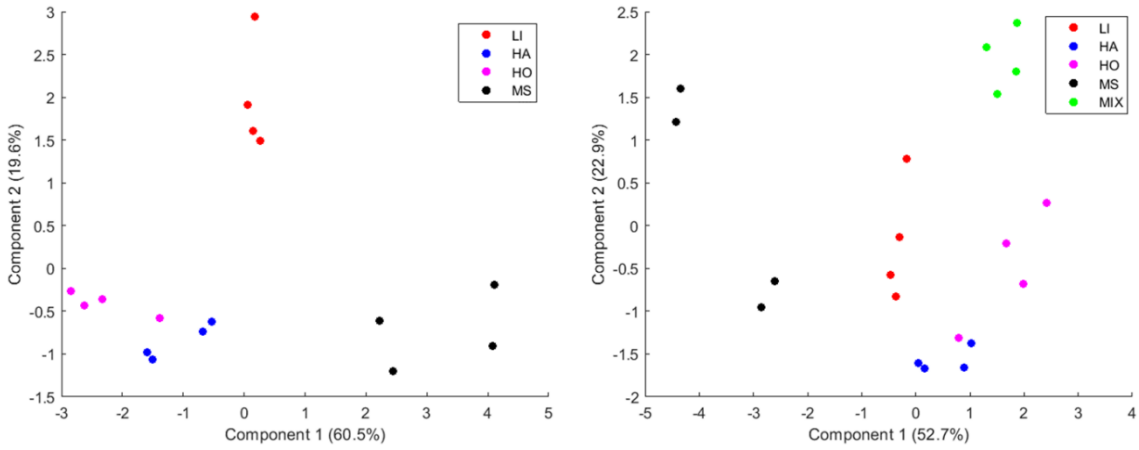

Figure 3.4 PCA plot for the discrimination of each VOC for 60 min (LI: Linalool, HA: Cis-3-hexenyl acetate, HO: Cis-3-hexen-1-ol, MS: Methyl salicylate, MIX: Mixture)

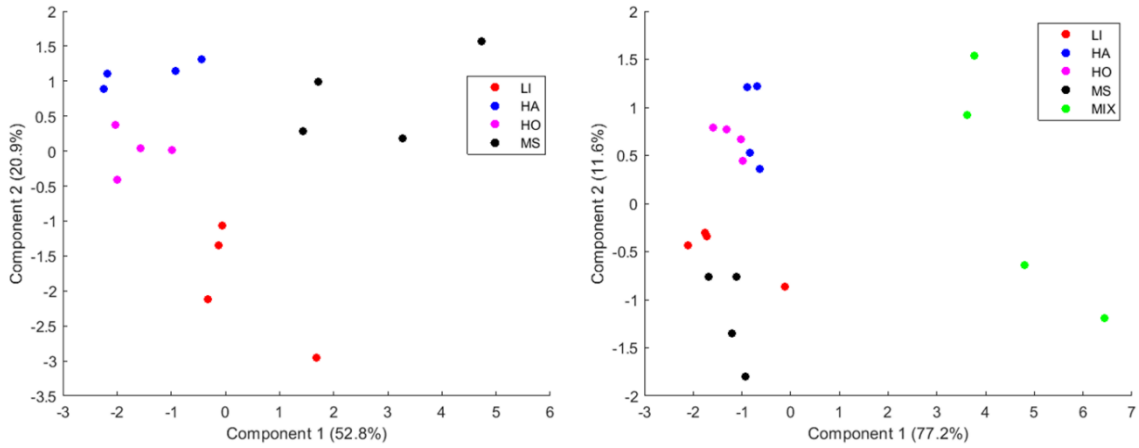

Figure 3.5 PCA plot for the discrimination of each VOC for 20 min (LI: Linalool, HA: Cis-3-hexenyl acetate, HO: Cis-3-hexen-1-ol, MS: Methyl salicylate, MIX: Mixture)

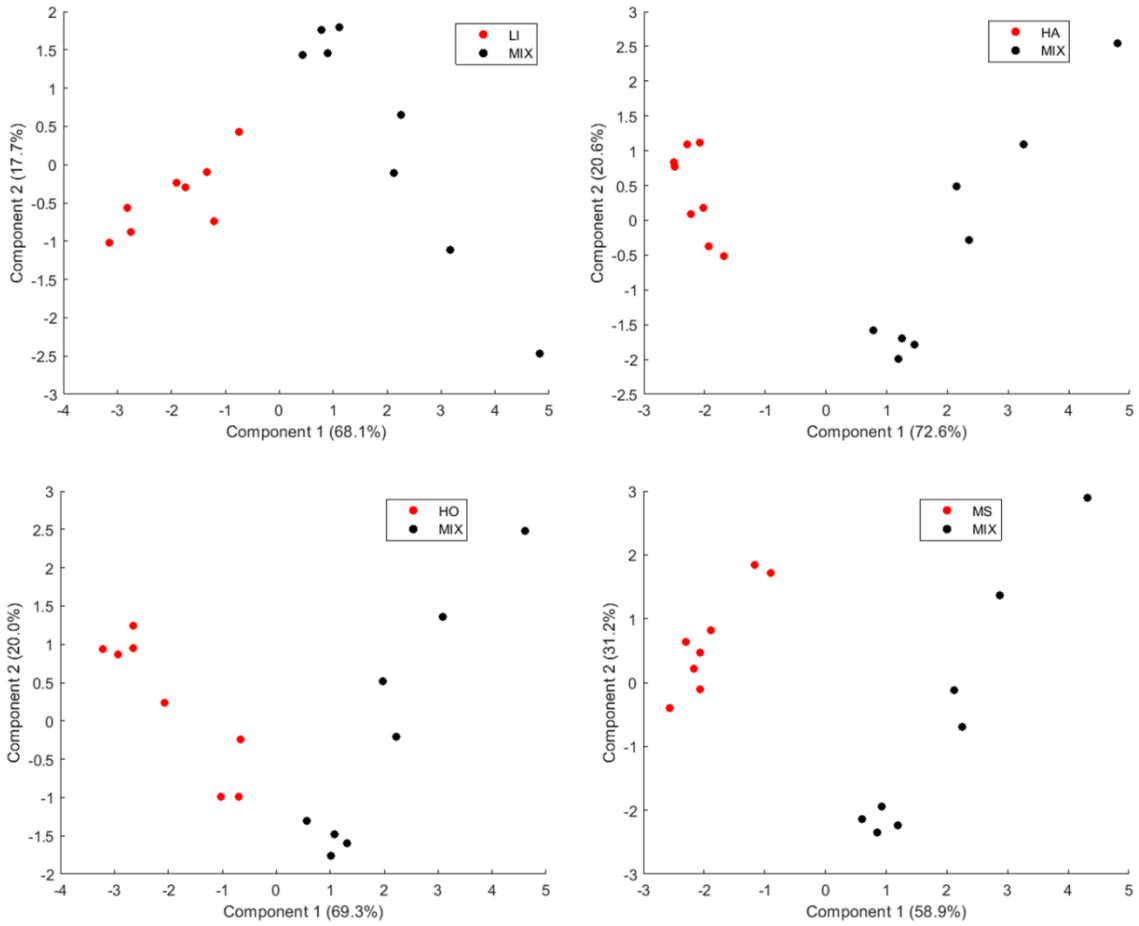

Figure 3.6 PCA plot for the discrimination of single VOC and mixture (LI: Linalool, HA: Cis-3-hexenyl acetate, HO: Cis-3-hexen-1-ol, MS: Methyl salicylate, MIX: Mixture)

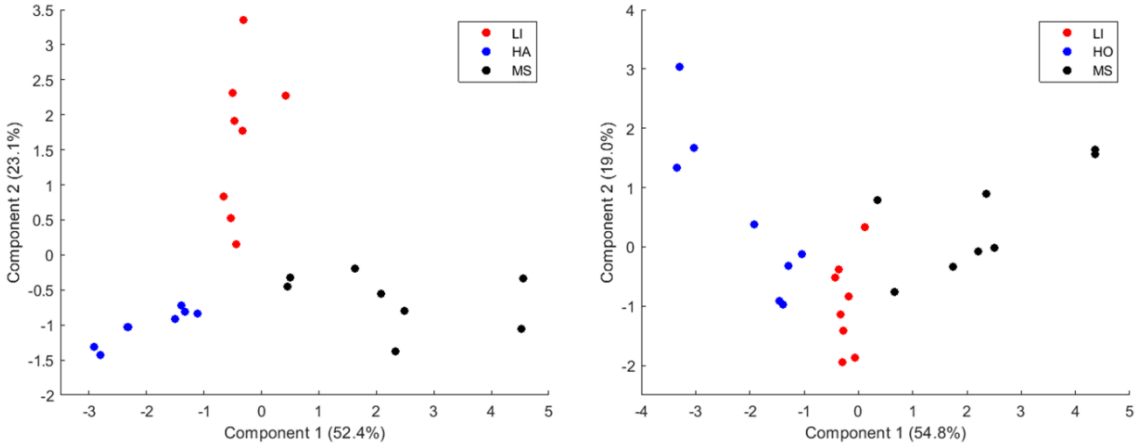

Figure 3.7 PCA plot for the discrimination of terpene, GLVs and aromatic (LI: Linalool, HA: Cis-3-hexenyl acetate, HO: Cis-3-hexen-1-ol, MS: Methyl salicylate)

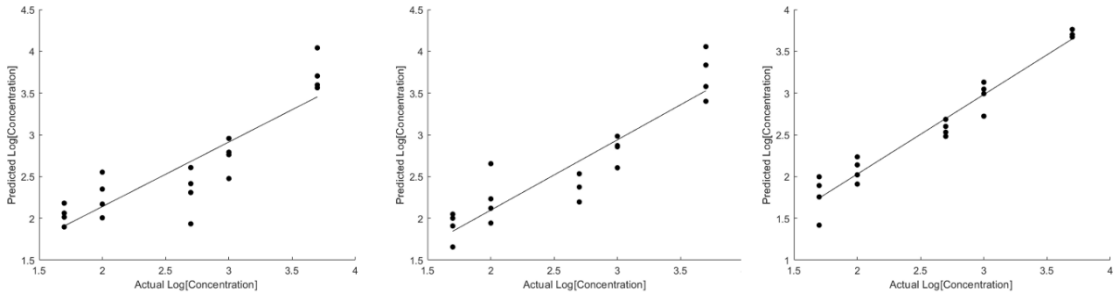

Figure 3.8 Linear regression model of PCR for three different cases (Left: only linear term, Middle: linear + quadratic, Right: linear + interaction)

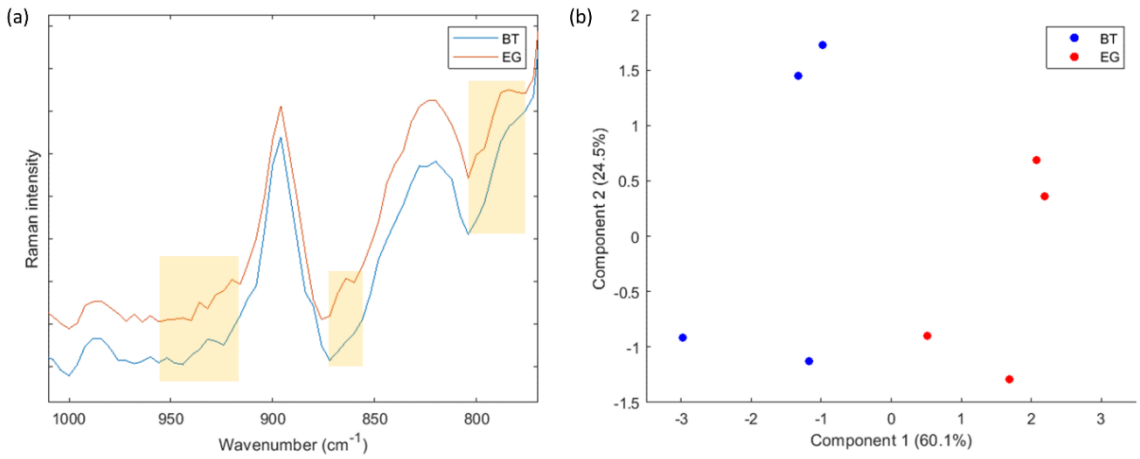

Figure 3.9 Raman spectra for each tea aroma (a) and PCA plot (b) (BT: black tea, EG: earl grey)

Table 3-1 Raman spectral signatures according to the VOCs

VOCs	Wavenumber (cm^{-1})	Mode
Linalool	1672	$\nu_{C=CH}$
	1643	$\nu_{C=CH2}$
Cis-3-hexen-1-ol	1654	$\nu_{C=CH}$
	865	*
	833	*
Cis-3-hexenyl acetate	1655	$\nu_{C=CH}$
	1680	$\nu_{C=O}$
Methyl salicylate	1031	δ_{CH}
	812	γ_{CH}

ν: stretching, γ: out-of-plane deformation, δ: in-plane deformation, *: not available

Table 3-2 LDA model validation by k-fold cross validation

Single volatile vs. Volatile mixture	
Different cases	Classification accuracy (%)
Linalool vs. Mixture	100
Cis-3-hexenyl acetate vs. Mixture	100
Cis-3-hexen-1-ol vs. Mixture	100
Methyl salicylate vs. Mixture	100
Terpene vs. GLVs vs. Aromatic	
Different cases	Classification accuracy (%)
Linalool vs. Cis-3-hexenyl acetate vs. methyl salicylate	92.9
Linalool vs. Cis-3-hexen-1-ol vs. methyl salicylate	95.8

Table 3-3 Summary of regression fit according to the three different representation

	Only linear	Linear + quadratic	Linear + interaction
R2	0.774	0.841	0.953
Adjusted R2	0.761	0.833	0.950
RMSE (Root mean square error)	0.314	0.275	0.159

Table 3-4 Relative composition for the identified VOCs from each tea sample

VOC	Relative percentage (%)	
	Black tea	Earl grey
Limonene	16.68	36.42
Linalyl acetate	0.23	12.51
β-pinene	0.25	9.53
Linalool	1.34	7.88
p-cymene	2.31	6.80
γ-terpinene	1.08	4.85
α-pinene	0	3.43
β-myrcene	0.60	2.80
Neophytadiene	22.04	1.48
Phytol	8.85	0
Phytol isomer	12.19	0

4. ELECTROSTATIC INTERACTION INDUCED PHASE TRANSFER OF AG-NANOSPHERE FOR SERS APPLICATION

4.1. Abstract

Surface-enhanced Raman spectroscopy (SERS), due to its good sensitivity and selectivity, has been widely investigated in many applications. However, only little work has been done on using SERS for the detection of volatile organic compounds (VOCs) primarily due to the challenges associated with fabricating SERS substrates with sufficient hot-spots for signal enhancement and good affinity for the VOCs. This study investigated whether or not Ag-nanospheres (AgNSs) can be transferred from aqueous phase to non-aqueous phase by electrostatic interaction induced by cationic surfactants, and if the AgNSs transferred from the aqueous can be utilized as SERS substrates for the determination of methyl salicylate as one of the VOCs. Results indicated that one of three cationic surfactants, tetraoctylammonium bromide (TOAB) dissolved in organic solvent showed good phase transfer of the AgNSs by efficient electrostatic interaction. The complex formed by hydrophobic interaction between the transferred AgNSs and Tenax-TA adsorbent polymer was able to be utilized as a SERS substrate, and the volatile of methyl salicylate could be easily determined from SERS measurements at 4 hours static volatile collection. Therefore, the proposed new techniques can be effectively employed to areas where many VOCs relevant to food and agriculture need to be analyzed.

4.2. Introduction

Plant-emitted volatile organic compounds (VOCs) are important constituents that may indicate a plant's physiological damage, potentially induced by abiotic or biotic stresses. Gas-chromatography/mass spectrometry (GC/MS) has been widely used to analyze VOCs due to its high sensitivity, but a great deal of time is required for the analysis, and it is not suitable for field application. Therefore, surface-enhanced Raman spectroscopy (SERS) using metallic nanostructure for signal enhancement is considered a potential alternative in field applications due to its reasonable sensitivity, selectivity and fast response [102]. To determine VOCs with SERS, key configuration requirements involve (1) using as many "hot-spots" on nanoparticles as possible to intensify the weak Raman signal from the VOCs, and (2) making the surface properties of the nanoparticle favorable to the VOCs so they have higher affinity for the surface.

There is greater need to develop 3D rather than 2D SERS substrates due to their stronger signal enhancement caused by the higher density of hot-spots in 3D structures. Most 3D substrates have been designed to make each nanoparticle aggregate unique, because signal enhancement at the gap between particles can be much stronger than at the surface of a single nanoparticle [103]. Research on fabricating nanoparticle aggregates as a SERS substrate has been done by several research groups.

An initial approach was to randomly deposit particle aggregates on a substrate. An Ag-nanoparticle (AgNP) aggregate was formed on copper foil by immersing the foil into the particle solution [104], and the AgNPs were also deposited on a glass substrate by a high-pressure sputtering technique [105]. However, there was a lack of regularity in the

number of hot-spots, resulting in an irreproducible and weak signal. Thus, it was necessary to develop a substrate with more uniform distribution of hot-spots in order to maximize the Raman intensity.

A subsequent approach was to use an additional guide structure patterned on the substrate to aid in depositing the particles on the structure. For instance, Si substrates were developed in patterns of nanorod, nanohump, and photolithographic microstructures so AgNPs could be deposited in efficient 3D hot-spots [106-108]. Also, poly(oligo(ethylene glycol)methacrylate) (POEGMA) brushes were prepared as substrates for sputtered AgNPs to increase hot-spot density [109]. Moreover, a nanoparticle film was formed on the surface of a non-plasmonic particle assembly such as iron nanoparticles [110] and reverse micelles of poly(styreneblock-2-vinylpyridine) (PS-b-P2VP) [111]. While these films turned out to be effective in detecting the analyte due to the intensified Raman signal, the methods for fabrication of the SERS substrates were complex and costly.

A cost-effective and functional approach was subsequently proposed as a 3D SERS substrate. The key component of that substrate was Ag-nanospheres (AgNSs) made of single Ag-nanocrystals (AgNCs) via bottom-up assembly by surfactants at an oil/water interface. The resulting colloidal spheres had many hot-spots at the gap between each crystal [112-113]. These AgNSs have been employed as the 3D SERS substrate in several different applications, such as the detection of pathogenic bacteria [114], melamine [115], maize toxin [116-117] and drugs in human urine [118].

The limitation of the AgNS approach was that the spheres were dispersible in water, so they were not compatible with samples based on organic solvents. Thus, a technique that can transfer the spheres from the water phase to the organic phase is needed when using SERS to sense organic samples. A number of different techniques have been investigated for the phase transfer of the nanoparticles [119], but only electrostatic interaction-based phase transfer processes relevant to our study have been considered at present.

Depending on the nature of molecules to be transferred in the organic solvent, several different techniques have been introduced. First, Au nanoparticles (AuNPs) modified with negatively charged valine [120] or carboxylate [121] were transferred to the organic solvent where primary amine was dissolved due to the interaction between the amine and the carboxylate.

Second, the most commonly used molecules in organic solvent were cationic surfactants, especially tetraoctylammonium bromide (TOAB) and cetrimonium bromide (CTAB). Many previous studies used mercaptocarboxylic acids as capping reagents of AuNPs, so the interaction between cations of the added surfactants in organic solvent and the carboxylate of the particle surface enabled them to be successfully transferred to the organic solvent phase [122-128]. In addition to mercaptocarboxylic acid, glutathione (GSH) having two carboxylic groups or calixresorcinarene as macrocycle were employed to cover the exterior of metal-based nanoparticles. In these cases, the nanoparticles protected by those molecules were finally transferred to organic solvent due to the cation of the added CTAB [129-130].

Similar to the results with cationic surfactants, alkyldimethyl(ferrocenylmethyl)ammonium ions also proved useful for phase transfer of AuNPs capped by thiolated cyclodextrins (CD) [131], and negatively charged polystyrene (PS) microspheres were utilized as carriers for the phase transfer of positively charged hydrophilic particles [132].

However, apparently no research has dealt with phase transfer of aggregates of nanoparticles rather than single nanoparticles, and the effect of the phase (either aqueous or non-aqueous) in which the added cationic surfactant is dissolved also has not been investigated.

Therefore, the objectives of this study were to make water-dispersible AgNSs, transfer them to an organic solvent via electrostatic interactions, and employ them as a 3D SERS substrate to identify VOCs relevant to plant defense systems.

4.3. Material and methods

4.3.1. Material description

Methyl salicylate standard, Tenax-TA (60/80 mesh), and chemicals used for manufacturing AgNSs (sodium oleate, oleic acid, cyclohexane, and sodium dodecyl sulfate) were purchased from Sigma Aldrich (St. Louis, MO). Silver nitrate (AgNO3) was obtained from Fisher Scientific (Pittsburgh, PA). All organic solvents, reagents, and chemicals were of analytical grade and used as received without further purification.

4.3.2. **Experimental procedure**

4.3.2.1. Fabrication of AgNSs

A two-step methodology for fabrication of AgNSs was based on previous research [116-117]. To fabricate AgNCs, a mixture including 0.5 g $AgNO_3$, 10 mL deionized (DI) water, 0.8 g sodium oleate, 1 mL oleic acid and 5 mL ethanol was added to a 20 mL glass vial under agitation. The vial was tightly sealed and stored in an oven at 150 ℃ overnight. Afterward the vial was washed out with ethanol and fully dried to create a layer of AgNCs at the bottom of the vial. To fabricate AgNSs, 80 mg of AgNCs from the first step was dissolved in 20 mL of cyclohexane, and 560 mg of sodium dodecyl sulfate (SDS) was also dissolved in 100 mL of DI water. These immiscible solutions were mixed and sonicated for 1 hour and then heated at 70 ℃ until the cyclohexane was mostly evaporated. The concentrated AgNSs were finally prepared by repeating the centrifugation and re-dispersion of DI water.

4.3.2.2. Phase transfer

The methodology for phase transfer was finally developed based on our previous work [133].

4.3.2.2.1. Cationic surfactants in aqueous phase

Three cationic surfactants, TOAB, CTAB and Benzalkonium chloride (BKC), were added separately to DI water on a hot plate until they were completely dissolved, to prepare 0.28 M solution of each. Three mixtures were made by mixing 100 µl of AgNSs with 100 µl of each cationic surfactant solution. Each AgNS mixture was vigorously vortexed for 1 min, and then 200 µl of dichloromethane was added into each mixture,

and each mixture of immiscible liquids was finally vortexed again for 1 min. The occurrence of phase transfer was confirmed by observing the color change at the bottom from clear to dark. If the AgNSs in DI water were transferred into the dichloromethane, only the transferred part at the bottom was collected and centrifuged to concentrate only the transferred AgNSs (TAgNSs), which were finally re-dispersed in 200 µl of dichloromethane for use as a 3D SERS substrate.

4.3.2.2.2. Cationic surfactants in non-aqueous phase

The same three cationic surfactants were dissolved in dichloromethane at a level of 0.14 M, and 100 µl of AgNSs were diluted with 100 µl of DI water. Then 200 µl of each surfactant in dichloromethane solution was mixed with 200 µl of two times diluted AgNS solution, and the mixture was vigorously vortexed for 1 min. Only the TAgNS solutions showing significant color change at the bottom were collected by centrifugation, and these were re-dispersed in 200 µl of dichloromethane for use as a 3D SERS substrate.

4.3.2.3. 3D SERS substrate

The SERS substrate was based on the complex between TAgNSs and Tenax-TA polymer, and three different complex solutions were prepared by dissolving Tenax-TA (1mg, 2mg and 3mg) into 150 µl TAgNS solution in dichloromethane. A 20 µl volume of each complex solution was drop-casted on a clean quartz substrate and fully dried.

4.3.2.4. Static volatile collection

For the generation of methyl salicylate (MeSA) volatile, 5 µl of the MeSA was dropped inside the jar with 120 ml, and three different SERS substrates were placed

inside the jar by facing the substrates to the evaporated reagent for two different collection times (4 hours and overnight).

4.3.2.5. Transmission electron microscope (TEM)

To determine the morphology of the AgNCs and AgNSs before and after phase transfer, carbon-coated 300 mesh grids were treated by glow discharge, and then approximately 2 to 3 µl of the samples (AgNCs, AgNSs and TAgNSs) were applied to the grid. After 10 seconds, the excess was blotted off with filter paper. The prepared specimens were observed in a JEOL 1200 EX transmission electron microscope (TEM) operated at an acceleration voltage of 100 kV. Electron micrographs were recorded at calibrated magnifications with a 3k slow-scan CCD camera (model 15C, SIA), and particle size was measured with ImageJ software.

To obtain elemental and crystallographic information from the AgNSs before and after phase transfer, approximately 2 to 3 µl of the samples (AgNSs and TAgNSs) were deposited onto TEM grids with a carbon film and dried on a paper filter. The spheres were characterized by FEI TECNAI G2 F20 Super-Twin TEM fitted with a Schottky field emission gun, a 2k x 2k Gatan CCD camera, and an Oxford windowless energy dispersive X-ray spectroscopy (EDX) detector (Oxford X-Max^N TSR) with a collection solid angle in the range 0.3 to 0.7 steradians. The elemental analysis was performed in the area of agglomerated AgNSs and TAgNSs at a 200 kV accelerating voltage, and the collected EDX spectra were exported from Oxford AZtec software. In addition to the chemical elements from the TEM-EDX system, electron diffraction patterns were also taken from the AgNSs and TAgNSs at a camera length of 200 mm.

4.3.2.6. UV/Vis spectroscopy

Both water-dispersible AgNSs and the TAgNSs solutions were prepared in a quartz cuvette, and UV/Vis-NIR spectra for both were acquired with a Hitachi U-4100 spectrophotometer.

4.3.2.7. Raman spectroscopy

Each substrate after static volatile collection was placed on the stage of a Raman spectroscopy instrument (RamanStation 400 F, Perkin-Elmer, Beaconsfield, Buckinghamshire, UK), which consists of a 256 × 1024 pixel CCD detector and a 175 mW near-infrared (785 nm) laser. Spectra were collected in quadruplicate with 2 s exposure at a spectral resolution of 4 cm^{-1} in the Raman shift range of 200 to 2,000 cm^{-1}. All collected spectra were exported from built-in software (The Spectrum v. 6.3) and finally processed with base-line correction and normalization in MATLAB's bioinformatics toolbox.

4.4. Results and discussion

4.4.1. Phase transfer of AgNSs

4.4.1.1. Cationic surfactants in aqueous solution

Distinct features of phase transfer (Figure 4.1) depended on the following: (1) what kind of cationic surfactant was used, and (2) in which phase (either aqueous or non-aqueous) the cationic surfactant was dissolved. When the cationic surfactant dissolved in water was added to AgNSs in the water, the phase transfer did not work at all for any of the surfactants. One reason might be low water solubility of each surfactant. In particular, TOAB was not more soluble than the others and required

continuous heating to maintain solubility due to its large hydrophobic tail area (Figure B 1). Results from the other two surfactants were also poor, even though their solubility was somewhat better. The AgNSs may have interacted with the micelle formed by adding surfactant during the first vortexing of the mixtures of AgNSs and added surfactant in water phase (Figure B 2). However, some of the added cationic surfactants may have started to move to the water/dichloromethane interface, and some of them may have interacted with the SDS right after the second vortexing with added dichloromethane. While interacting with the SDS, they may have either been inserted into the spot where the SDS layer had formed or attached to the head of the SDS by electrostatic interaction. The hydrophobic tail area of the other two surfactants was smaller than that of TOAB, so they may have been inserted at the interface where anionic SDS surfactant had already been aligned (Figure B 1). As a result, the electrostatic interaction between the cationic surfactant of one AgNS and the anionic surfactant of another AgNS may induce aggregation (Figure B 2, a). The aggregation of AgNSs may also be explained in different way (Figure B 2, b). The added cationic surfactants may have been attracted to the anionic surfactant by electrostatic interaction, and the hydrophobic tails of the cationic surfactants may have been exposed to the water phase, not a favorable situation. Therefore, the modified AgNSs with the added surfactants may have been trying to aggregate together to minimize the exposed hydrophobic area in the water phase. Finally, the aggregates (based on either possible explanation) may have a much greater diameter than the original AgNS, which can be confirmed by a color change from dark green to brown (Figure 4.1). In accordance with

the first explanation, it has been reported that cetyltrimethylammonium chloride (CTACl) cationic surfactant can interact with negatively charged AuNPs, with the aggregation confirmed by a color change from red to blue [134]. Whether the phase transfer can occur during vortexing can be determined largely by how well the AgNSs can be modified with the cationic surfactant to increase hydrophobicity, in which case the aggregates would still have a chance to meet other cationic surfactants aligned at the water/dichloromethane interface. However, there may be no way to make the surfactants cover the surface of the aggregates due to their increased surface area, so inadequate hydrophobicity could be the reason they were not driven to the organic phase.

4.4.1.2. Cationic surfactants in non-aqueous solution

A major consideration is that each cationic surfactant had a different effect on phase transfer (Figure 4.1). When BKC cationic surfactants were added, phase transfer did not occur at all (no color change). However, the addition of CTAB or TOAB cationic surfactants did result in a color change, and a clear color change was observed in the case of TOAB surfactants, meaning that most of the AgNSs in water phase were transferred to the organic phase. The key factor in the difference appears to be the hydrophobicity of the surfactants, such that if the AgNSs modified with the cationic surfactant by electrostatic interaction at the water/dichloromethane interface become hydrophobic enough, they are finally moved from the water to the organic phase. Again, the TOAB that was not dissolved in water had four hydrocarbon tails rather than only one tail like the other two surfactants. Thus, if it is assumed that one mole of each cationic surfactant is attached to one mole of the SDS anionic surfactant of the AgNSs, a

much greater hydrophobicity can be exerted on the AgNSs in the TOAB case, and a lesser number of moles should be enough to transfer them to the organic phase. The TOAB induced phase transfer procedure is shown in Figure B 3. A slight color change was found at the bottom of the organic phase as a result of adding CTAB, meaning that only a few AgNSs were transferred to the bottom. This result can be explained similarly, such that a larger number of moles of CTAB might be needed to produce the same hydrophobicity induced by TOAB. The phase transfer induced by TOAB was also confirmed by TEM (Figure 4.2), and the spherical aggregates representing the AgNSs were found in both cases (before and after phase transfer). The successful effect of TOAB was additionally analyzed by EDS (Figure 4.3), and the bromide peak that was only visible after phase transfer could be strong evidence that AgNSs were well-modified with the added TOAB during phase transfer. In addition, the crystallinity of the AgNSs was examined by analyzing the diffraction pattern, and spot and ring patterns were clearly identified from both cases (Figure 4.4), confirming that the quality of crystal structure was not affected by the addition of TOAB.

The successful phase transfer of the AgNSs raises the question, how is it possible to transfer AgNSs with diameter above 50nm by using TOAB? Cheng et al. used TOAB to make AuNPs covered with citrate phase transferred from water to toluene by electrostatic interaction. They found that phase transfer by electrostatic interaction alone was not effective for nanoparticles above 10 nm in diameter due to the decreased surface area to volume ratio [135]. In other words, the TOAB coverage on the surface of the nanoparticles was less for larger particles, contrary to our results. Therefore, the

nanoparticles must be considered in-detail to elucidate the difference. The AuNPs of Cheng et al. were formed by citrate reduction of $HAuCl^4$, so the particles were highly stabilized by the citrate anion uniformly covering them [136]. The citrate anion layer on the AuNPs was also considered to unveil the exact mechanism of formation. The citrate trimer, having two absorbed molecules and one dangling molecule, may be a unit of the layer, with surface coverage of 2.8×10^{-6} mol/m^2. The central COO^- group of the exposed dangling citrate may be the main source for negative charge [137], and many other polar groups including hydroxyl and other carboxyls can be major factors in making the particle hydrophilic. However, the AgNSs used in our experiment were formed by hydrophobic interaction between a cluster of AgNCs and the tail of the SDS anionic surfactants, so how regularly the SDS anionic surfactants were packed at the water-oil interface where the AgNCs were dissolved needs to be known. If the surfactants were sparsely positioned at the interface, a smaller number of the cationic surfactants might have been needed to induce the electrostatic interaction between them, a possibility supported by previous research [138]. The hydrophobic tail of the SDS is not positioned in an orderly way in the oil phase, even in contact with water, so the surface area is about several hundred square angstroms, corresponding to a surface coverage of 3.92×10^{-7} mol/m^2 and comparable to the surface area of citrate with about ten times difference in quantity. Furthermore, the disorder of the hydrophobic tail inside the oil phase might help the particles transfer to the organic phase due to more exposed hydrophobic area into the water. This possibility is different from the case of citrate in that some of the polar groups might keep the particles from being hydrophobic even after interacting with

the added TOAB. Taken together, these two points may explain how large particles can be transferred from water to organic phase.

4.4.2. **SERS application for the determination of MeSA**

The UV/Vis absorption intensity of AgNSs at around 450 nm before phase transfer was higher than after phase transfer (Figure 4.5). Not all the particles from the water phase could be transferred to the organic phase, so the final concentration after phase transfer was less than the original concentration, resulting in lower absorption intensity. However, the shape of the spectrum was maintained, and the absorption peaks after phase transfer were located around 400 and 500nm, similar to the absorption spectra of the AgNSs used as SERS substrate [114]. Therefore, the AgNSs after phase transfer were used as a 3D SERS substrate to detect MeSA, an important VOC for plant systematic defense [139]. Tenax TA, poly(2,6-diphenylene oxide), is known to be an effective adsorbent polymer for collecting a wide range of VOCs emitted from plants and foods. It is usually used with GC/MS analysis, and a thermal μ-preconcentrator where the adsorbent is coated has also been developed for detecting VOCs [13, 140]. However, this combined technique requires a thermal desorption step before detecting VOCs, and the configuration is complicated to fabricate. In contrast to GC/MS analysis, our 3D SERS substrate does not need thermal desorption. The 3D SERS substrate was tested to determine whether it can directly measure pre-concentrated MeSA at different concentrations in the adsorbent polymer.

Due to surface property changes of TAgNSs, the added polymer was well-dispersed in the TAgNSs solution, and the film from the complex solution was

uniformly formed on a quartz substrate. The hydrophobic interaction between phenyl groups of the polymer and hydrophobic tail of the TOAB on TAgNSs should be the main force for formation of the complex, and this notion has been confirmed; hydrophobic polymer above a certain concentration or chain length can successfully interact with the hydrophobic core of a lipid membrane similar to the TOAB amphiphilic molecule [141]. The film formed from the complex solution was easily deposited on the quartz substrate immediately after evaporation of the dichloromethane solvent, and the film ultimately deposited on the quartz substrate is shown with the plausible scheme in Figure 4.6. TAgNSs appeared to be immobilized on the quartz substrate, where they were surrounded by the polymer matrix. This observation is supported by a previous fundamental study about solid film generated from a nanoparticle-polymer complex of the solution, even though the complex was dispersed in aqueous solution, not organic solution like in our case [142]. The solid film was finally tested with MeSA in the vapor phase to determine whether the film could efficiently capture the vapor as it was naturally evaporated from its liquid phase depending on its vapor pressure. Four different SERS spectra of the vapor are shown in Figure 4.7. After 4 hours of vapor capture, the case with the highest polymer concentration looked better than the other two cases. The three spectra had similar features, with one unique peak at the 812 cm^{-1} wavenumber region due to out-of-plane deformation of C-H. However, two other peaks at 1032 and 1676 cm^{-1} from in-plane deformation of C-H and stretching of C=O were relatively weak [143]. All three peaks became dominant after overnight collection regardless of the added polymer concentrations, and another small peak was observed at

1620 cm^{-1} from stretching of the phenyl group [143]. Evaporation of a liquid drop of MeSA may take some time to reach a certain vapor pressure, so the amount of volatile produced during 4 hours is likely to be lower than that for overnight. In addition, another study was done to observe how the use of the adsorbent polymer could affect the enhancement of the SERS spectra, and the comparison whether or not to use the adsorbent is shown in Figure 4.8. If only TAgNSs were used as a SERS substrate, no significant peaks from the MeSA VOC were not identified even for overnight collection. However, the addition of the adsorbent layer might be able to improve the VOC collection efficiency, producing three significant MeSA VOC peaks from the overnight collection. Nevertheless, the uniformity of the distance between the polymer surface and the TAgNSs surface may factor into the difference in spectral intensity. If the adsorbed molecule at the surface of the polymer is located far away from the TAgNSs (Figure 4.6, red double arrow), the SERS intensity from the molecule may be weaker than from a molecule near the TAgNSs (Figure 4.6, white double arrow) due to decreased light penetration [34, 144]. Thus, uniformity should be improved to intensify the SERS signal. Nevertheless, detecting MeSA in the vapor phase by using simple complexes between TAgNSs and adsorbent is notable, and multiplex detection of VOCs warrants further study.

4.5. Conclusion

Spherical aggregates of single nanoparticles were successfully transferred from aqueous phase to a non-aqueous phase by electrostatic interaction induced by TOAB surfactants. The key idea is to use an aggregate covered by surfactants with enlarged

surface area, a useful concept for the phase transfer of large nanoparticles in many applications. The transferred AgNSs were well-mixed with polymer adsorbent, and the complex between the AgNSs and polymer adsorbent were successfully used as an ADS-SERS substrate. After static collection of the volatile of MeSA by the substrate, spectra at several wavenumbers could clearly identify the MeSA, and peak intensity at each wavenumber was dramatically increased for overnight collection, suggesting the possibility for quantitative detection of MeSA volatile. The ADS-SERS technique shows promise for a sensor to detect MeSA volatile, and other VOCs in food and agriculture should be tested in the near future.

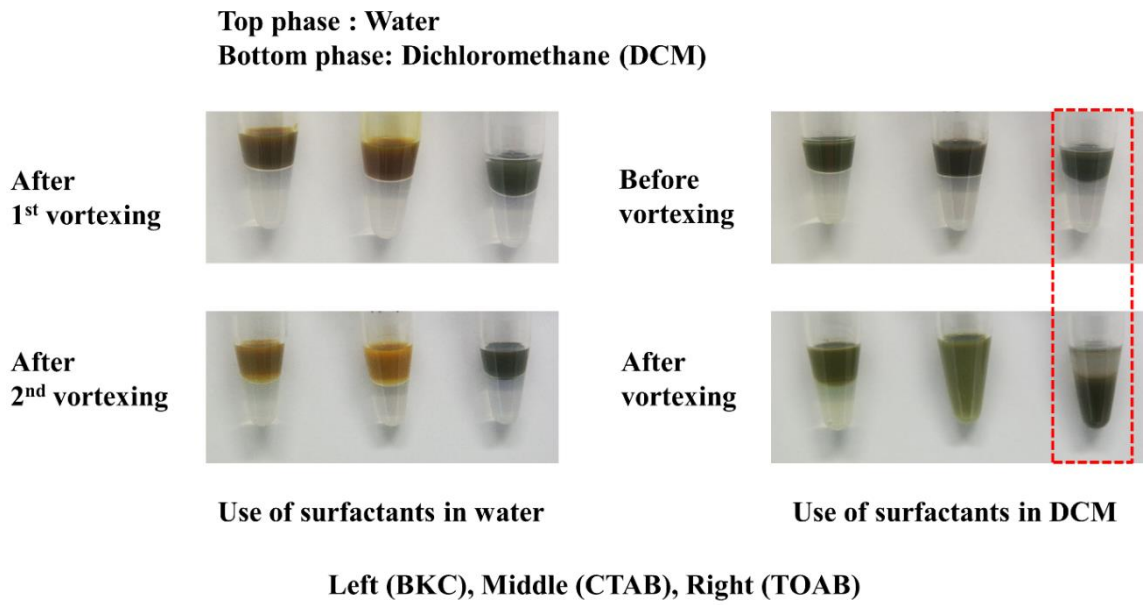

Figure 4.1 Phase transfer of AgNSs from water to dichloromethane by different cationic surfactants

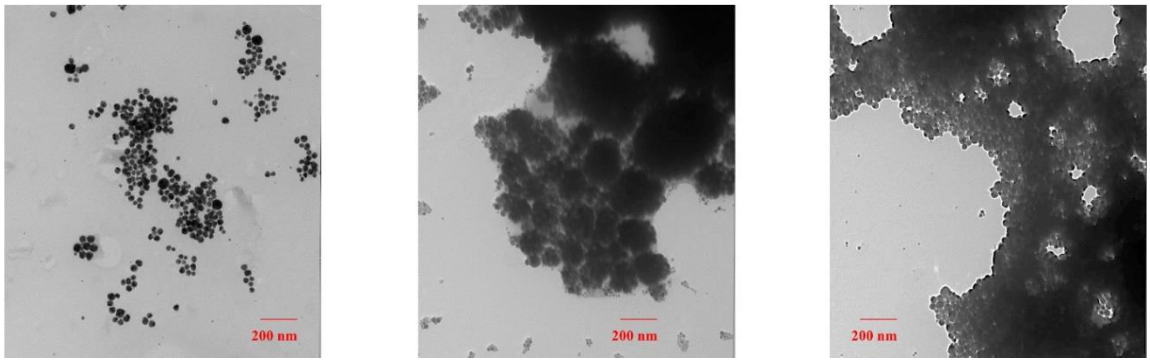

Figure 4.2 TEM images of AgNCs and AgNSs before/after phase transfer (Left: AgNCs, Middle: AgNSs before phase transfer, Right: AgNSs after phase transfer)

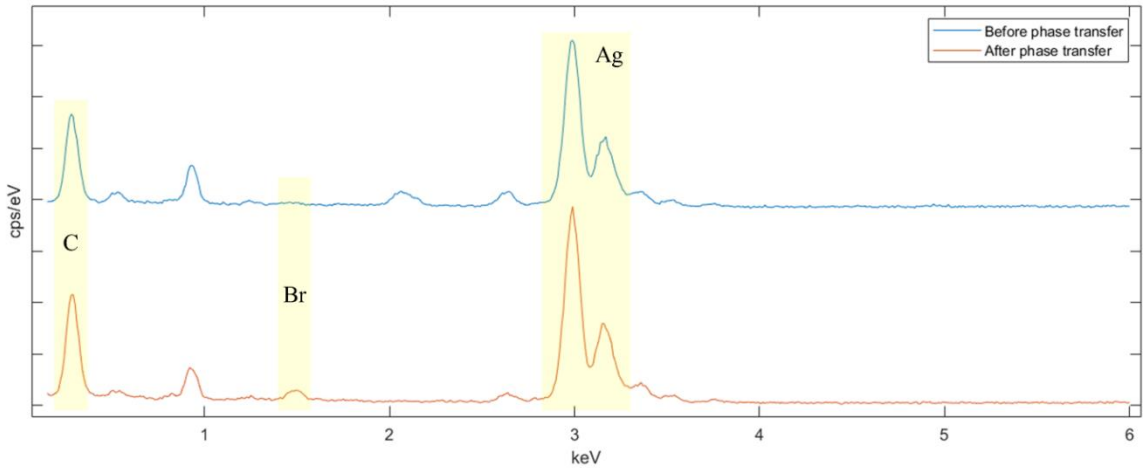

Figure 4.3 EDS spectra of AgNSs before/after phase transfer

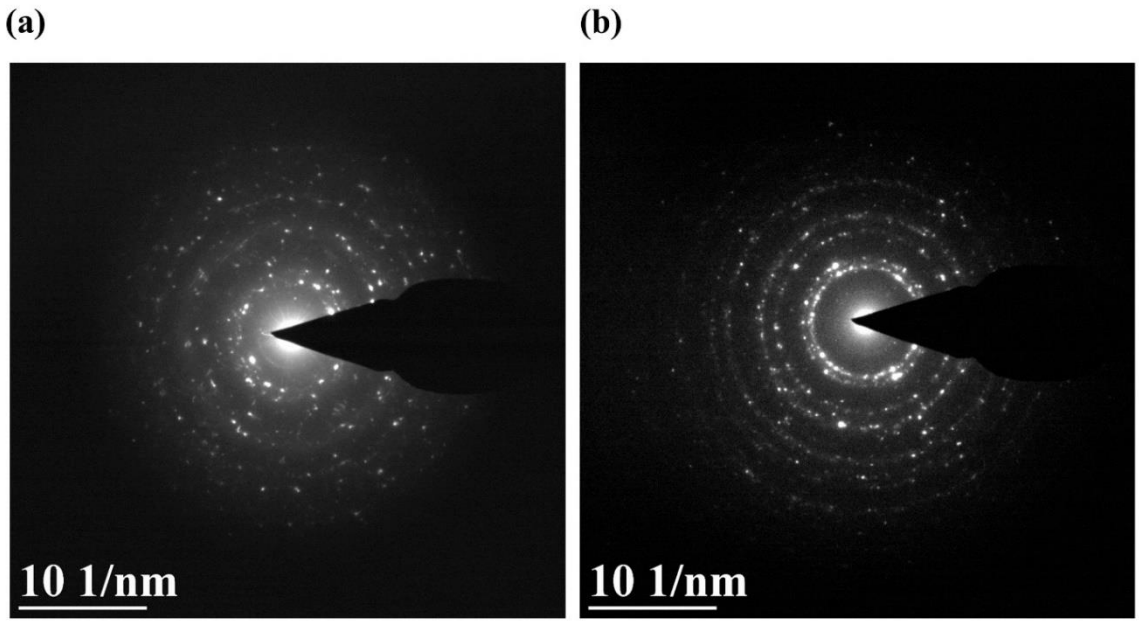

Figure 4.4 Crystal diffraction pattern of AgNSs (a) before phase transfer (b) after phase transfer

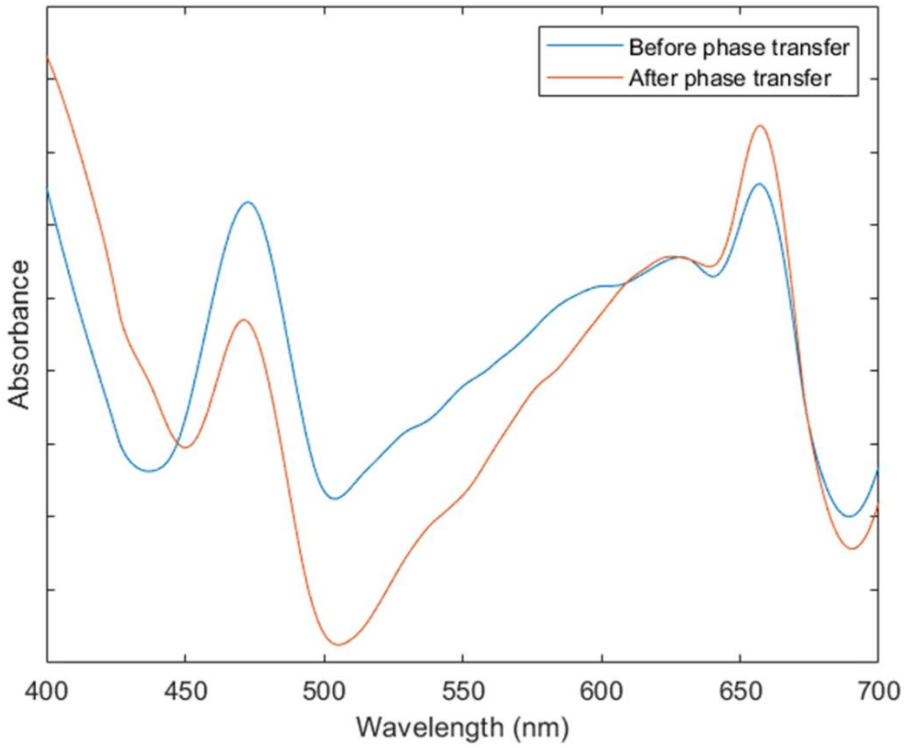

Figure 4.5 UV/Vis absorption spectrum of AgNSs before/after phase transfer

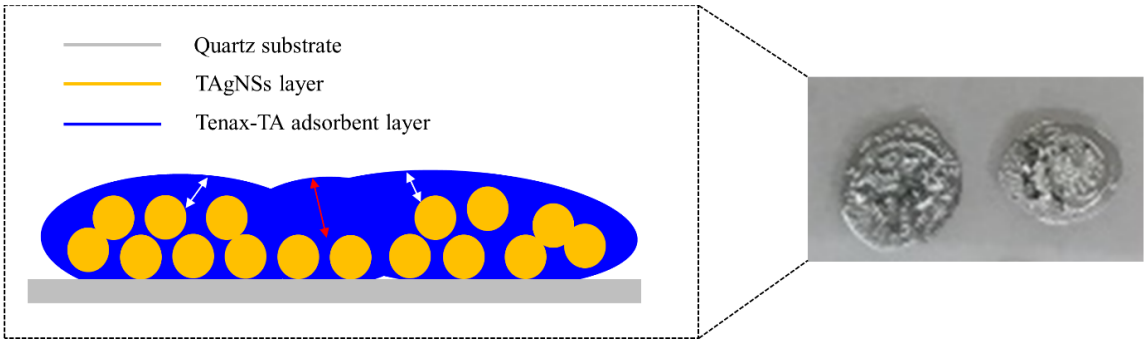

Figure 4.6 Scheme of TAgNSs-polymer complex-based SERS substrate

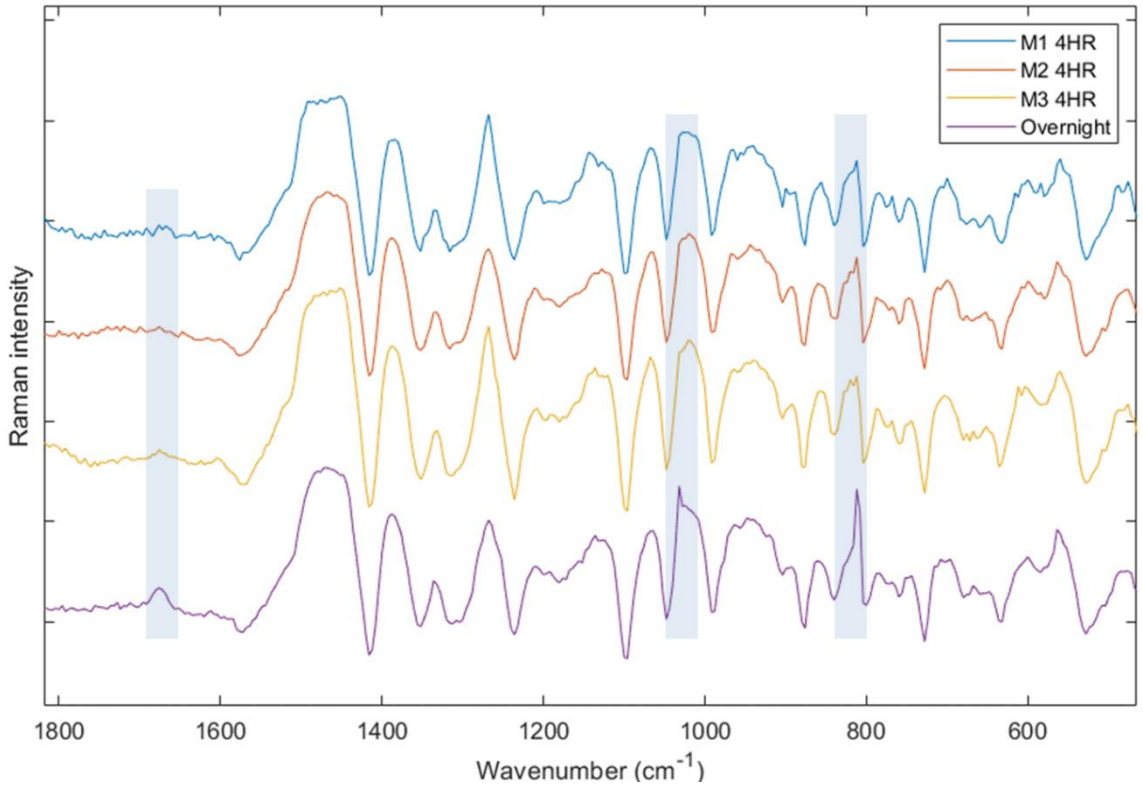

Figure 4.7 SERS spectra of MeSA VOC according to the collection times (M1 4HR: Mixture with 1 mg polymer for 4 hours, M2 4HR: Mixture with 2 mg polymer for 4 hours, M3 4HR: Mixture with 3 mg polymer for 4 hours, Overnight: Averaged over three concentrations for overnight)

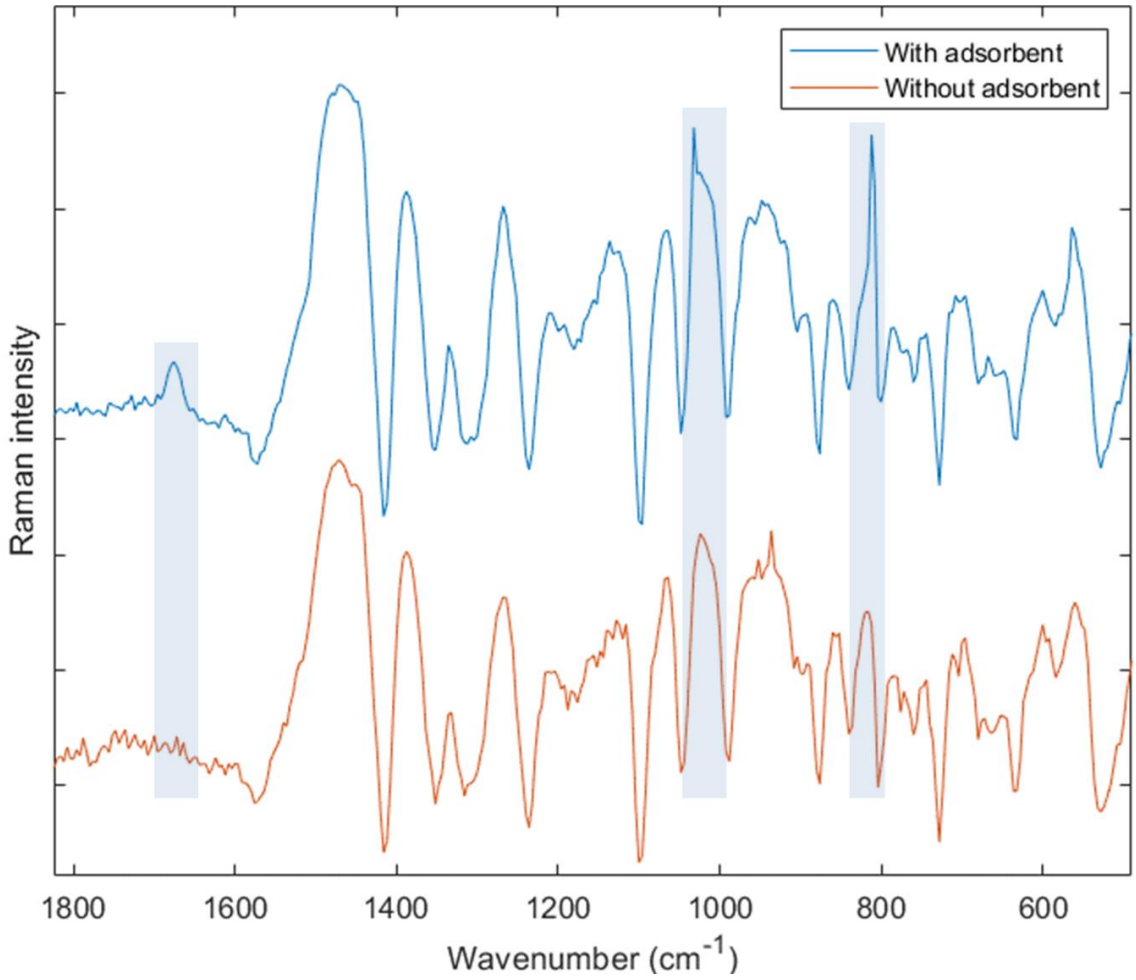

Figure 4.8 The effect of adsorbent on SERS spectra of MeSA VOC

5. ADSORBENT-SERS TECHNIQUE FOR DETERMINATION OF PLANT VOCS FROM LIVE COTTON PLANTS AND DRIED TEAS

5.1. Abstract

We developed a novel substrate for the collection of volatile organic compounds emitted from either living or dried plant material to be analyzed by surface-enhanced Raman spectroscopy. We demonstrated that this substrate can be utilized to differentiate emissions from blends of three teas, and to differentiate emissions from healthy cotton plants versus caterpillar-infested cotton plants. The substrate we developed can adsorb volatiles in static headspace sampling environments, and differences in volatile profiles were confirmed with collections on Super-Q resin for dynamic headspace and solid-phase micro-extraction for static head-space sampling followed by gas chromatography to mass spectrometry. Our results indicate that both qualitative and quantitative differences can be detected by surface-enhanced Raman spectroscopy of our substrate although we find the detection of quantitative differences could be improved.

5.2. Introduction

Volatile organic compounds (VOCs) are odorant compounds emitted from plant tissues. VOCs are responsible for the distinct aroma of certain dried plants, including tea, Camellia sinensis. As such, VOCs can be used as an indicator of tea quality [145-146]. In addition, the VOCs emitted from live plants have an important ecological role by attracting predators to insect herbivores feeding on the plant [147]. Cotton (Gossypium hirsutum) is an important crop for fiber production, but its productivity has been

significantly affected by major pests: cotton aphid (*Aphis gossypii*), cotton bollworm (*Helicoverpa armigera*), beet armyworm (*Spodoptera exigua*) and stink bug (*Nezara viridula*) [148-149]. Herbivore-induced cotton volatiles can be utilized as a reliable indicator to tell whether a plant is being infested by the insect [74].

A popular contemporary method for analyzing VOCs is gas chromatography/mass spectrometry (GC/MS). VOC collection methods such as indirect extraction by solid-phase micro-extraction (SPME) fiber in static headspace [11, 150], purge and trap dynamic sampling involving drawing headspace air through a column packed with different adsorbent resins [11], or direct extraction by distillation [150] are required prior to GC/MS analysis. For tea aroma analysis, black, green, white, oolong, and pu-erh teas can be analyzed for quality by their VOC emissions. SPME is the most widely used technique for the analysis of the VOCs from tea samples [151-155], but dynamic headspace sampling [156] and distillation [157-159] are also used. Cotton plant VOC emissions induced by insect herbivores are typically analyzed by dynamic headspace sampling with different adsorbents [52, 160-162], but SPME has also been used [163]. Regardless of the extraction method, the VOCs needs to be analyzed by the GC/MS and this is generally very time-consuming process, requiring at least half an hour to complete just one analysis.

To overcome the lack of the rapidity of the GC/MS, electronic nose (e-nose) sensors have been developed [164-165]. For the analysis of tea aroma, dynamic sampling methods were coupled to the e-nose sensor. The FOX 4000 from Alpha-MOS was applied to different tea infusions (green, black and oolong) to evaluate its performance

on the discrimination of the grade level [166-167], and the EOS835 from Sacmi Imola s.c.a.r.l. was also tested with green tea infusions to classify green tea samples with different storage periods [168]. Additionally, the PEN from AIRSENSE Analytics was selected as a sensor to investigate tea aroma profile difference between tea infusion and tea leaves [169], and to discriminate green tea samples with different grades directly from tea leaves [170]. Likewise, a hand-held e-nose system was fabricated for black tea aroma detection [171] based on optimized selection of four commercial tin-oxide based MOS sensors, and the Pd doped SnO2 film deposited on an interdigitated Au electrode was studied to evaluate its functionality for linalool tea aroma sensing [172].

As for e-nose applications in cotton, the Cyranose 320 has been used to analyze stink bug damaged cotton bolls or stink bug itself [173-175]. In addition to using the commercial sensor, a low-cost portable e-nose sensor was designed by optimizing carbon black-polymer composites to detect the VOCs released from stink bug damaged cotton bolls [23]. Although the e-nose has reasonable sensitivity for VOC detection with good rapidity, it requires additional training specific to the application before analysis, and cannot always detect individual compounds.

Given the shortcomings of the two methods mentioned above, surface-enhanced Raman spectroscopy (SERS) can be great platform to analyze VOCs due to its specificity, rapidity, and sensitivity. Although there have apparently been no studies for the determination of VOC emissions from live plants by the SERS technique, a few studies investigated whether it can discriminate different tea samples based on unique spectral information. In these studies, each tea infusion was vigorously mixed with Ag-

nanoparticles or drop-casted on commercial SERS substrate [176-177]. However, those methods are not applicable to the analysis of VOCs emitted from live plants. Therefore, a detection system that can act as pre-concentrator and SERS substrate at the same time is herein proposed and investigated for the analysis of VOCs from dried teas and live cotton plants.

Metal–organic frameworks (MOFs) have been widely studied for capturing VOCs, and some studies integrated MOFs with SERS for the direct detection of VOCs. One MOF, zeolitic imidazolate framework (ZIF), was grown on the surface of SERS substrate for the pre-concentration of a wide range of toxic VOCs, and the detection of the VOCs including benzene and toluene was successfully achieved at the ppm level [178-179]. However, whether the film can be effective for collection of VOCs released from live plants has not been determined. Tenax-TA, 2,6-diphenyl-p-phenylene oxide porous polymer, has been widely applied to studies in which VOCs from botanicals and food needed to be effectively collected as one of the adsorbents in dynamic sampling [180-181], and it is easily dissolved in organic solvent, enhancing its processability as a film from the dissolved polymer solution [182].

In this study, a unique SERS substrate, Tenax-TA deposited on a layer of Ag-nanospheres (AgNSs), was developed and tested. The three objectives were to evaluate SERS spectra for multiplex detection of VOCs given off by three different groups of sources: authenticated VOC standards, three different tea samples, and cotton plants infested by beet armyworm caterpillars.

5.3. Material and methods

5.3.1. Material description

VOC standards including linalool, cis-3-hexen-ol and methyl salicylate and Tenax-TA (60/80 mesh) adsorbent were purchased from Sigma Aldrich.

5.3.2. Adsorbent coated SERS substrate

The fabrication of adsorbent coated SERS (ADS-SERS) substrate was composed of three steps: (1) the fabrication of water-dispersible AgNSs (WAgNSs) [116-117], (2) phase transfer of the AgNSs to organic solvent, and (3) adsorbent polymer deposition on the transferred AgNSs (TAgNSs) film. The phase transfer of the AgNSs was performed with some modifications to our previous methodology [133], and the fabrication of ADS-SERS substrate will be introduced here. For the fabrication of AgNSs, 0.5 g AgNO3, 10 mL deionized (DI) water, 0.8 g sodium oleate, 1 mL oleic acid and 5 mL ethanol were mixed together in a glass vial under agitation. The vial was sealed and heated overnight at 150 ℃. A layer of Ag-nanocrystal formed at the bottom of the vial, 80 mg of which was dissolved in 20 mL of cyclohexane. 560 mg of sodium dodecyl sulfate was dissolved in 100 mL of DI water, and the two solutions were mixed together. The AgNSs were finally prepared by sonicating the mixture for 1 hour and heating it at 70 ℃ until the cyclohexane was almost completely evaporated. For the phase transfer of the AgNSs, tetraoctylammonium bromide cationic surfactant solution was prepared by dissolving it in 0.14 M dichloromethane, and 100 µl of the surfactant solution was mixed with 100 µl of the AgNSs solution. Then, the mixture was vortexed for 1 min and the TAgNSs concentrated by centrifugation and re-dispersion with dichloromethane. For the

fabrication of ADS-SERS substrate, Tenax-TA polymer was dissolved in dichloromethane (10mg/ml) for the adsorbent solution, and a 5µl volume of the TAgNSs solution was first drop-casted on the cleaned quartz substrate and fully dried. Thereafter, 5µl of the adsorbent solution was also deposited on the spot where the TAgNSs were first coated and again fully dried.

5.3.3. **Cotton and caterpillar herbivory**

Cotton seeds (Phytogen 367) were planted in 8.5 x 8.5 x 8.5 cm plastic pots filled with store-bought potting soil (SunGro Metro Mix 900) and arranged in trays. We added water to the trays as needed by the plants and fertilized plants biweekly with Botanicare CNS17 at a rate of 10 mL fertilizer per liter of water. Plants were reared in Percival environmental chambers on 14:10 h light:dark cycle at 29°:25°C until the seventh true leaf was fully expanded and the first square (flower bud) was developing. We wrapped the pots in aluminum foil pressed closed around the base of the plant stalk to minimize the emissions of soil-borne volatiles in close proximity to the SERS substrate. On the outside of the foil we incorporated a plastic mesh to facilitate the caterpillars' crawling back up to the leaves after falling, which they often did at the beginning of the experiment when being placed on the plants.

The insects, Spodoptera exigua larvae, were purchased as eggs from Benzon Research and reared on artificial diet for Helicoverpa zea purchased from Southland Products Incorporated, and supplemented with 7 mL raw linseed oil per batch of diet. Insect rearing conditions were light:dark for 14:10 h at 28°:25°C. Insects were reared until the 3rd instar on artificial diet and then transferred into glass petri dishes with

excised leaves of conventional (non-genetically modified) cotton. They were allowed to feed on the conventional cotton leaves for at least 24 hours before being used in experiments. This acclimated the larvae to feeding on plant material so that they would readily accept the leaves as food during the experiments.

5.3.4. VOCs collection by ADS-SERS substrate

The prepared ADS-SERS substrate was finally used for the pre-concentration of VOCs from various sources in the static headspace sampling set-up (Figure C 1), and the size of the chamber varied depending on what kinds of samples were prepared as VOC sources.

5.3.4.1. VOCs standards

Three 5 µl droplets of linalool, cis-3-hexen-1-ol and methyl salicylate were dispensed in a 120 ml jar. The ADS-SERS substrate was situated against the wall of the jar facing the three droplets (Figure C 1-(a)). Three trials were performed with collection times of 1hr, 3hrs, and overnight. As a control, one substrate was kept inside an empty jar. All were replicated 4 times.

5.3.4.2. Tea aroma

10 g of each tea sample was placed inside a 120 mL glass for 3 hours as well as for overnight, and the ADS-SERS substrate was also located against the wall of the glass facing the tea sample (Figure C 1-(b)). These experiments were replicated 4 times.

5.3.4.3. Cotton VOCs

A single plant was placed inside a chamber. We fashioned a stand out of metal wire which hung off the side of the pot and held the ADS-SERS substrate (Figure C 1-

(c)). The substrate was held with the narrow edge vertical so that droppings from the caterpillars would not land on the substrate and contaminate the sample. Experimental conditions were the same as rearing conditions other than the fact that the plants were inside glass chambers with static headspace for the experiments. Using soft forceps, we placed 5 total 3rd and 4th instar larvae in one experimental chamber, the other chamber was herbivore-free, and both chambers were then sealed. The experiments took place over 48 hours with the plants being enclosed and removed midday. This experiment was replicated 3 times.

5.3.5. **VOCs collection by commercial adsorbent**

5.3.5.1. Dynamic sampling for tea aroma

10g of each tea sample was placed inside a 120 mL glass jar capped with a Teflon lid. Each glass jar was connected to two glass columns (178 mm length x 6 mm O.D.; Supelco, Bellafonte, PA) filled with a 5-cm bed of Hayesep Q resin (80/100 Mesh; Hayes Separations, Inc., Bandera, TX): one column was for dynamic VOC collection, and the other was for cleaning the air entering the jar. The VOC dynamic collection was performed with a diaphragm pump (Thomas Scientific, USA) at a rate of 1 liter/min for 1 hour.

5.3.5.2. Static sampling for cotton VOCs

PDMS/DVB/Carbowax 50/30 µm coating SPME fibers by Supelco (Millipore-Sigma, St. Louis, MO) were exposed to the static headspace of the chamber during the final 30 minutes of the experiment (Figure C 1-(c)).

5.3.6. **Equipment used**

5.3.6.1. Adsorbent-GC/MS

The VOCs collected dynamically were eluted from the resin with 500µl dichloromethane and analyzed by a Shimadzu GCMS-QP2010 Ultra (Shimadzu Scientific Instruments (Oceania) Pty Ltd, Henderson, New Zealand). We used the Zebron ZB-WAXplus capillary GC column from Phenomenex, which is 30 m in length with an internal diameter of 0.25 mm and a film thickness of 0.25 µm. The temperature at the injection port with a flow rate of 1.5 mL/min was 250°C, and a 1µL eluate was injected with a split ratio of 1. Oven temperature program initiated at 40°C held for 3 min, increased 240°C at 5 °C/min and held for 3 min, then increased to 250°C at 40°/min to purge the column.

Manual injections with the SPME fibers were performed with a hollow-bore splitless injection port and a desorption time of 2 min at 230°C with total injection port air flow at 1.5 mL/min. The oven temperature program was initiated at 60°C and held for 2 min, increased to 180°C at 4°/min, then increased to 250°C at 50°/min and held for 4 minutes to purge the column. Identification of VOCs was based on the comparison of retention times to authentic standards and mass spectra stored in the National Institute of Standards and Technology (NIST) and Wiley Registry (10th edition).

5.3.6.2. Raman spectroscopy

All ADS-SERS substrates were analyzed by Raman spectroscopy (RamanStation 400 F, Perkin-Elmer, Beaconsfield, Buckinghamshire, UK) with a 256 × 1024 pixel CCD detector and a 785nm near-infrared laser with 175 mW power. They were placed

on the stage of the Raman spectrometer, and a spectrum was collected with 2 s exposure time at the spectral resolution of 4 cm^{-1} in the Raman shift range of 200 to 2,000 cm^{-1}. The spectra were finally compared to the VOCs identified by GC/MS using commercial Raman libraries (KnowItAll Informatics System 2018, Bio-Rad Laboratories, Inc., USA).

5.3.6.3. Transmission electron microscope (TEM)

A few µl of the TAgNSs were sampled to the grid and perfectly dried. The finally dried sample on the grid was analyzed in a JEOL 1200 EX transmission electron microscope (TEM) operated at an acceleration voltage of 100 kV, and morphological images was captured with a 3k slow-scan CCD camera (model 15C, SIA).

5.3.6.4. UV/Vis spectroscopy

A 100 µl of the TAgNSs were sampled inside a quartz cuvette, and UV/Vis-NIR spectra were collected with a Hitachi U-4100 spectrophotometer.

5.3.7. Statistical analysis

5.3.7.1. Descriptive statistics

For GC/MS data, the peak area for each identified VOC was calculated with Shimadzu GCMSsolution (version 2.7) package software. Relative abundance of the VOCs was calculated by dividing the integration of an individual by the total integrated values for the chromatogram.

For Raman data, all spectral information was exported from The Spectrum (v. 6.3) software, and the data were preprocessed by baseline correction and normalization

with the bioinformatics toolbox of MATLAB. The processed data were finally averaged out from all replicated data.

5.3.7.2. Multivariate analysis

Optimal sets of wavenumber variables were selected for the Raman data based on the identified peaks associated with the three VOCs. Principal component analysis (PCA) was performed in JMP 13 Pro (SAS Institute Inc.) with the selected variables. Finally, the first two principal components were plotted to determine whether the replicates could be clustered according to collection time.

To determine tea variety, specific wavenumbers were chosen as a final variable set from the identified peaks induced by the aromas of three teas. PCA was also applied to the Raman tea data with this variable set. The first two principal components were again plotted to determine how the replicates from the three tea samples could be clustered. In addition, linear discriminant analysis (LDA) was applied in R software to the same data set to create an LDA classification model that can predict which tea variety each data point belongs to. Model accuracy was evaluated by 4-fold cross-validation with custom R code that divided all the data into four groups, and each group included three data points randomly selected from each tea sample.

To detect caterpillar infestation on cotton, variable optimization was again done by selecting wavenumbers associated with cotton VOCs, and PCA was run with the selected data set. The first two principal components were again plotted to determine whether the replicates from the infested and non-infested cotton samples could be clustered.

5.4. Results and discussion

5.4.1. **Fabrication of ADS-SERS substrate**

A TEM image (Figure 5.1-(a)) shows that TAgNSs about 100 nm in diameter were formed from many Ag-nanocrystals less than 10 nm diameter, and they had an adsorption peak around 450 nm (Figure 5.1-(b)), making them suitable as a SERS substrate.

A unique feature in our developed SERS substrate was the combination of the adsorbent polymer layer for VOC pre-concentration with the SERS layer (Figure 5.1-(c)). When the TAgNSs were used as the material for the first layer, the adsorbent layer was very well formed on the TAgNSs layer due to hydrophobic interaction between the phenyl group of the adsorbent polymer and the hydrocarbon tail of the added surfactant on the surface of the TAgNSs.

When the TAgNSs based substrate was compared with the WAgNSs based substrate, polymer solution contact angle on the solid film and quality of adhesion were different between them. In case of WAgNSs, the polymer solution contact angle was higher, and adhesion quality was poor. With TAgNSs, the adsorbent polymer layer was uniformly formed in a relatively larger area of the film, and great adhesion was observed, possibly due to substantial work of adhesion from hydrophobic interactions [183-184]. The differences are related to interfacial phenomena between TAgNSs solid film and adsorbent polymer in liquid, and can also be explained by two well-known equations regarding interfacial energy [185].

$$\cos\theta = -1 + \frac{2\sqrt{\gamma_s^d \gamma_l^d}}{\gamma_l} + \frac{2\sqrt{\gamma_s^p \gamma_l^p}}{\gamma_l} \quad \text{(Equation 6)}$$

$$W_a = 2\left(\sqrt{\gamma_s^d \gamma_l^d} + \sqrt{\gamma_s^p \gamma_l^p}\right) \quad \text{(Equation 7)}$$

θ: contact angle (°), W_a: work of adhesion, γ: surface energy (J/m^2), d: non-polar dispersion part, p: polar part, s: AgNSs solid film, l: polymer in liquid

From these equations, both contact angle and work of adhesion between two surfaces could be determined by non-polar and polar molecular interaction, and the polar term can be ignored in our case due to the strongly non-polar property of polymer. Therefore, only the non-polar dispersion term needs to be considered, and TAgNSs with a higher non-polar portion than WAgNSs can result in larger surface energy in the non-polar term, which eventually causes larger values of $\cos\theta$ (small contact angle) and W_a.

5.4.2. **Determination of VOC standards**

The SERS spectrum from each VOC adsorbed on the polymer was compared according to the collection times in Figure 5.2 (a-c), and notably, the multiplex detection of three VOCs could be achieved even at 3 hours collection time.

The identified wavenumbers are summarized in Table 5-1, and the spectra from both linalool and methyl salicylate were more pronounced than cis-3-hexen-1-ol. The vapor from three droplets of VOC standards was generated by their vapor pressures at 25 ℃ and could be assumed to reach saturation at a certain time. Based on the ideal gas law, the maximum concentration for each volatile could be approximated (supplementary 1), and the actual concentration should be lower than maximum until the vapor becomes saturated. This idea is supported by the fact that the peak intensity for the

identified wavenumbers was more pronounced as collection time increased, and the maximum could be reached after overnight saturation. Quantitative differences between collection times were confirmed by PCA (Figure 5.2-(d)), and all replicates from the 1-hour collection were clearly separated from those from 3-hours and overnight collection. In addition, the data for 3-hours were closely located to those for overnight, showing that most of the VOCs could be saturated within 3 hours, and they could be effectively pre-concentrated on the ADS-SERS substrate.

The maximum concentration for methyl salicylate was the lowest among the three compounds (Table C 1). However, many wavenumber peaks induced by methyl salicylate were observable in the SERS spectra. This fact could be explained in that Tenax-TA adsorbent was more effective for the pre-concentration of the VOCs with lower polarity and higher boiling point [186-187]. Although cis-3-hexen-1-ol or linalool was first attached on the adsorbent, they may have been displaced by methyl salicylate due to its phenyl group having higher affinity to the adsorbent. A few studies have developed a sensor to identify the VOCs used in our experiment, but they focused on a single VOC rather than combined detection of multiple VOCs. For instance, a quartz crystal microbalance (QCM) sensor coated with an adsorbent layer such as Polyethylene glycol (PEG) or maltodextrin (MDEX) was proposed to identify the linalool or methyl salicylate from black tea [188-189]. However, this type of sensor could not detect two VOCs simultaneously. In addition, the SERS technique in which the AgNPs were modified with a specific linkage molecule was specifically designed only for the detection of

methyl salicylate [190]. However, it was tested with the methyl salicylate in liquid phase, not gas phase, and might not be effective for molecules other than methyl salicylate.

5.4.3. **Determination of tea aroma**

Major compounds identified through GC/MS analysis of tea were qualitatively different for each sample (Table 5-2**)**. Easily noticeable is a higher proportion of phthalate ester in the black tea sample, a compound known as a carcinogenic material that can directly affect human health. Other reports have detected phthalate ester in tea samples contaminated by environmental sources or plastic [191-192], so our finding could be a result of contamination in the black tea samples. Many different terpenes were detected from the earl grey tea samples; both linalool and linalool oxides are important terpene derivatives that can contribute to tea flavor and aroma [145-146]. Lastly, several VOCs including acetoin and butyric acid were identified from rooibos tea samples, and they also have been previously reported as volatile components from rooibos tea [193-194].

Raman spectra of the VOCs identified by GC/MS were investigated using commercial libraries, and possible matching with the SERS spectra from each tea (Figure 5.3**)** was summarized (Table 5-1**)**. From the SERS spectra of black tea samples, several intense peaks were observed at three wavenumber regions of 1072, 1452, and 1496 cm^{-1}, and three phthalate esters from black tea may be the main components affecting those peaks. As the commercial libraries of any phthalate ester were not available, an additional function in KnowItAll software aided selection of molecular groups based on the peak locations (Figure C 2). An aromatic component with ortho-disubstituted was suggested as a possible candidate (Figure C 2-(a)), and its Raman

peaks have been identified at regions similar to those from black tea and are associated with several vibrational modes of aromatic ring bending-stretching [143] and C-H in-plane H bending. The general structure of phthalate is that of an ortho-disubstituted aromatic compound, so several phthalate esters from black tea may strongly affect those three wavenumbers. A previous article regarding the detection of the phthalate ester in plastics by Raman showed that two characteristic peaks were found at 1450 and 1040 cm-$^{-1}$, which could support our result [195]. The other two intense peaks were also shown at the wavenumbers of 1144, and 1268 cm^{-1}, and any secondary or tertiary alcohol that can result in two wavenumber regions by C-O-H deformation and C-C-O stretching were suggested in Figure C 2-(b). Therefore, two alcohols in Table 5-1, 2-Hydroxyisobutyric acid for tertiary and 3-Penten-2-ol for secondary, might be also possible VOCs affecting those two wavenumbers. A strong and broad peak was found in the SERS spectra from earl grey tea at the 1620 cm^{-1} wavenumber, and it is associated with the mode of bending-stretching by the aromatic ring of *p*-cymene [95]**.** Two small peaks between 900 and 800 cm^{-1} corresponded to the spectra from *p*-cymene and β-pinene. In the case of rooibos tea, no significant peak was observed relative to the other two teas, but two small peaks were found at 768 cm^{-1} corresponding to acetoin and 856 cm^{-1} related to butyric acid.

Two multivariate analyses with the identified wavenumbers showed great discrimination among the three tea samples (Figure 5.4). From the data for 3 hours collection, one replicate for black tea did not separate well from rooibos, but all the data points were clearly separated for each tea after overnight collection due to increased

intensities at the identified wavenumbers. In addition to PCA, the classification accuracy for the LDA model is summarized in Table 5-3, averaged from ten replicates. The overnight experiment provided nearly perfect classification (98 % accuracy), while the 3 hours experiment resulted in 80% accuracy.

5.4.4. **Determination of caterpillar-induced cotton VOCs**

The SPME collections from healthy and infested cotton plants revealed qualitative differences in the relative abundance of VOCs (Figure 5.5**)**. Caryophyllene, Z-3-hexenyl acetate, humulene, and sabinene were detected in emissions from caterpillar-infested plants but not from healthy plants. The composition of VOCs emitted was dominated by α-pinene, with that compound representing >70% of the blend from healthy plants and >40% of the blend from infested plants. Phellandrene and DMNT (3,8-dimethyl-1,4,7-nonatriene) were more represented in the emissions of caterpillar infested plants.

Some wavenumber regions (Figure 5.6 (a-b)) that could differentiate between healthy and infested cotton plants were identified, and most of them were located between 1750 and 1550 cm^{-1}. First, 1620 cm^{-1} was clearly identified only in infested cotton, but the specific VOC responsible was not determined. A possible VOC affecting the peak at that wavenumber is caryophyllene, with a characteristic peak at 1630 cm^{-1}. The peak shift of more than 10 cm^{-1} can be explained by geometric orientation of the adsorbed molecule to the surface of the SERS substrate[196]. Second, two other peaks were also shown at 1744 and 1584 cm^{-1} only in the infested case, and these fairly closely correspond to the main characteristic peak of Z-3-hexenyl acetate and phellandrene,

respectively. Third, a peak at 1604 cm^{-1} was detected in healthy and infested cotton, so a shared compound could be responsible, possibly ocimene, with a weak band at that wavenumber. Lastly, two other peaks were also observed at 828 and 672 cm^{-1} only in the infested case, and they may be associated with the vibrational property caused by α-pinene. Although the peak intensities for all the identified VOCs that could differentiate between the two treatments were not high, the PCA plot in Figure 5.6-(c) showed clear discrimination, such that all the replicates from healthy cotton were located along the negative component 1 axis, but those from infested cotton were located along the positive axis.

5.5. Conclusion

A simple and cost-effective SERS substrate was developed to determine the VOCs given off by dried teas and live cotton plants. Three tests were successfully used to demonstrate this SERS substrate's ability for simultaneous detection of multiple VOCs qualitatively. We also found potential for quantification, because there was a large intensity difference associated with VOC collection times. To the best of our knowledge, our study is the first to report direct SERS sensing of VOCs emitted from either a live plant or a food source. Future studies will include the optimization of the SERS substrate to maximize VOC quantification and its application to other types of samples.

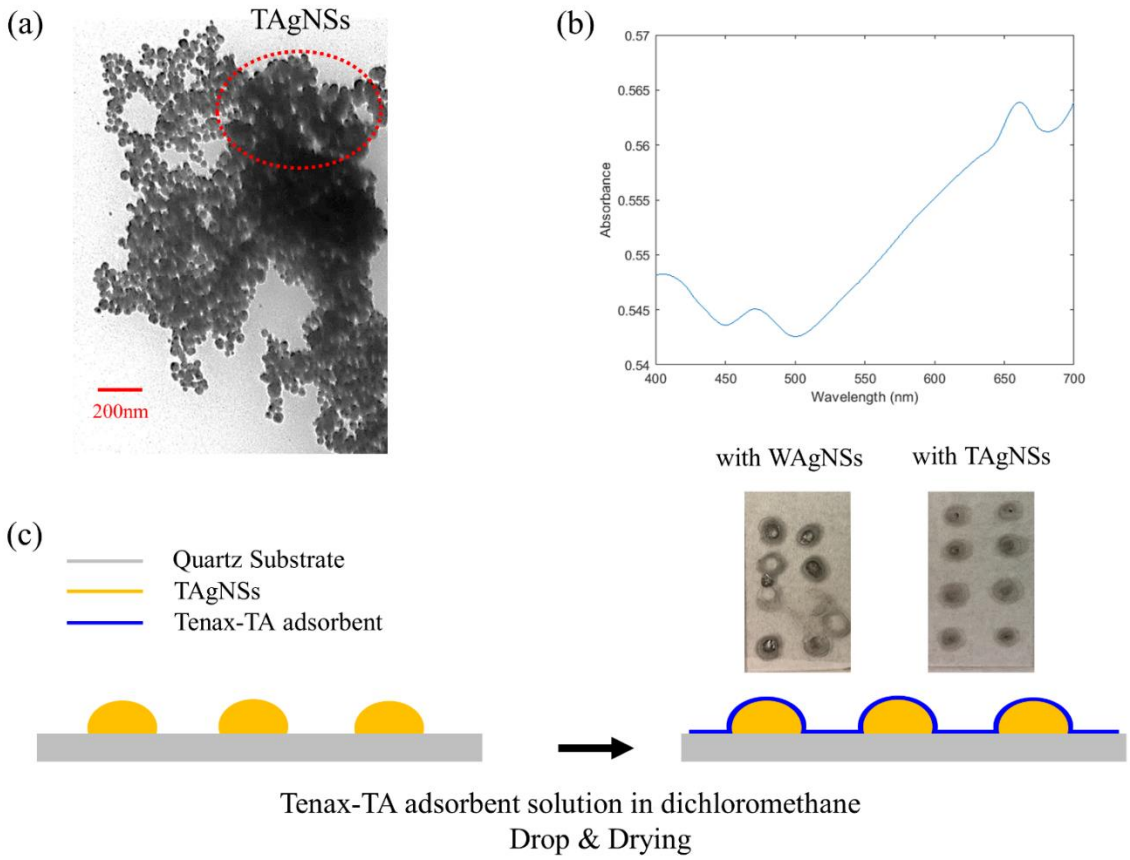

Figure 5.1 (a) TEM image of TAgNSs (b) UV-Vis absorption spectrum of TAgNSs (c) Fabrication of ADS-SERS substrate and comparison between water-dispersible AgNSs (WAgNSs) based substrate and TAgNSs based substrate

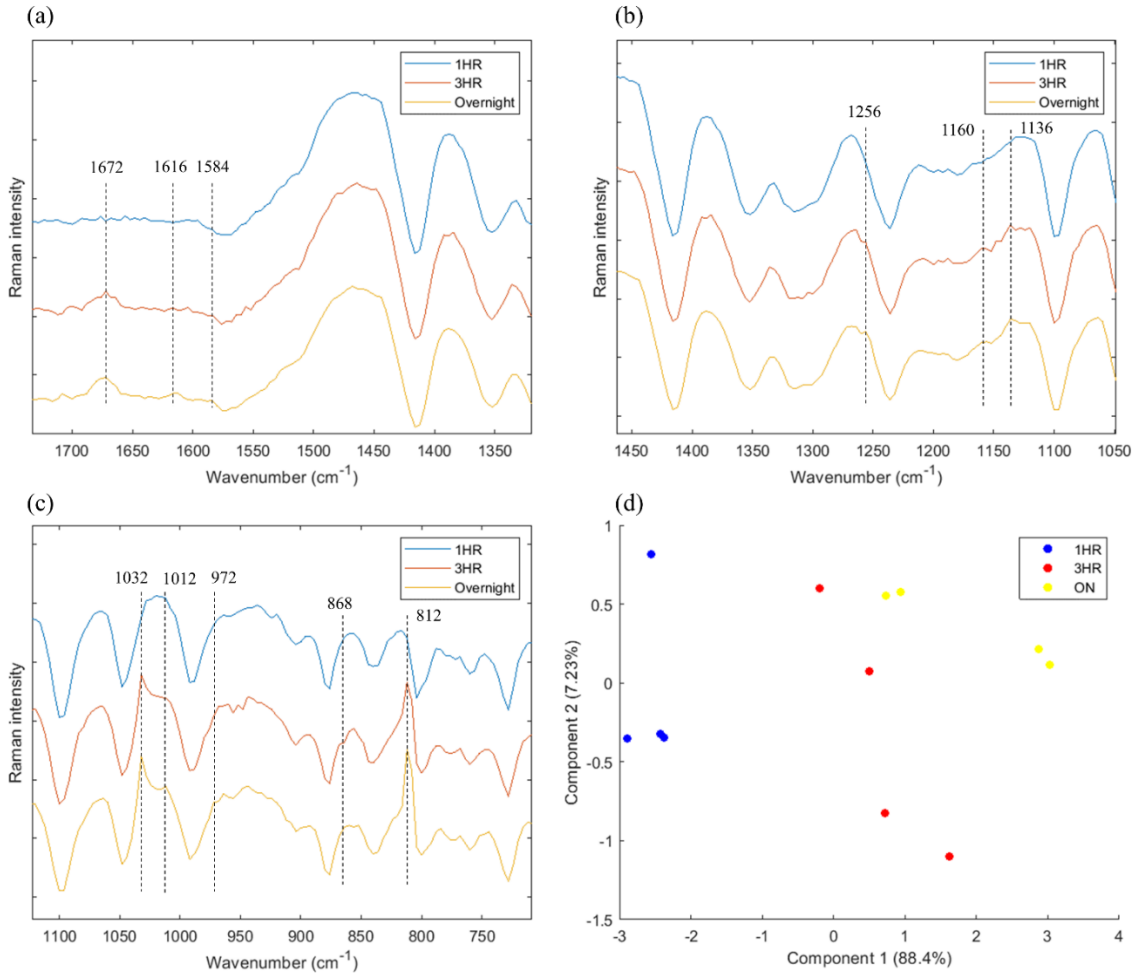

Figure 5.2 (a-c) (a-c) Comparison of SERS spectra from the VOCs evaporated three standards according to the three different collection times (d) PCA plot based on SERS spectra

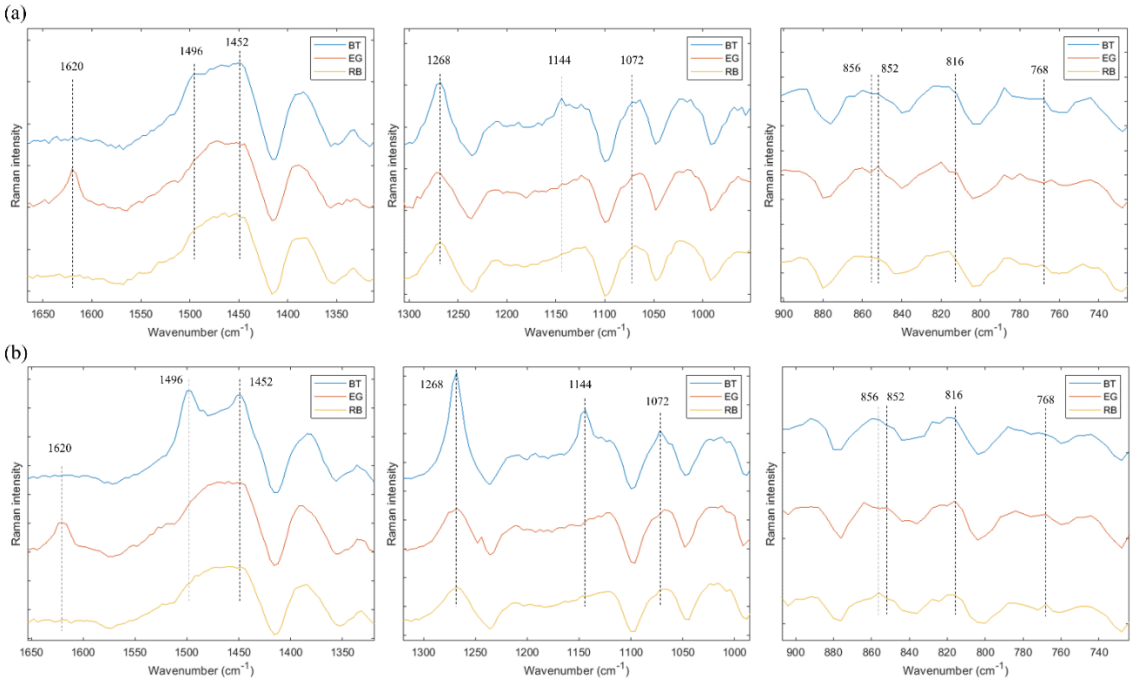

Figure 5.3 (a) Comparison of SERS spectra from three different tea aroma for 3 hours collection (b) Comparison of SERS spectra from three different tea aroma for overnight collection

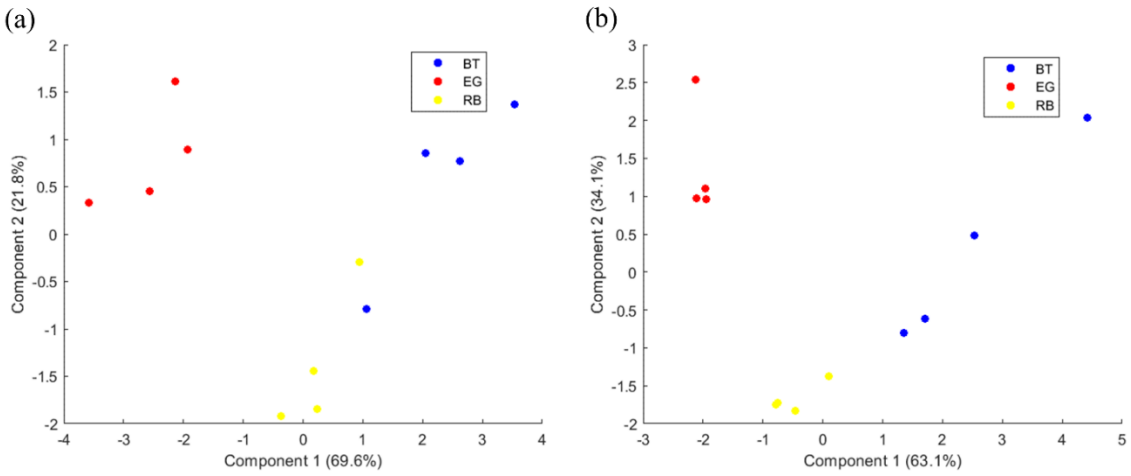

Figure 5.4 (a) PCA plot based on SERS spectra of teas aroma for 3 hours collection (b) PCA plot based on SERS spectra of teas aroma for overnight collection

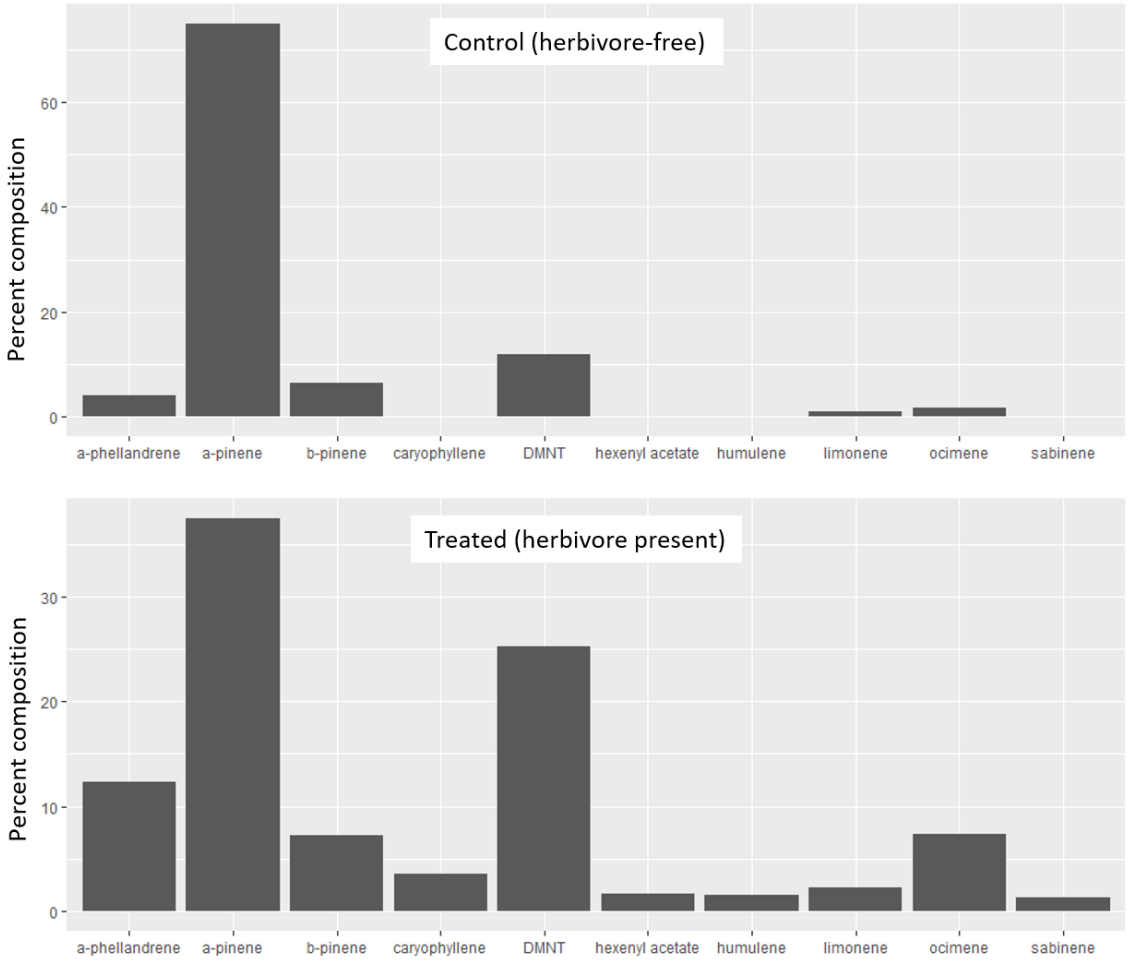

Figure 5.5 Comparison of relative intensity of the identified VOCs by GC/MS between healthy and infested cotton

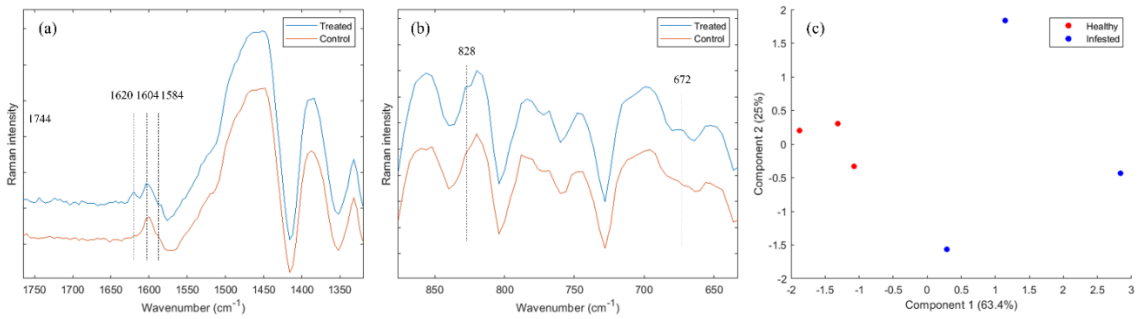

Figure 5.6 (a-b) Comparison of SERS spectra of the VOCs given off from healthy and infested cotton plant (c) PCA plot based on cotton VOCs SERS spectra

Table 5-1 List of the VOCs affecting the SERS spectra
*** Possible molecular group that can affect those wavenumber regions**

Samples	Identified wavenumber (cm^{-1})	VOCs
Three standards	1672	Linalool (1672 cm^{-1})
	868 972 1012	Cis-3-hexen-1-ol (868, 971, 1020 cm^{-1})
	812 1032 1136 1160 1256 1584 1616	Methyl salicylate (810, 1033, 1135, 1158, 1252, 1585, 1615 cm^{-1})
Black tea	1144 1268	Any compound with secondary or tertiary alcohols*
	1072 1452 1496	Any compound with Aromatic component with ortho-disubstituted*
Earl grey	852	β-pinene (852 cm^{-1})
	816 1620	*p*-cymene (818, 1618 cm^{-1})
Rooibos	768	Acetoin (768 cm^{-1})
	856	Butyric acid (863 cm^{-1})
Cotton	672 828	α-pinene (668, 840 cm^{-1})
	1584	Phellandrene (1585 cm^{-1})

Table 5.1 Continued

Samples	Identified wavenumber (cm^{-1})	VOCs
Cotton	1604	Ocimene (1604 cm^{-1})
	1620	Caryophyllene (1630 cm^{-1})
	1744	Z-3-hexenyl acetate (1742 cm^{-1})

Table 5-2 Major VOCs of each tea sample identified by GC/MS

Tea samples	VOCs	Percentage (%)
Black tea	Diethyl phthalate	33.67
	Dimethyl phthalate	4.62
	Diisononyl phthalate	4.08
	2-Hydroxyisobutyric acid	1.60
	3-Penten-2-ol	1.17
Earl grey	Limonene	35.62
	Linalyl acetate	20.25
	L-Linalool	12.58
	β-pinene	6.2
	p-cymene	5.51
Rooibos	Butyric acid	10.54
	Acetoin	7.13
	Isobornyl isovalerate	5.6
	γ-octalactone	5.28
	γ-decanolactone	4.21

Table 5-3 LDA model validation by k-fold cross validation

Black tea vs. Earl grey vs. Rooibos

Different cases	LDA Classification accuracy (%)										Average (%)
3 hours collection	92	92	75	83	83	67	75	75	83	75	80
Overnight collection	100	100	100	100	92	100	100	92	100	100	98

6. CONCLUSIONS AND FUTURE STUDIES

6.1. Conclusions

Damage on crop plants from insect pests causes severe problems worldwide, and early detection of infestations should be addressed to minimize the damage. For this purpose, HIPVs were selected as a phenome to assess insect infestation and were extensively studied to develop a unique technique. Two important crops, sorghum and cotton, were considered as host plants, and two severe pests, SCA and BAW caterpillar, were selected as herbivorous insects to the host plants, respectively.

First, specific blends of HIPVs were analyzed by adsorbent-GC/MS to see how insect herbivores can affect the VOC emission from host plants. One result from the interaction between sorghum and SCA was that the VOC profile had no qualitative difference between healthy and infested sorghum, meaning that same VOCs were identified from both cases. However, only a quantitative difference (difference in VOCs concentration) could be observed. Relative abundance of the VOCs was significantly changed after one-day infestation, and multivariate statistical analysis based on the relative abundance showed good discrimination between healthy and infested plants, suggesting that the relative amount could be used as a useful parameter for the infestation detection. Another result came from the interaction between cotton and BAW caterpillar. This result was different from the previous result in that qualitative VOC differences between healthy and infested cotton were clearly observed. The specifically identified VOCs different between the two cases could be easily utilized as another parameter for estimating the infestation.

Second, based on these results and previous studies by other research groups, four representative HIPVs were selected for our study, and our developed system was tested with the HIPVs to prove system functionality regarding multiplex detection of HIPVs. The system combined VOC collection by adsorbent and Raman spectroscopy, in which VOC eluate from the adsorbent was directly analyzed by Raman spectroscopy. Multivariate statistical analyses of Raman spectra confirmed that the four HIPVs tested could be successfully discriminated even in 20 min dynamic collection, and an HIPV mixture down to ppm level was detected.

However, the limit of detection for the proposed system would not enable detection of plant-emitting VOCs down to ppb level. Therefore, additional studies to enhance the detection limit needed to be addressed, which involved the utilization of TAgNSs for SERS application.

Third, the developed system was upgraded to two ways: 1. Sensitivity improvement by SERS rather than simply standard Raman spectroscopy. 2. Usability improvement by integrating the pre-concentration step with adsorbent into VOC detection. The SERS technique was developed based on TAgNSs in non-aqueous solution that could be phase-transferred from AgNSs in aqueous solution by TOAB surfactant-induced electrostatic interaction. Thus, the TAgNSs could be compatible with organic materials including VOCs and adsorbent polymers. After successful phase transfer, the complexes (ADS-SERS) could be made by hydrophobic interaction between TAgNSs and Tenax-TA adsorbent polymers, and they were finally used as a unique SERS substrate in which HIPVs could be collected on the adsorbent, and the collected

VOCs were measured by SERS at the same time. The upgraded system was also evaluated with the same HIPVs used in the multiplex detection, and detection could be achieved even within a few hours of static collection. As compared with the spectra of the HIPVs by standard Raman, SERS based spectra of the HIPVs was much stronger, and many peaks induced from the HIPVs could be easily identified.

Lastly, the established detection system was applied to plant leaves including dried tea and living plants, and the feasibility of detecting VOCs from agricultural samples was confirmed. To evaluate dried tea, three tea varieties were prepared as VOC sources, and overnight static collection from each tea sample produced unique SERS spectra, making it possible to differentiate each tea variety by multivariate analysis. To investigate a living plant, the cotton and BAW caterpillar that resulted in qualitative HIPV differences were used again, and the identified HIPVs from the caterpillar infested cotton were found to effect SERS spectra differences between healthy and infested cotton.

Although future work is still required to improve the detection system, the work described in this dissertation should be valuable in that plant-emitting VOCs were detected by an ADS-SERS technique, and insect infestation was identified by this technique for the first time.

6.2. Future studies

Future studies may include three additional objectives: 1. Optimization of adsorbent polymer thickness. 2. Development of another methodology for phase transfer

that can enhance transfer efficiency of AgNSs for SERS application. 3. Development of possible VOC collectors for field application.

6.2.1. **Film thickness**

Our SERS substrate consist of two layers: TAgNSs at the bottom for signal enhancement and Tenax-TA adsorbent polymer layer on top of the TAgNS layer for VOC pre-concentration. If the adsorbent polymer layer is too thick, VOC collection efficiency should be adequate, but the laser cannot pass through the layer well, and the collected VOCs on the layer might be located far away from the TAgNS layer. Even the enhanced electric field by the penetrated laser thus cannot interact with the VOCs very well, causing the SERS signal to be weak. Conversely, if the adsorbent polymer layer is too thin, VOC collection cannot be performed well. Therefore, it is important to find an optimal thickness of the polymer layer so it can collect VOC efficiently and not prohibit the incoming laser from penetrating onto the layer at the same time.

A spin coating technique might be the answer for controlling the thickness precisely. Spin coating is a technique to deposit the thin film very uniformly on the substrate, so the quality of the film can be improved compared to the drop casting method used in the dissertation. To control the film thickness, the rotation speed can be adjusted by a spin coater, and different film thicknesses can be tested to find an optimal condition in which a strong SERS signal from the VOCs can be produced. Similar work regarding film thickness control for SERS application was already done by the spin coating technique, in which very thin layers were produced, down to 15-25 nm [92].

6.2.2. **Phase transfer**

Another idea based on different molecular interactions can be proposed for phase transfer (Figure 6.1). The covalent bonding between the carboxylic group (COOH) of AgNSs and the amine group (NH_2) of added surfactants can be induced by two specific molecules, 1-ethyl-3-(3-dimethylaminopropyl)carbodiimide hydrochloride (EDC) and N-hydroxysulfosuccinimide (Sulfo-NHS). A similar concept was successfully applied in a different application such that the peptide could be attached to gold nanoparticles by this covalent bonding [197]. We already fabricated AgNSs capped with sodium decanoate, and success was confirmed by TEM image (Figure 6.1). Thus, the new concept is ready to be tested with AgNSs to check whether the efficiency for phase transfer can be improved.

6.2.3. **Field VOC detection**

For field application, direct detection of VOCs in the field would likely not be possible due to lack of sensitivity by any commercially available gas sensor. However, a plausible scenario is to pre-concentrate the VOCs as has been discussed previously. A field VOC collector needs to be prepared for the collection of the VOCs given off in the field, and then the collected VOCs could be analyzed with a portable Raman spectroscope in the field or by GC/MS in a laboratory.

A proposed field VOC collector (Figure 6.2) includes the following: 1. microcontroller to control a motor drive. 2. battery to power the system. 3. two motor drives to control two diaphragm pumps independently. 4. two diaphragm pumps to draw the VOCs from the field. 5. a PTFE sampling tube and frame to which Super-Q resin

(for GC/MS) or ADS-SERS substrate (for Raman) could be connected for VOC sampling.

Depending on activation by the motor drive under the microcontroller, each pump would work independently to pre-concentrate field VOCs from ambient air on Super-Q resin or SERS substrate through each sampling frame for a specified time. Also, either Super-Q resin or SERS substrate could be detached from the frame for the final VOC analysis. Micro diaphragm pumps and plastic materials for the frame and case could be fabricated by 3D printer to minimize the total weight, so it should be no problem to deploy a portable VOC collector with an agricultural robotic platform.

Figure 6.3 shows a plausible configuration of an agricultural ground robot deployed with the proposed field portable VOC collector including SERS substrate. The portable VOC collector could be installed on a ground robot, and the robot could move to pre-defined locations in which field VOCs need to be collected. Pump actuation would be controlled by the microcontroller to pro-concentrate the field VOCs at that location. After pre-concentration of VOCs onto the SERS substrate, the SERS substrate chamber would be opened, and SERS spectra from the VOCs collected on the substrate would be repeatedly obtained (Figure 6.3, top right).

Alternatively, to a ground robot, the portable VOC collector could be deployed with an unmanned aerial vehicle (UAV), although the payload might present problems. Several references regarding deployment of a VOC sampler at the bottom of a UAV [198-200] are available, and their common concept was to use GC/MS adsorbent cartridges for field VOC collection by continuous air pumping over 20 min and to analyze the cartridges

in a lab after the flight. In our case, the SERS substrate will also be added in the VOC sampler, so the pre-concentrated VOCs on the SERS substrate could be analyzed by a portable spectrometer. However, it may not be possible to add the portable Raman on a UAV due to payload limitations, so field VOC collection might be the only aspect done during the flight, with Raman measurement being done after the flight.

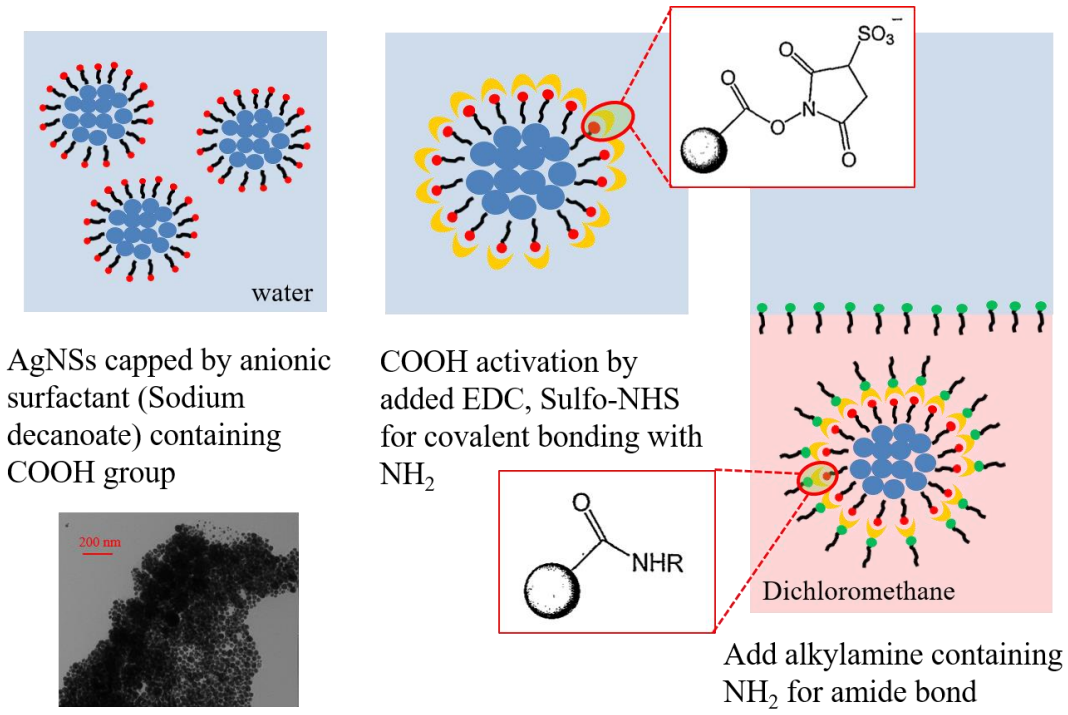

Figure 6.1 New concept of phase transfer using EDC, Sulfo-NHS crosslinker

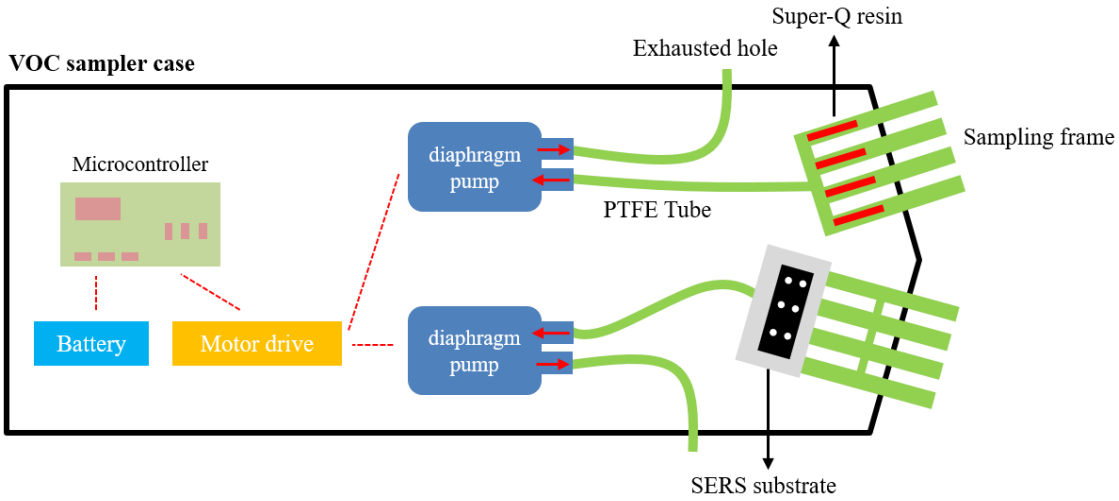

Figure 6.2 Design of a field VOC collector compatible with GC/MS and Raman

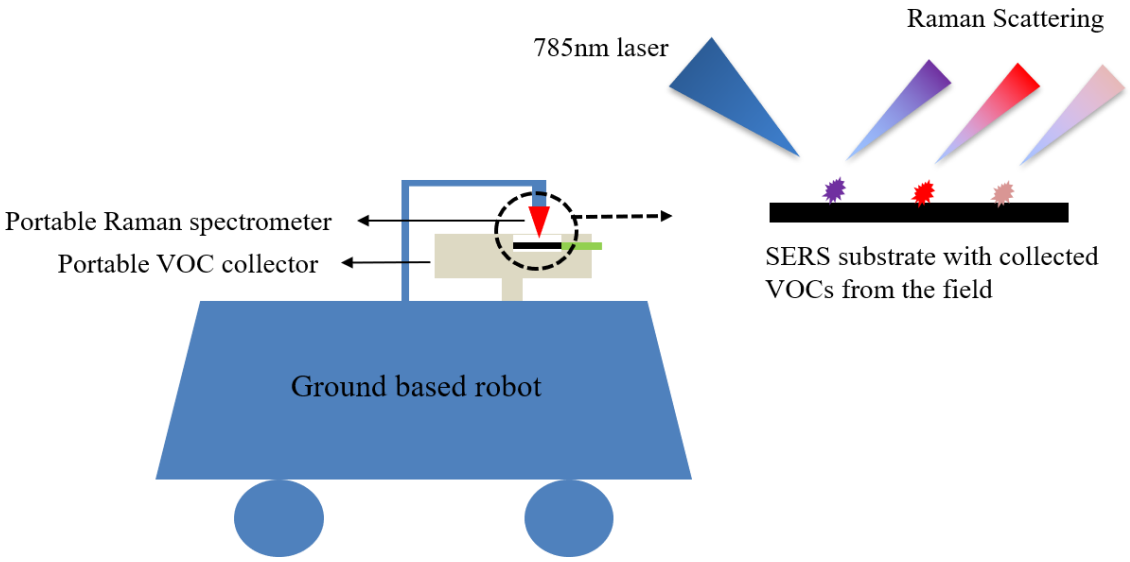

Figure 6.3 Scheme of a portable VOC collector deployment on a ground-based robot

REFERENCES

1. Dhaliwal, G.; Jindal, V.; Dhawan, A., Insect pest problems and crop losses: changing trends. *Indian Journal of Ecology* **2010,** *37* (1), 1-7.
2. Bowling, R. D.; Brewer, M. J.; Kerns, D. L.; Gordy, J.; Seiter, N.; Elliott, N. E.; Buntin, G. D.; Way, M.; Royer, T.; Biles, S., Sugarcane aphid (Hemiptera: Aphididae): a new pest on sorghum in North America. *Journal of Integrated Pest Management* **2016,** *7* (1).
3. Luo, J. H.; Huang, W. J.; Zhao, J. L.; Zhang, J. C.; Zhao, C. J.; Ma, R. H., Detecting Aphid Density of Winter Wheat Leaf Using Hyperspectral Measurements. *Ieee Journal of Selected Topics in Applied Earth Observations and Remote Sensing* **2013,** *6* (2), 690-698.
4. Luo, J. H.; Huang, W. J.; Yuan, L.; Zhao, C. J.; Du, S. Z.; Zhang, J. C.; Zhao, J. L., Evaluation of spectral indices and continuous wavelet analysis to quantify aphid infestation in wheat. *Precision Agriculture* **2013,** *14* (2), 151-161.
5. Huang, W. J.; Guan, Q. S.; Luo, J. H.; Zhang, J. C.; Zhao, J. L.; Liang, D.; Huang, L. S.; Zhang, D. Y., New Optimized Spectral Indices for Identifying and Monitoring Winter Wheat Diseases. *Ieee Journal of Selected Topics in Applied Earth Observations and Remote Sensing* **2014,** *7* (6), 2516-2524.
6. Prabhakar, M.; Prasad, Y. G.; Vennila, S.; Thirupathi, M.; Sreedevi, G.; Rao, G. R.; Venkateswarlu, B., Hyperspectral indices for assessing damage by the solenopsis mealybug (Hemiptera: Pseudococcidae) in cotton. *Computers and Electronics in Agriculture* **2013,** *97*, 61-70.
7. Kumar, J.; Vashisth, A.; Sehgal, V. K.; Gupta, V. K., Assessment of Aphid Infestation in Mustard by Hyperspectral Remote Sensing. *Journal of the Indian Society of Remote Sensing* **2013,** *41* (1), 83-90.
8. Mirik, M.; Ansley, R. J.; Steddom, K.; Rush, C. M.; Michels, G. J.; Workneh, F.; Cui, S.; Elliott, N. C., High spectral and spatial resolution hyperspectral imagery for quantifying Russian wheat aphid infestation in wheat using the constrained energy minimization classifier. *Journal of Applied Remote Sensing* **2014,** *8*.
9. Backoulou, G. F.; Elliott, N. C.; Giles, K. L., Using Multispectral Imagery to Compare the Spatial Pattern of Injury to Wheat Caused by Russian Wheat Aphid and Greenbug. *Southwestern Entomologist* **2016,** *41* (1), 1-7.
10. Elliott, N. C.; Backoulou, G. F.; Brewer, M. J.; Giles, K. L., NDVI to Detect Sugarcane Aphid Injury to Grain Sorghum. *Journal of Economic Entomology* **2015,** *108* (3), 1452-1455.
11. Tholl, D.; Boland, W.; Hansel, A.; Loreto, F.; Röse, U. S.; Schnitzler, J. P., Practical approaches to plant volatile analysis. *The Plant Journal* **2006,** *45* (4), 540-560.
12. Dudareva, N.; Pichersky, E., *Biology of floral scent*. CRC Press: 2006.
13. Alfeeli, B.; Jain, V.; Johnson, R. K.; Beyer, F. L.; Heflin, J. R.; Agah, M., Characterization of poly (2, 6-diphenyl-p-phenylene oxide) films as adsorbent for microfabricated preconcentrators. *Microchemical Journal* **2011,** *98* (2), 240-245.

14. Yang, C.; Wang, J.; Li, D., Microextraction techniques for the determination of volatile and semivolatile organic compounds from plants: a review. *Analytica chimica acta* **2013,** *799*, 8-22.
15. Verheggen, F. J.; Haubruge, E.; De Moraes, C. M.; Mescher, M. C., Aphid responses to volatile cues from turnip plants (*Brassica rapa*) infested with phloem-feeding and chewing herbivores. *Arthropod-Plant Interactions* **2013,** *7* (5), 567-577.
16. Pareja, M.; Qvarfordt, E.; Webster, B.; Mayon, P.; Pickett, J.; Birkett, M.; Glinwood, R., Herbivory by a Phloem-Feeding Insect Inhibits Floral Volatile Production. *Plos One* **2012,** *7* (2), 11.
17. Saad, K. A.; Roff, M. N. M.; Hallett, R. H.; Idris, A. B., Aphid-induced Defences in Chilli Affect Preferences of the Whitefly, *Bemisia tabaci* (Hemiptera: Aleyrodidae). *Scientific Reports* **2015,** *5*.
18. Hegde, M.; Oliveira, J. N.; da Costa, J. G.; Bleicher, E.; Santana, A. E. G.; Bruce, T. J. A.; Caulfield, J.; Dewhirst, S. Y.; Woodcock, C. M.; Pickett, J. A.; Birkett, M. A., Identification of Semiochemicals Released by Cotton, *Gossypium hirsutum*, Upon Infestation by the Cotton Aphid, *Aphis gossypii*. *Journal of Chemical Ecology* **2011,** *37* (7), 741-750.
19. Cai, L.; Koziel, J. A.; O'Neal, M. E., Studying plant–insect interactions with solid phase microextraction: screening for airborne volatile emissions response of soybeans to the soybean aphid, *Aphis glycines* Matsumura (Hemiptera: Aphididae). *Chromatography* **2015,** *2* (2), 265-276.
20. Markom, M. A.; Shakaff, A. M.; Adom, A.; Ahmad, M.; Hidayat, W.; Abdullah, A.; Fikri, N. A., Intelligent electronic nose system for basal stem rot disease detection. *Computers and Electronics in Agriculture* **2009,** *66* (2), 140-146.
21. Laothawornkitkul, J.; Moore, J. P.; Taylor, J. E.; Possell, M.; Gibson, T. D.; Hewitt, C. N.; Paul, N. D., Discrimination of plant volatile signatures by an electronic nose: a potential technology for plant pest and disease monitoring. *Environmental Science & Technology* **2008,** *42* (22), 8433-8439.
22. Weerakoon, K. A.; Shu, J. H.; Park, M.-K.; Auad, M. A.; Chin, B. A., Detecting insect infestation using a polymer based sensor array. *Sensors and Actuators B: Chemical* **2012,** *174*, 506-512.
23. Lampson, B. D.; Khalilian, A.; Greene, J. K.; Han, Y. J.; Degenhardt, D. C., Development of a Portable Electronic Nose for Detection of Cotton Damaged by *Nezara viridula* (Hemiptera: Pentatomidae). *Journal of Insects* **2014,** *2014*.
24. Padmaja, P. G.; Woodcock, C. M.; Bruce, T. J., Electrophysiological and behavioral responses of sorghum shoot fly, *Atherigona soccata*, to sorghum volatiles. *Journal of chemical ecology* **2010,** *36* (12), 1346-1353.
25. Zhuang, X.; Köllner, T. G.; Zhao, N.; Li, G.; Jiang, Y.; Zhu, L.; Ma, J.; Degenhardt, J.; Chen, F., Dynamic evolution of herbivore-induced sesquiterpene biosynthesis in sorghum and related grass crops. *The Plant Journal* **2012,** *69* (1), 70-80.
26. Holopainen, J. K.; Gershenzon, J., Multiple stress factors and the emission of plant VOCs. *Trends in plant science* **2010,** *15* (3), 176-184.

27. Fontana, A.; Reichelt, M.; Hempel, S.; Gershenzon, J.; Unsicker, S. B., The effects of arbuscular mycorrhizal fungi on direct and indirect defense metabolites of Plantago lanceolata L. *Journal of Chemical Ecology* **2009,** *35* (7), 833-843.
28. Harmel, N.; Almohamad, R.; FAUCONNIER, M. L.; Du Jardin, P.; Verheggen, F.; Marlier, M.; Haubruge, E.; Francis, F., Role of terpenes from aphid-infested potato on searching and oviposition behavior of *Episyrphus balteatus*. *Insect Science* **2007,** *14* (1), 57-63.
29. Mithöfer, A.; Wanner, G.; Boland, W., Effects of feeding Spodoptera littoralis on lima bean leaves. II. Continuous mechanical wounding resembling insect feeding is sufficient to elicit herbivory-related volatile emission. *Plant Physiol.* **2005,** *137* (3), 1160-1168.
30. Piesik, D.; Pańka, D.; Delaney, K. J.; Skoczek, A.; Lamparski, R.; Weaver, D. K., Cereal crop volatile organic compound induction after mechanical injury, beetle herbivory (Oulema spp.), or fungal infection (Fusarium spp.). *Journal of plant physiology* **2011,** *168* (9), 878-886.
31. Nwaneshiudu, I. C.; Yu, Q.; Schwartz, D. T., Quantitative Solid-Phase Microextraction (SPME)–Raman spectroscopy for the detection of trace organics in water. *Applied spectroscopy* **2012,** *66* (12), 1487-1491.
32. Ewing, K.; Nau, G.; Bilodeau, T.; Dagenais, D.; Bucholtz, F.; Aggarwal, I., Monitoring the absorption of organic vapors to a solid phase extraction medium applications to detection of trace volatile organic compounds by integration of solid phase absorbents with fiber optic Raman spectroscopy. *Analytica chimica acta* **1997,** *340* (1), 227-232.
33. Caballero-Díaz, E.; Simonet, B. M.; Valcárcel, M., Microextraction by packed sorbents combined with surface-enhanced Raman spectroscopy for determination of musk ketone in river water. *Analytical and bioanalytical chemistry* **2013,** *405* (23), 7251-7257.
34. Xia, D.; Guo, Q. H.; Ge, M.; Yuan, Y. X.; Xu, M. M.; Yao, J. L., On-line sensitive detection of aromatic vapor through PDMS/C3H7S-assisted SERS amplification. *RSC Adv.* **2016,** *6* (58), 53289-53295.
35. Kant, M.; Jonckheere, W.; Knegt, B.; Lemos, F.; Liu, J.; Schimmel, B.; Villarroel, C.; Ataide, L.; Dermauw, W.; Glas, J., Mechanisms and ecological consequences of plant defence induction and suppression in herbivore communities. *Annals of botany* **2015,** *115* (7), 1015-1051.
36. Paré, P. W.; Tumlinson, J. H., Plant volatiles as a defense against insect herbivores. *Plant Physiol.* **1999,** *121* (2), 325-332.
37. Rodriguez-Saona, C. R.; Stelinski, L. L., Behavior-modifying strategies in IPM: theory and practice. In *Integrated pest management: innovation-development process*, Springer: 2009; pp 263-315.
38. Truong, D. H.; Delory, B. M.; Vanderplanck, M.; Brostaux, Y.; Vandereycken, A.; Heuskin, S.; Delaplace, P.; Francis, F.; Lognay, G., Temperature regimes and aphid density interactions differentially influence VOC emissions in Arabidopsis. *Arthropod-Plant Interactions* **2014,** *8* (4), 317-327.

39. Gosset, V.; Harmel, N.; Göbel, C.; Francis, F.; Haubruge, E.; Wathelet, J.-P.; Du Jardin, P.; Feussner, I.; Fauconnier, M.-L., Attacks by a piercing-sucking insect (*Myzus persicae* Sultzer) or a chewing insect (*Leptinotarsa decemlineata* Say) on potato plants (*Solanum tuberosum* L.) induce differential changes in volatile compound release and oxylipin synthesis. *Journal of experimental botany* **2009**, erp015.
40. Verheggen, F. J.; Capella, Q.; Wathelet, J. P.; Haubruge, E., What makes Episyrphus balteatus (Diptera: Syrphidae) oviposit on aphid infested tomato plants? *Communications in agricultural and applied biological sciences* **2008,** *73* (3), 371-81.
41. Giorgi, A.; Panseri, S.; Nanayakkara, N.; Chiesa, L. M., HS-SPME-GC/MS analysis of the volatile compounds of *Achillea collina*: Evaluation of the emissions fingerprint induced by *Myzus persicae* infestation. *Journal of Plant Biology* **2012,** *55* (3), 251-260.
42. Errard, A.; Ulrichs, C.; Kuhne, S.; Mewis, I.; Drungowski, M.; Schreiner, M.; Baldermann, S., Single- versus Multiple-Pest Infestation Affects Differently the Biochemistry of Tomato (Solanum lycopersicum 'Ailsa Craig'). *Journal of Agricultural and Food Chemistry* **2015,** *63* (46), 10103-10111.
43. Giorgi, A.; Manzo, A.; Nanayakkara, N.; Giupponi, L.; Cocucci, M.; Panseri, S., Effect of biotic and abiotic stresses on volatile emission of *Achillea collina* Becker ex Rchb. *Natural Product Research* **2015,** *29* (18), 1695-1702.
44. Francis, F. D.; Martin, T.; Lognay, G.; Haubruge, E., Role of (E)-beta-farnesene in systematic aphid prey location by Episyrphus balteatus larvae (Diptera : Syrphidae). *European Journal of Entomology* **2005,** *102* (3), 431-436.
45. Pettersson, M.; Unelius, C. R.; Valterova, I.; Borg-Karlson, A.-K., Semiochemicals related to the aphid *Cinara pilicornis* and its host, *Picea abies*: A method to assign nepetalactone diastereomers. *Journal of Chromatography A* **2008,** *1180* (1-2), 165-170.
46. Sun, H. N.; Zhang, F.; Chen, S. M.; Guan, Z. Y.; Jiang, J. F.; Fang, W. M.; Chen, F. D., Effects of aphid herbivory on volatile organic compounds of *Artemisia annua* and *Chrysanthemum morifolium*. *Biochemical Systematics and Ecology* **2015,** *60*, 225-233.
47. Moayeri, H. R. S.; Ashouri, A.; Poll, L.; Enkegaard, A., Olfactory response of a predatory mirid to herbivore induced plant volatiles: multiple herbivory vs. single herbivory. *Journal of Applied Entomology* **2007,** *131* (5), 326-332.
48. Zhu, J. W.; Park, K. C., Methyl salicylate, a soybean aphid-induced plant volatile attractive to the predator *Coccinella septempunctata*. *Journal of Chemical Ecology* **2005,** *31* (8), 1733-1746.
49. Ren, Q.; Cao, L. Z.; Su, J. W.; Xie, M. H.; Zhang, Q. W.; Liu, X. X., Volatile Emissions from the Invasive Weed *Eupatorium adenophorum* Induced by *Aphis gossypii* Feeding and Methyl Jasmonate Treatment. *Weed Sci.* **2010,** *58* (3), 252-257.
50. da Costa, J. G.; Pires, E. V.; Riffel, A.; Birkett, M. A.; Bleicher, E.; Sant'Ana, A. E. G., Differential preference of *Capsicum* spp. cultivars by *Aphis gossypii* is conferred by variation in volatile semiochemistry. *Euphytica* **2011,** *177* (3), 299-307.
51. Campbell, C.; Pettersson, J.; Pickett, J.; Wadhams, L.; Woodcock, C., Spring migration of damson-hop aphid, *Phorodon humuli* (Homoptera, Aphididae), and summer

host plant-derived semiochemicals released on feeding. *Journal of Chemical Ecology* **1993,** *19* (7), 1569-1576.
52. Du, Y.; Poppy, G. M.; Powell, W.; Pickett, J. A.; Wadhams, L. J.; Woodcock, C. M., Identification of semiochemicals released during aphid feeding that attract parasitoid *Aphidius ervi*. *Journal of Chemical Ecology* **1998,** *24* (8), 1355-1368.
53. Sasso, R.; Iodice, L.; Digilio, M. C.; Carretta, A.; Ariati, L.; Guerrieri, E., Host-locating response by the aphid parasitoid *Aphidius ervi* to tomato plant volatiles. *J. Plant Interact.* **2007,** *2* (3), 175-183.
54. Yan, Z. G.; Wang, C. Z., Similar attractiveness of maize volatiles induced by *Helicoverpa armigera* and *Pseudaletia separata* to the generalist parasitoid *Campoletis chlorideae*. *Entomologia Experimentalis Et Applicata* **2006,** *118* (2), 87-96.
55. Yan, Z. G.; Wang, C. Z., Identification of *Mythmna separata*-induced maize volatile synomones that attract the parasitoid *Campoletis chlorideae*. *Journal of Applied Entomology* **2006,** *130* (4), 213-219.
56. Rasmann, S.; Turlings, T. C. J., Simultaneous feeding by aboveground and belowground herbivores attenuates plant-mediated attraction of their respective natural enemies. *Ecol. Lett.* **2007,** *10* (10), 926-936.
57. Pinto-Zevallos, D. M.; Strapasson, P.; Zarbin, P. H. G., Herbivore-induced volatile organic compounds emitted by maize: Electrophysiological responses in *Spodoptera frugiperda* females. *Phytochem. Lett.* **2016,** *16*, 70-74.
58. Williams, L.; Rodriguez-Saona, C.; Pare, P. W.; Crafts-Brandner, S. J., The piercing-sucking herbivores *Lygus hesperus* and *Nezara viridula* induce volatile emissions in plants. *Arch. Insect Biochem. Physiol.* **2005,** *58* (2), 84-96.
59. Oluwafemi, S.; Bruce, T. J. A.; Pickett, J. A.; Ton, J.; Birkett, M. A., Behavioral Responses of the Leafhopper, *Cicadulina storeyi* China, a Major Vector of Maize Streak Virus, to Volatile Cues from Intact and Leafhopper-Damaged Maize. *Journal of Chemical Ecology* **2011,** *37* (1), 40-48.
60. Rodriguez-Saona, C.; Crafts-Brandner, S. J.; Cañas, L. A., Volatile emissions triggered by multiple herbivore damage: beet armyworm and whitefly feeding on cotton plants. *Journal of chemical ecology* **2003,** *29* (11), 2539-2550.
61. Zhang, P.-J.; Zheng, S.-J.; van Loon, J. J.; Boland, W.; David, A.; Mumm, R.; Dicke, M., Whiteflies interfere with indirect plant defense against spider mites in Lima bean. *Proceedings of the National Academy of Sciences* **2009,** *106* (50), 21202-21207.
62. Kant, M. R.; Sabelis, M. W.; Haring, M. A.; Schuurink, R. C., Intraspecific variation in a generalist herbivore accounts for differential induction and impact of host plant defences. *Proceedings of the Royal Society of London B: Biological Sciences* **2008,** *275* (1633), 443-452.
63. Sarmento, R. A.; Lemos, F.; Bleeker, P. M.; Schuurink, R. C.; Pallini, A.; Oliveira, M. G. A.; Lima, E. R.; Kant, M.; Sabelis, M. W.; Janssen, A., A herbivore that manipulates plant defence. *Ecol. Lett.* **2011,** *14* (3), 229-236.
64. Schwartzberg, E. G.; Böröczky, K.; Tumlinson, J. H., Pea aphids, *Acyrthosiphon pisum*, suppress induced plant volatiles in broad bean, *Vicia faba*. *Journal of Chemical Ecology* **2011,** *37* (10), 1055.

65. Turlings, T. C.; Bernasconi, M.; Bertossa, R.; Bigler, F.; Caloz, G.; Dorn, S., The induction of volatile emissions in maize by three herbivore species with different feeding habits: possible consequences for their natural enemies. *Biol. Control* **1998,** *11* (2), 122-129.
66. Lwande, W.; Bentley, M., Volatiles of Sorghum bicolor seedlings. *Journal of natural products* **1987,** *50* (5), 950-952.
67. Sun, X.-G.; Tang, M., Effect of arbuscular mycorrhizal fungi inoculation on root traits and root volatile organic compound emissions of Sorghum bicolor. *South African Journal of Botany* **2013,** *88*, 373-379.
68. Brewer, M. J.; Gordy, J. W.; Kerns, D. L.; Woolley, J. B.; Rooney, W. L.; Bowling, R. D., Sugarcane aphid population growth, plant injury, and natural enemies on selected grain sorghum hybrids in Texas and Louisiana. *Journal of economic entomology* **2017,** *110* (5), 2109-2118.
69. Dean, J. M.; De Moraes, C. M., Effects of genetic modification on herbivore-induced volatiles from maize. *Journal of Chemical Ecology* **2006,** *32* (4), 713-724.
70. Kiani, M.; Szczepaniec, A., Effects of sugarcane aphid herbivory on transcriptional responses of resistant and susceptible sorghum. *BMC genomics* **2018,** *19* (1), 774.
71. Degen, T.; Dillmann, C.; Marion-Poll, F.; Turlings, T. C. J., High genetic variability of herbivore-induced volatile emission within a broad range of maize inbred lines. *Plant Physiol.* **2004,** *135* (4), 1928-1938.
72. Gouinguene, S.; Degen, T.; Turlings, T. C. J., Variability in herbivore-induced odour emissions among maize cultivars and their wild ancestors (teosinte). *Chemoecology* **2001,** *11* (1), 9-16.
73. Hoballah, M. E. F.; Tamo, C.; Turlings, T. C. J., Differential attractiveness of induced odors emitted by eight maize varieties for the parasitoid *Cotesia marginiventris*: Is quality or quantity important? *Journal of Chemical Ecology* **2002,** *28* (5), 951-968.
74. Niederbacher, B.; Winkler, J.; Schnitzler, J., Volatile organic compounds as non-invasive markers for plant phenotyping. *Journal of experimental botany* **2015,** *66* (18), 5403-5416.
75. ŠPÁNIK, N. J. O. V. I., Identification of volatile organic compounds in honeydew honeys using comprehensive gas chromatography. *Journal of Food and Nutrition Research (ISSN 1336-8672)* **2014,** *53* (4), 353-362.
76. Mannucci, A.; Serra, A.; Remorini, D.; Castagna, A.; Mele, M.; Scartazza, A.; Ranieri, A., Aroma profile of Fuji apples treated with gelatin edible coating during their storage. *LWT-Food Science and Technology* **2017,** *85*, 28-36.
77. Jiménez, B.; Rivas, A.; Lorenzo, M. L.; Sánchez-Ortiz, A., Chemosensory characterization of virgin olive oils obtained from organic and conventional practices during fruit ripening. *Flavour and Fragrance Journal* **2017,** *32* (4), 294-304.
78. Lv, S.-D.; Wu, Y.-S.; Song, Y.-Z.; Zhou, J.-S.; Lian, M.; Wang, C.; Liu, L.; Meng, Q.-X., Multivariate Analysis Based on GC-MS Fingerprint and Volatile Composition for the Quality Evaluation of Pu-Erh Green Tea. *Food Analytical Methods* **2015,** *8* (2), 321-333.

79. Chiu, S.-W.; Tang, K.-T., Towards a chemiresistive sensor-integrated electronic nose: A review. *Sensors* **2013,** *13* (10), 14214-14247.
80. Casalinuovo, I. A.; Di Pierro, D.; Coletta, M.; Di Francesco, P., Application of electronic noses for disease diagnosis and food spoilage detection. *Sensors* **2006,** *6* (11), 1428-1439.
81. Concina, I.; Falasconi, M.; Gobbi, E.; Bianchi, F.; Musci, M.; Mattarozzi, M.; Pardo, M.; Mangia, A.; Careri, M.; Sberveglieri, G., Early detection of microbial contamination in processed tomatoes by electronic nose. *Food Control* **2009,** *20* (10), 873-880.
82. Sberveglieri, V.; Bhandari, M. P.; Núñez Carmona, E.; Betto, G.; Sberveglieri, G., A Novel MOS Nanowire Gas Sensor Device (S3) and GC-MS-Based Approach for the Characterization of Grated Parmigiano Reggiano Cheese. *Biosensors* **2016,** *6* (4), 60.
83. Heidarbeigi, K.; Mohtasebi, S. S.; Foroughirad, A.; Ghasemi-Varnamkhasti, M.; Rafiee, S.; Rezaei, K., Detection of adulteration in saffron samples using electronic nose. *International Journal of Food Properties* **2015,** *18* (7), 1391-1401.
84. Di Pietrantonio, F.; Benetti, M.; Cannatà, D.; Verona, E.; Palla-Papavlu, A.; Fernández-Pradas, J.; Serra, P.; Staiano, M.; Varriale, A.; D'Auria, S., A surface acoustic wave bio-electronic nose for detection of volatile odorant molecules. *Biosensors and Bioelectronics* **2015,** *67*, 516-523.
85. Kim, K.; Lee, J. W.; Shin, K. S., Cyanide SERS as a platform for detection of volatile organic compounds and hazardous transition metal ions. *Analyst* **2013,** *138* (10), 2988-2994.
86. Kim, K.; Lee, J. W.; Shin, D. H.; Choi, J. Y.; Shin, K. S., Organic isocyanide-adsorbed gold nanostructure: a SERS sensory device for indirect peak-shift detection of volatile organic compounds. *Analyst* **2012,** *137* (8), 1930-1936.
87. Wang, J. P.; Yang, L.; Liu, B. H.; Jiang, H. H.; Liu, R. Y.; Yang, J. W.; Han, G. M.; Mei, Q. S.; Zhang, Z. P., Inkjet-Printed Silver Nanoparticle Paper Detects Airborne Species from Crystalline Explosives and Their Ultratrace Residues in Open Environment. *Anal. Chem.* **2014,** *86* (7), 3338-3345.
88. Myoung, N.; Yoo, H. K.; Hwang, I. W., Surface-enhanced Raman scattering detection of toluene and dichlorobenzene vapors using 1-propanethiol-linked Ag nanoparticles. *J. Nanophotonics* **2014,** *8*, 7.
89. Marega, C.; Maculan, J.; Rizzi, G. A.; Saini, R.; Cavaliere, E.; Gavioli, L.; Cattelan, M.; Giallongo, G.; Marigo, A.; Granozzi, G., Polyvinyl alcohol electrospun nanofibers containing Ag nanoparticles used as sensors for the detection of biogenic amines. *Nanotechnology* **2015,** *26* (7), 9.
90. Wong, C. L.; Dinish, U. S.; Schmidt, M. S.; Olivo, M., Non-labeling multiplex surface enhanced Raman scattering (SERS) detection of volatile organic compounds (VOCs). *Analytica Chimica Acta* **2014,** *844*, 54-60.
91. Wong, C. L.; Dinish, U. S.; Buddharaju, K. D.; Schmidt, M. S.; Olivo, M., Surface-enhanced Raman scattering (SERS)-based volatile organic compounds (VOCs) detection using plasmonic bimetallic nanogap substrate. *Appl. Phys. A-Mater. Sci. Process.* **2014,** *117* (2), 687-692.

92. Xia, D.; Guo, Q.; Ge, M.; Yuan, Y.; Xu, M.; Yao, J., On-line sensitive detection of aromatic vapor through PDMS/C 3 H 7 S-assisted SERS amplification. *RSC Adv.* **2016,** *6* (58), 53289-53295.
93. Park, K. J.; Wu, C.; Mercer-Smith, A. R.; Dodson, R. A.; Moersch, T. L.; Koonath, P.; Pipino, A. C.; Lu, H.-W.; Yang, Y.; Sapirstein, V. S., Raman system for sensitive and selective identification of volatile organic compounds. *Sensors and Actuators B: Chemical* **2015,** *220*, 491-499.
94. Vargas Jentzsch, P.; Ciobotă, V., Raman spectroscopy as an analytical tool for analysis of vegetable and essential oils. *Flavour and fragrance journal* **2014,** *29* (5), 287-295.
95. Jentzsch, P. V.; Ramos, L. A.; Ciobotă, V., Handheld Raman spectroscopy for the distinction of essential oils used in the cosmetics industry. *Cosmetics* **2015,** *2* (2), 162-176.
96. Lafhal, S.; Vanloot, P.; Bombarda, I.; Valls, R.; Kister, J.; Dupuy, N., Raman spectroscopy for identification and quantification analysis of essential oil varieties: a multivariate approach applied to lavender and lavandin essential oils. *Journal of Raman Spectroscopy* **2015,** *46* (6), 577-585.
97. Fang, Y.; Bullock, H.; Lee, S. A.; Sekar, N.; Eiteman, M. A.; Whitman, W. B.; Ramasamy, R. P., Detection of methyl salicylate using bi-enzyme electrochemical sensor consisting salicylate hydroxylase and tyrosinase. *Biosensors and Bioelectronics* **2016,** *85*, 603-610.
98. Vogt, N., Polynomial principal component regression: an approach to analysis and interpretation of complex mixture relationships in multivariate environmental data. *Chemometrics and intelligent laboratory systems* **1989,** *7* (1-2), 119-130.
99. Ureña, F. P.; Moreno, J. R. A.; González, J. J. L., Conformational study of (R)-(+)-limonene in the liquid phase using vibrational spectroscopy (IR, Raman, and VCD) and DFT calculations. *Tetrahedron: Asymmetry* **2009,** *20* (1), 89-97.
100. Jentzsch, P.; Ramos, L.; Ciobotă, V., Handheld Raman spectroscopy for the distinction of essential oils used in the cosmetics industry. *Cosmetics* **2015,** *2* (2), 162-176.
101. Skoczek, A.; Piesik, D.; Wenda-Piesik, A.; Buszewski, B.; Bocianowski, J.; Wawrzyniak, M., Volatile organic compounds released by maize following herbivory or insect extract application and communication between plants. *Journal of Applied Entomology* **2017,** *141* (8), 630-643.
102. Mosier-Boss, P. A., Review of SERS substrates for chemical sensing. *Nanomaterials* **2017,** *7* (6), 142.
103. Xu, H.; Aizpurua, J.; Käll, M.; Apell, P., Electromagnetic contributions to single-molecule sensitivity in surface-enhanced Raman scattering. *Physical Review E* **2000,** *62* (3), 4318.
104. Jiang, X.; Lai, Y.; Yang, M.; Yang, H.; Jiang, W.; Zhan, J., Silver nanoparticle aggregates on copper foil for reliable quantitative SERS analysis of polycyclic aromatic hydrocarbons with a portable Raman spectrometer. *Analyst* **2012,** *137* (17), 3995-4000.

105. Chen, J.; Qin, G.; Wang, J.; Yu, J.; Shen, B.; Li, S.; Ren, Y.; Zuo, L.; Shen, W.; Das, B., One-step fabrication of sub-10-nm plasmonic nanogaps for reliable SERS sensing of microorganisms. *Biosensors and Bioelectronics* **2013,** *44*, 191-197.
106. Tang, H.; Meng, G.; Huang, Q.; Zhang, Z.; Huang, Z.; Zhu, C., Arrays of Cone-Shaped ZnO Nanorods Decorated with Ag Nanoparticles as 3D Surface-Enhanced Raman Scattering Substrates for Rapid Detection of Trace Polychlorinated Biphenyls. *Advanced Functional Materials* **2012,** *22* (1), 218-224.
107. Li, Z.; Meng, G.; Huang, Q.; Hu, X.; He, X.; Tang, H.; Wang, Z.; Li, F., Ag Nanoparticle-Grafted PAN-Nanohump Array Films with 3D High-Density Hot Spots as Flexible and Reliable SERS Substrates. *Small* **2015,** *11* (40), 5452-5459.
108. Zhang, Q.; Lee, Y. H.; Phang, I. Y.; Lee, C. K.; Ling, X. Y., Hierarchical 3D SERS Substrates Fabricated by Integrating Photolithographic Microstructures and Self-Assembly of Silver Nanoparticles. *Small* **2014,** *10* (13), 2703-2711.
109. Zhang, Q.; Wang, X.-D.; Tian, T.; Chu, L.-Q., Incorporation of multilayered silver nanoparticles into polymer brushes as 3-dimensional SERS substrates and their application for bacteria detection. *Applied Surface Science* **2017,** *407*, 185-191.
110. Fan, Z.; Senapati, D.; Khan, S. A.; Singh, A. K.; Hamme, A.; Yust, B.; Sardar, D.; Ray, P. C., Popcorn-Shaped Magnetic Core–Plasmonic Shell Multifunctional Nanoparticles for the Targeted Magnetic Separation and Enrichment, Label-Free SERS Imaging, and Photothermal Destruction of Multidrug-Resistant Bacteria. *Chemistry-A European Journal* **2013,** *19* (8), 2839-2847.
111. Yap, F. L.; Thoniyot, P.; Krishnan, S.; Krishnamoorthy, S., Nanoparticle cluster arrays for high-performance SERS through directed self-assembly on flat substrates and on optical fibers. *Acs Nano* **2012,** *6* (3), 2056-2070.
112. Wang, X.; Zhuang, J.; Peng, Q.; Li, Y., A general strategy for nanocrystal synthesis. *Nature* **2005,** *437* (7055), 121.
113. Bai, F.; Wang, D.; Huo, Z.; Chen, W.; Liu, L.; Liang, X.; Chen, C.; Wang, X.; Peng, Q.; Li, Y., A Versatile Bottom-up Assembly Approach to Colloidal Spheres from Nanocrystals. *Angewandte Chemie International Edition* **2007,** *46* (35), 6650-6653.
114. Wang, Y.; Lee, K.; Irudayaraj, J., Silver nanosphere SERS probes for sensitive identification of pathogens. *The Journal of Physical Chemistry C* **2010,** *114* (39), 16122-16128.
115. Liu, Y.; Zhang, Y.; Ding, H.; Xu, S.; Li, M.; Kong, F.; Luo, Y.; Li, G., Self-assembly of noble metallic spherical aggregates from monodisperse nanoparticles: their synthesis and pronounced SERS and catalytic properties. *Journal of Materials Chemistry A* **2013,** *1* (10), 3362-3371.
116. Lee, K.-M.; Herrman, T. J.; Bisrat, Y.; Murray, S. C., Feasibility of surface-enhanced raman spectroscopy for rapid detection of aflatoxins in maize. *Journal of agricultural and food chemistry* **2014,** *62* (19), 4466-4474.
117. Lee, K.-M.; Herrman, T. J., Determination and prediction of fumonisin contamination in maize by surface–enhanced Raman spectroscopy (SERS). *Food and bioprocess technology* **2016,** *9* (4), 588-603.
118. Han, Z.; Liu, H.; Wang, B.; Weng, S.; Yang, L.; Liu, J., Three-dimensional surface-enhanced Raman scattering hotspots in spherical colloidal superstructure for

identification and detection of drugs in human urine. *Anal. Chem.* **2015,** *87* (9), 4821-4828.
119. Yang, J.; Lee, J. Y.; Ying, J. Y., Phase transfer and its applications in nanotechnology. *Chemical Society Reviews* **2011,** *40* (3), 1672-1696.
120. Kumar, A.; Mukherjee, P.; Guha, A.; Adyantaya, S.; Mandale, A.; Kumar, R.; Sastry, M., Amphoterization of colloidal gold particles by capping with valine molecules and their phase transfer from water to toluene by electrostatic coordination with fatty amine molecules. *Langmuir* **2000,** *16* (25), 9775-9783.
121. Mayya, K. S.; Caruso, F., Phase transfer of surface-modified gold nanoparticles by hydrophobization with alkylamines. *Langmuir* **2003,** *19* (17), 6987-6993.
122. Yao, H.; Momozawa, O.; Hamatani, T.; Kimura, K., Phase transfer of gold nanoparticles across a water/oil interface by stoichiometric ion-pair formation on particle surfaces. *Bulletin of the Chemical Society of Japan* **2000,** *73* (12), 2675-2678.
123. Yao, H.; Momozawa, O.; Hamatani, T.; Kimura, K., Stepwise size-selective extraction of carboxylate-modified gold nanoparticles from an aqueous suspension into toluene with tetraoctylammonium cations. *Chemistry of materials* **2001,** *13* (12), 4692-4697.
124. Devarajan, S.; Vimalan, B.; Sampath, S., Phase transfer of Au–Ag alloy nanoparticles from aqueous medium to an organic solvent: effect of aging of surfactant on the formation of Ag-rich alloy compositions. *Journal of colloid and interface science* **2004,** *278* (1), 126-132.
125. Cheng, H.-W.; Schadt, M. J.; Young, K.; Luo, J.; Zhong, C.-J., Determination of ion pairing on capping structures of gold nanoparticles by phase extraction. *Analyst* **2015,** *140* (18), 6239-6244.
126. Cheng, H.-W.; Schadt, M. J.; Zhong, C.-J., Titration of gold nanoparticles in phase extraction. *Analyst* **2015,** *140* (23), 8023-8032.
127. Guo, H.; Xing, B.; White, J. C.; Mukherjee, A.; He, L., Ultra-sensitive determination of silver nanoparticles by surface-enhanced Raman spectroscopy (SERS) after hydrophobization-mediated extraction. *Analyst* **2016,** *141* (18), 5261-5264.
128. Yao, Q.; Yuan, X.; Yu, Y.; Yu, Y.; Xie, J.; Lee, J. Y., Introducing amphiphilicity to noble metal nanoclusters via phase-transfer driven ion-pairing reaction. *Journal of the American Chemical Society* **2015,** *137* (5), 2128-2136.
129. Yuan, X.; Luo, Z.; Zhang, Q.; Zhang, X.; Zheng, Y.; Lee, J. Y.; Xie, J., Synthesis of highly fluorescent metal (Ag, Au, Pt, and Cu) nanoclusters by electrostatically induced reversible phase transfer. *Acs Nano* **2011,** *5* (11), 8800-8808.
130. Ermakova, A. M.; Morozova, J. E.; Shalaeva, Y. V.; Syakaev, V. V.; Nizameev, I. R.; Kadirov, M. K.; Antipin, I. S.; Konovalov, A. I., The supramolecular approach to the phase transfer of carboxylic calixresorcinarene-capped silver nanoparticles. *Colloids and Surfaces A: Physicochemical and Engineering Aspects* **2017,** *524*, 127-134.
131. Liu, J.; Alvarez, J.; Ong, W.; Román, E.; Kaifer, A. E., Phase transfer of hydrophilic, cyclodextrin-modified gold nanoparticles to chloroform solutions. *Journal of the American Chemical Society* **2001,** *123* (45), 11148-11154.

132. Sapoletova, N. A.; Kushnir, S. E.; Kushnir, A. E.; Kocherginskaya, P. B.; Kazin, P. E.; Napolskii, K. S., Simple phase transfer of nanoparticles from aqueous to organic media using polymer colloids as carriers. *RSC Adv.* **2016,** *6* (113), 112409-112412.
133. Park, J.; Thomasson, J. A.; Lee, K.-M. In *Volatile Detection from Plant Headspace with Modified Surface-Enhanced Raman Spectroscopy*, 2017 ASABE Annual International Meeting, American Society of Agricultural and Biological Engineers: 2017; p 1.
134. Kazakova, J.; García-Povea, A.; Fernández-Palacios, M.; Villar-Navarro, M.; Carnerero, J. M.; Jimenez-Ruiz, A.; Prado-Gotor, R., A colorimetric study of the interaction of cationic and anionic surfactants with anionic gold nanoparticles. *Colloid and Polymer Science* **2017,** *295* (11), 2141-2149.
135. Cheng, W.; Wang, E., Size-dependent phase transfer of gold nanoparticles from water into toluene by tetraoctylammonium cations: a wholly electrostatic interaction. *The Journal of Physical Chemistry B* **2004,** *108* (1), 24-26.
136. Frens, G., Controlled nucleation for the regulation of the particle size in monodisperse gold suspensions. *Nature physical science* **1973,** *241* (105), 20.
137. Park, J.-W.; Shumaker-Parry, J. S., Structural study of citrate layers on gold nanoparticles: role of intermolecular interactions in stabilizing nanoparticles. *Journal of the American Chemical Society* **2014,** *136* (5), 1907-1921.
138. De Aguiar, H. B.; Strader, M. L.; de Beer, A. G.; Roke, S., Surface structure of sodium dodecyl sulfate surfactant and oil at the oil-in-water droplet liquid/liquid interface: a manifestation of a nonequilibrium surface state. *The Journal of Physical Chemistry B* **2011,** *115* (12), 2970-2978.
139. Park, S.-W.; Kaimoyo, E.; Kumar, D.; Mosher, S.; Klessig, D. F., Methyl salicylate is a critical mobile signal for plant systemic acquired resistance. *Science* **2007,** *318* (5847), 113-116.
140. Chae, M.-S.; Kim, J.; Yoo, Y. K.; Kang, J. Y.; Lee, J. H.; Hwang, K. S., A micro-preconcentrator combined olfactory sensing system with a micromechanical cantilever sensor for detecting 2, 4-dinitrotoluene gas vapor. *Sensors* **2015,** *15* (8), 18167-18177.
141. Drenscko, M.; Loverde, S. M., Molecular dynamics simulations of the interaction of phospholipid bilayers with polycaprolactone. *Molecular Simulation* **2019,** *45* (11), 859-867.
142. Berret, J.-F.; Yokota, K.; Morvan, M.; Schweins, R., Polymer− nanoparticle complexes: From dilute solution to solid state. *The Journal of Physical Chemistry B* **2006,** *110* (39), 19140-19146.
143. Varghese, H. T.; Panicker, C. Y.; Philip, D.; Mannekutla, J. R.; Inamdar, S., IR, Raman and SERS studies of methyl salicylate. *Spectrochimica Acta Part A: Molecular and Biomolecular Spectroscopy* **2007,** *66* (4-5), 959-963.
144. Li, M.; Qiu, Y.; Fan, C.; Cui, K.; Zhang, Y.; Xiao, Z., Design of SERS nanoprobes for Raman imaging: materials, critical factors and architectures. *Acta pharmaceutica sinica B* **2018,** *8* (3), 381-389.
145. Yang, Z.; Baldermann, S.; Watanabe, N., Recent studies of the volatile compounds in tea. *Food Research International* **2013,** *53* (2), 585-599.

146. Zheng, X.-Q.; Li, Q.-S.; Xiang, L.-P.; Liang, Y.-R., Recent advances in volatiles of teas. *Molecules* **2016,** *21* (3), 338.
147. Brilli, F.; Loreto, F.; Baccelli, I., Exploiting plant volatile organic compounds (VOCs) in agriculture to improve sustainable defense strategies and productivity of crops. *Frontiers in Plant Science* **2019,** *10*, 264.
148. Sakthivel, S.; Habeeb, S.; Raman, C., Screening of broad spectrum natural pesticides against conserved target arginine kinase in cotton pests by molecular modeling. *Journal of Biomolecular Structure and Dynamics* **2019,** *37* (4), 1022-1042.
149. Naranjo, S. E.; Luttrell, R. G., Cotton arthropod IPM. *Integrated pest management* **2009**, 324-340.
150. Ormeno, E.; Goldstein, A.; Niinemets, Ü., Extracting and trapping biogenic volatile organic compounds stored in plant species. *TrAC Trends in Analytical Chemistry* **2011,** *30* (7), 978-989.
151. Lv, S.; Wu, Y.; Zhou, J.; Lian, M.; Li, C.; Xu, Y.; Liu, S.; Wang, C.; Meng, Q., The study of fingerprint characteristics of Dayi Pu-erh tea using a fully Automatic HS-SPME/GC–MS and combined chemometrics method. *PloS one* **2014,** *9* (12), e116428.
152. Zhu, J.; Chen, F.; Wang, L.; Niu, Y.; Yu, D.; Shu, C.; Chen, H.; Wang, H.; Xiao, Z., Comparison of aroma-active volatiles in oolong tea infusions using GC–olfactometry, GC–FPD, and GC–MS. *Journal of agricultural and food chemistry* **2015,** *63* (34), 7499-7510.
153. He, C.; Guo, X.; Yang, Y.; Xie, Y.; Ju, F.; Guo, W., Characterization of the aromatic profile in "zijuan" and "pu-erh" green teas by headspace solid-phase microextraction coupled with GC-O and GC-MS. *Anal. Methods* **2016,** *8* (23), 4727-4735.
154. Magagna, F.; Cordero, C.; Cagliero, C.; Liberto, E.; Rubiolo, P.; Sgorbini, B.; Bicchi, C., Black tea volatiles fingerprinting by comprehensive two-dimensional gas chromatography–Mass spectrometry combined with high concentration capacity sample preparation techniques: Toward a fully automated sensomic assessment. *Food chemistry* **2017,** *225*, 276-287.
155. Lau, H.; Liu, S. Q.; Xu, Y. Q.; Lassabliere, B.; Sun, J.; Yu, B., Characterising volatiles in tea (Camellia sinensis). Part I: Comparison of headspace-solid phase microextraction and solvent assisted flavour evaporation. *LWT* **2018,** *94*, 178-189.
156. Arceusz, A.; Occhipinti, A.; Capuzzo, A.; Maffei, M. E., Comparison of different extraction methods for the determination of α-and β-thujone in sage (Salvia officinalis L.) herbal tea. *Journal of separation science* **2013,** *36* (18), 3130-3134.
157. Zhang, L.; Zeng, Z.; Zhao, C.; Kong, H.; Lu, X.; Xu, G., A comparative study of volatile components in green, oolong and black teas by using comprehensive two-dimensional gas chromatography–time-of-flight mass spectrometry and multivariate data analysis. *Journal of chromatography A* **2013,** *1313*, 245-252.
158. Xiao, Z.; Wang, H.; Niu, Y.; Liu, Q.; Zhu, J.; Chen, H.; Ma, N., Characterization of aroma compositions in different Chinese congou black teas using GC–MS and GC–O combined with partial least squares regression. *Flavour and Fragrance Journal* **2017,** *32* (4), 265-276.

159. Zhu, Y.; Lv, H.-P.; Shao, C.-Y.; Kang, S.; Zhang, Y.; Guo, L.; Dai, W.-D.; Tan, J.-F.; Peng, Q.-H.; Lin, Z., Identification of key odorants responsible for chestnut-like aroma quality of green teas. *Food Research International* **2018,** *108*, 74-82.
160. Rose, U. S.; Manukian, A.; Heath, R. R.; Tumlinson, J. H., Volatile semiochemicals released from undamaged cotton leaves (a systemic response of living plants to caterpillar damage). *Plant Physiol.* **1996,** *111* (2), 487-495.
161. Yu, H.; Zhang, Y.; Wyckhuys, K. A.; Wu, K.; Gao, X.; Guo, Y., Electrophysiological and behavioral responses of Microplitis mediator (Hymenoptera: Braconidae) to caterpillar-induced volatiles from cotton. *Environmental entomology* **2010,** *39* (2), 600-609.
162. Huang, X.-Z.; Chen, J.-Y.; Xiao, H.-J.; Xiao, Y.-T.; Wu, J.; Wu, J.-X.; Zhou, J.-J.; Zhang, Y.-J.; Guo, Y.-Y., Dynamic transcriptome analysis and volatile profiling of Gossypium hirsutum in response to the cotton bollworm Helicoverpa armigera. *Scientific reports* **2015,** *5*, 11867.
163. Byers, J. A., A cost of alarm pheromone production in cotton aphids, Aphis gossypii. *Naturwissenschaften* **2005,** *92* (2), 69-72.
164. Kiani, S.; Minaei, S.; Ghasemi-Varnamkhasti, M., Application of electronic nose systems for assessing quality of medicinal and aromatic plant products: A review. *Journal of Applied Research on Medicinal and Aromatic Plants* **2016,** *3* (1), 1-9.
165. Loutfi, A.; Coradeschi, S.; Mani, G. K.; Shankar, P.; Rayappan, J. B. B., Electronic noses for food quality: A review. *Journal of Food Engineering* **2015,** *144*, 103-111.
166. Qin, Z.; Pang, X.; Chen, D.; Cheng, H.; Hu, X.; Wu, J., Evaluation of Chinese tea by the electronic nose and gas chromatography–mass spectrometry: Correlation with sensory properties and classification according to grade level. *Food research international* **2013,** *53* (2), 864-874.
167. Zhu, J.; Chen, F.; Wang, L.; Niu, Y.; Xiao, Z., Evaluation of the synergism among volatile compounds in Oolong tea infusion by odour threshold with sensory analysis and E-nose. *Food chemistry* **2017,** *221*, 1484-1490.
168. Mirasoli, M.; Gotti, R.; Di Fusco, M.; Leoni, A.; Colliva, C.; Roda, A., Electronic nose and chiral-capillary electrophoresis in evaluation of the quality changes in commercial green tea leaves during a long-term storage. *Talanta* **2014,** *129*, 32-38.
169. Torri, L.; Rinaldi, M.; Chiavaro, E., Electronic nose evaluation of volatile emission of Chinese teas: from leaves to infusions. *International journal of food science & technology* **2014,** *49* (5), 1315-1323.
170. Wang, J.; Wei, Z., The classification and prediction of green teas by electrochemical response data extraction and fusion approaches based on the combination of e-nose and e-tongue. *RSC Adv.* **2015,** *5* (129), 106959-106970.
171. Dutta, L.; Talukdar, C.; Hazarika, A.; Bhuyan, M., A Novel Low-Cost Hand-Held Tea Flavor Estimation System. *IEEE Transactions on Industrial Electronics* **2018,** *65* (6), 4983-4990.
172. Kakoty, P.; Bhuyan, M.; Das, K., Performance of Pd Doped SnO 2 as Sensing Material for Tea Aromatic Chemicals. *IEEE Sensors Journal* **2018,** *18* (11), 4392-4398.

173. Lan, Y. B.; Zheng, X. Z.; Westbrook, J. K.; Lopez, J.; Lacey, R.; Hoffmann, W. C., Identification of Stink Bugs Using an Electronic Nose. *J. Bionic Eng.* **2008,** *5*, 172-180.
174. Henderson, W. G.; Khalilian, A.; Han, Y. J.; Greene, J. K.; Degenhardt, D. C., Detecting stink bugs/damage in cotton utilizing a portable electronic nose. *Computers and Electronics in Agriculture* **2010,** *70* (1), 157-162.
175. Degenhardt, D. C.; Greene, J. K.; Khalilian, A., Temporal dynamics and electronic nose detection of stink bug-induced volatile emissions from cotton bolls. *Psyche: A Journal of Entomology* **2012,** *2012*.
176. Buyukgoz, G. G.; Soforoglu, M.; Akgul, N. B.; Boyaci, I. H., Spectroscopic fingerprint of tea varieties by surface enhanced Raman spectroscopy. *Journal of food science and technology* **2016,** *53* (3), 1709-1716.
177. Liao, Y.-W.; Chen, S.-F. In *Discriminant Analysis of the Geographical Origins of Oolong Tea Using Surface-Enhanced Raman Spectroscopy*, 2017 ASABE Annual International Meeting, American Society of Agricultural and Biological Engineers: 2017; p 1.
178. Kreno, L. E.; Greeneltch, N. G.; Farha, O. K.; Hupp, J. T.; Van Duyne, R. P., SERS of molecules that do not adsorb on Ag surfaces: a metal-organic framework-based functionalization strategy. *Analyst* **2014,** *139* (16), 4073-4080.
179. Koh, C. S. L.; Lee, H. K.; Han, X.; Sim, H. Y. F.; Ling, X. Y., Plasmonic nose: integrating the MOF-enabled molecular preconcentration effect with a plasmonic array for recognition of molecular-level volatile organic compounds. *Chemical Communications* **2018,** *54* (20), 2546-2549.
180. Shulaev, V.; Silverman, P.; Raskin, I., Airborne signalling by methyl salicylate in plant pathogen resistance. *Nature* **1997,** *385* (6618), 718.
181. Van Den Boom, C. E.; Van Beek, T. A.; Posthumus, M. A.; De Groot, A.; Dicke, M., Qualitative and quantitative variation among volatile profiles induced by Tetranychus urticae feeding on plants from various families. *Journal of chemical ecology* **2004,** *30* (1), 69-89.
182. Akbar, M.; Wang, D.; Goodman, R.; Hoover, A.; Rice, G.; Heflin, J. R.; Agah, M., Improved performance of micro-fabricated preconcentrators using silica nanoparticles as a surface template. *Journal of Chromatography A* **2013,** *1322*, 1-7.
183. Meyer, E. E.; Rosenberg, K. J.; Israelachvili, J., Recent progress in understanding hydrophobic interactions. *Proceedings of the National Academy of Sciences* **2006,** *103* (43), 15739-15746.
184. Talwar, S.; Scanu, L. F.; Khan, S. A., Hydrophobic interactions in associative polymer/nonionic surfactant systems: Effects of surfactant architecture and system parameters. *Journal of Rheology* **2006,** *50* (6), 831-847.
185. Stöckelhuber, K. W.; Das, A.; Jurk, R.; Heinrich, G., Contribution of physico-chemical properties of interfaces on dispersibility, adhesion and flocculation of filler particles in rubber. *Polymer* **2010,** *51* (9), 1954-1963.
186. Borusiewicz, R.; Zięba-Palus, J., Comparison of the effectiveness of Tenax TA® and Carbotrap 300® in concentration of flammable liquids compounds. *Journal of forensic sciences* **2007,** *52* (1), 70-74.

187. Chu, L.; Deng, S.; Zhao, R.; Deng, J.; Kang, X., Comparison of adsorption/desorption of volatile organic compounds (VOCs) on electrospun nanofibers with tenax TA for potential application in sampling. *PloS one* **2016,** *11* (10), e0163388.
188. Sharma, P.; Ghosh, A.; Tudu, B.; Bhuyan, L. P.; Tamuly, P.; Bhattacharyya, N.; Bandyopadhyay, R.; Chatterjee, A., Detection of linalool in black tea using a quartz crystal microbalance sensor. *Sensors and Actuators B: Chemical* **2014,** *190*, 318-325.
189. Sharma, P.; Tudu, B.; Bhuyan, L. P.; Tamuly, P.; Bhattacharyya, N.; Bandyopadhyay, R., Detection of methyl salicylate in black tea using a quartz crystal microbalance sensor. *IEEE Sensors Journal* **2016,** *16* (13), 5160-5166.
190. Li, Y.; Li, Q.; Wang, Y.; Oh, J.; Jin, S.; Park, Y.; Zhou, T.; Zhao, B.; Ruan, W.; Jung, Y. M., A reagent-assisted method in SERS detection of methyl salicylate. *Spectrochimica Acta Part A: Molecular and Biomolecular Spectroscopy* **2018,** *195*, 172-175.
191. Du, L.; Ma, L.; Qiao, Y.; Lu, Y.; Xiao, D., Determination of phthalate esters in teas and tea infusions by gas chromatography–mass spectrometry. *Food chemistry* **2016,** *197*, 1200-1206.
192. Yin, P.; Liu, X.; Chen, H.; Pan, R.; Ma, G., Determination of 16 phthalate esters in tea samples using a modified QuEChERS sample preparation method combined with GC-MS/MS. *Food Additives & Contaminants: Part A* **2014,** *31* (8), 1406-1413.
193. Habu, T.; Flath, R. A.; Mon, T. R.; Morton, J. F., Volatile components of rooibos tea (Aspalathus linearis). *Journal of Agricultural and Food Chemistry* **1985,** *33* (2), 249-254.
194. Kawakami, M.; Kobayashi, A.; Kator, K., Volatile constituents of rooibos tea (Aspalathus linearis) as affected by extraction process. *Journal of agricultural and food chemistry* **1993,** *41* (4), 633-636.
195. Nørbygaard, T.; Berg, R. W., Analysis of phthalate ester content in poly (vinyl chloride) plastics by means of Fourier transform Raman spectroscopy. *Applied spectroscopy* **2004,** *58* (4), 410-413.
196. Fleger, Y.; Mastai, Y.; Rosenbluh, M.; Dressler, D., SERS as a probe for adsorbate orientation on silver nanoclusters. *Journal of Raman Spectroscopy: An International Journal for Original Work in all Aspects of Raman Spectroscopy, Including Higher Order Processes, and also Brillouin and Rayleigh Scattering* **2009,** *40* (11), 1572-1577.
197. Bartczak, D.; Kanaras, A. G., Preparation of peptide-functionalized gold nanoparticles using one pot EDC/sulfo-NHS coupling. *Langmuir* **2011,** *27* (16), 10119-10123.
198. Black, O.; Chen, J.; Scircle, A.; Zhou, Y.; Cizdziel, J. V., Adaption and use of a quadcopter for targeted sampling of gaseous mercury in the atmosphere. *Environmental Science and Pollution Research* **2018,** *25* (13), 13195-13202.
199. Chang, C.-C.; Wang, J.-L.; Chang, C.-Y.; Liang, M.-C.; Lin, M.-R., Development of a multicopter-carried whole air sampling apparatus and its applications in environmental studies. *Chemosphere* **2016,** *144*, 484-492.
200. McKinney, K. A.; Wang, D.; Ye, J.; de Fouchier, J.-B.; Guimarães, P. C.; Batista, C. E.; Souza, R. A.; Alves, E. G.; Gu, D.; Guenther, A. B., A sampler for

atmospheric volatile organic compounds by copter unmanned aerial vehicles. *Atmospheric Measurement Techniques Discussions* **2018**.

APPENDIX A

SUPPLEMENT FOR CHAPTER 3

A. 1 Gas concentration approximation

a. Maximum limit based on the assumption that the liquid drop was fully evaporated

We can approximate the amount of the vapor due to vapor pressure based on the equation expressed in previous question.

$$n_{VOC} = \frac{P_{VOC} V_{Total}}{RT}$$

From the evaporated amount from 5µl each reagent drops, we can finally approximate the concentration when it will be fully evaporated.

$$C_{VOC,max}[ppmv] = \frac{\frac{P_{VOC}}{P_{atm}} \times 10^6 \times V_{total\ reagent}}{n_{VOC} \times \frac{Molar\ mass}{Density}} = \frac{RT \times 10^6 \times V_{total\ reagent}}{V_{Total} \times \frac{Molar\ mass}{Density}}$$

Table A 1 Maximum concentration limit for each VOC

VOC	Amount (mole)	Density (g/ml)	Molar mass (g/mol)	$C_{VOC,max}$ $[ppmv]$
Linalool	1.08 X 10^{-6}	0.86	154.25	5683
Cis-3-hexen-1-ol	5.89 X 10^{-6}	0.846	100.159	8610
Cis-3-hexenyl-acetate	7.85 X 10^{-6}	0.897	142.198	6430
Methyl salicylate	2.2 X 10^{-7}	1.174	152.149	7865

b. Approximation of mixture concentration

$$\text{Concentration} = \text{Volume percent ratio} \times \text{Density}_{Mixture} \times 10^6 \quad (\frac{mg}{L} = \frac{\mu g}{ml})$$

$$Density_{Mixture} = \frac{Density_{Linalool} + Density_{Cis-3-hexen-1-ol} + Density_{Methyl\ salicylate}}{3}$$

Table A 2 Loading matrix of PC 1 for the case study (VOC vs. Mixture)

Wavenumber (cm^{-1})	LI vs. MIX	HA vs. MIX	HO vs. MIX	MS vs. MIX
808	0.7863	0.7871	0.7973	0.4319
812	0.8176	0.8231	0.8062	0.5845
1032	0.9494	0.9403	0.9179	0.7480
1040	0.8603	0.7720	0.7616	0.7631
1644	0.8978	0.9310	0.9190	0.8907
1652	0.8171	0.8114	0.7051	0.8425
1656	0.8574	0.8370	0.8563	0.8782
1672	0.5559	0.8986	0.8716	0.8745

Table A 3 Cumulative percentage of PC of mixture for PCR

PC number	Eigenvalue	Percent (%)	Cumulative percentage (%)
1	2.9477	42.110	42.110
2	1.4194	20.276	62.386
3	0.9911	14.159	76.545
4	0.8430	12.043	88.588
5	0.3864	5.520	94.108
6	0.2646	3.780	97.888
7	0.1479	2.112	100.000

Table A 4 Loading matrix of PC 1 and PC 2 of mixture for PCR

Wavenumber (cm^{-1})	PC 1	PC 2
808	0.8244	0.2459
812	0.9086	0.1640
1032	0.8879	-0.1987
1644	0.2518	0.8721
1656	0.5740	-0.5649
1676	0.3075	0.2685
1680	0.4085	-0.3750

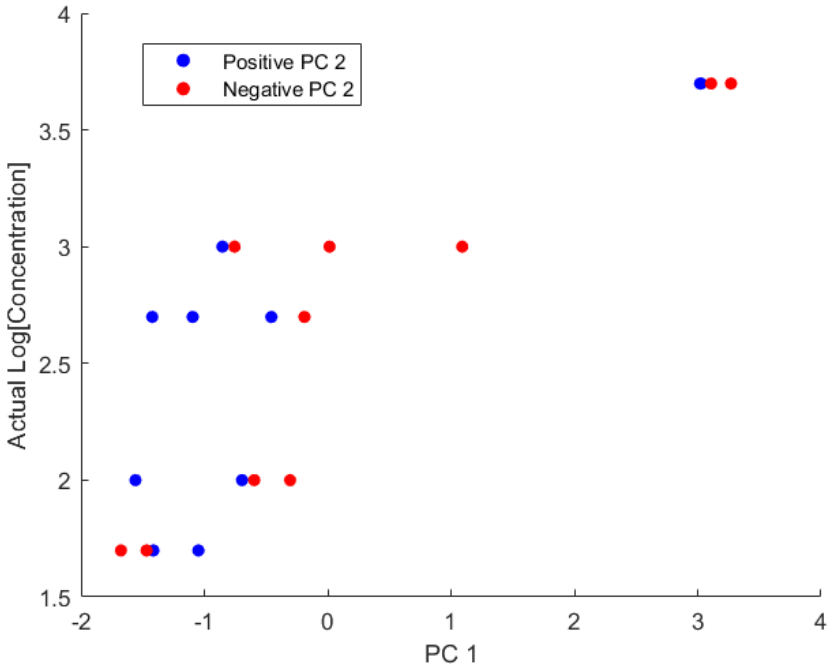

Figure A 1 Plot of PC 1 versus concentration according to the sign of PC 2

APPENDIX B

SUPPLEMENT FOR CHAPTER 4

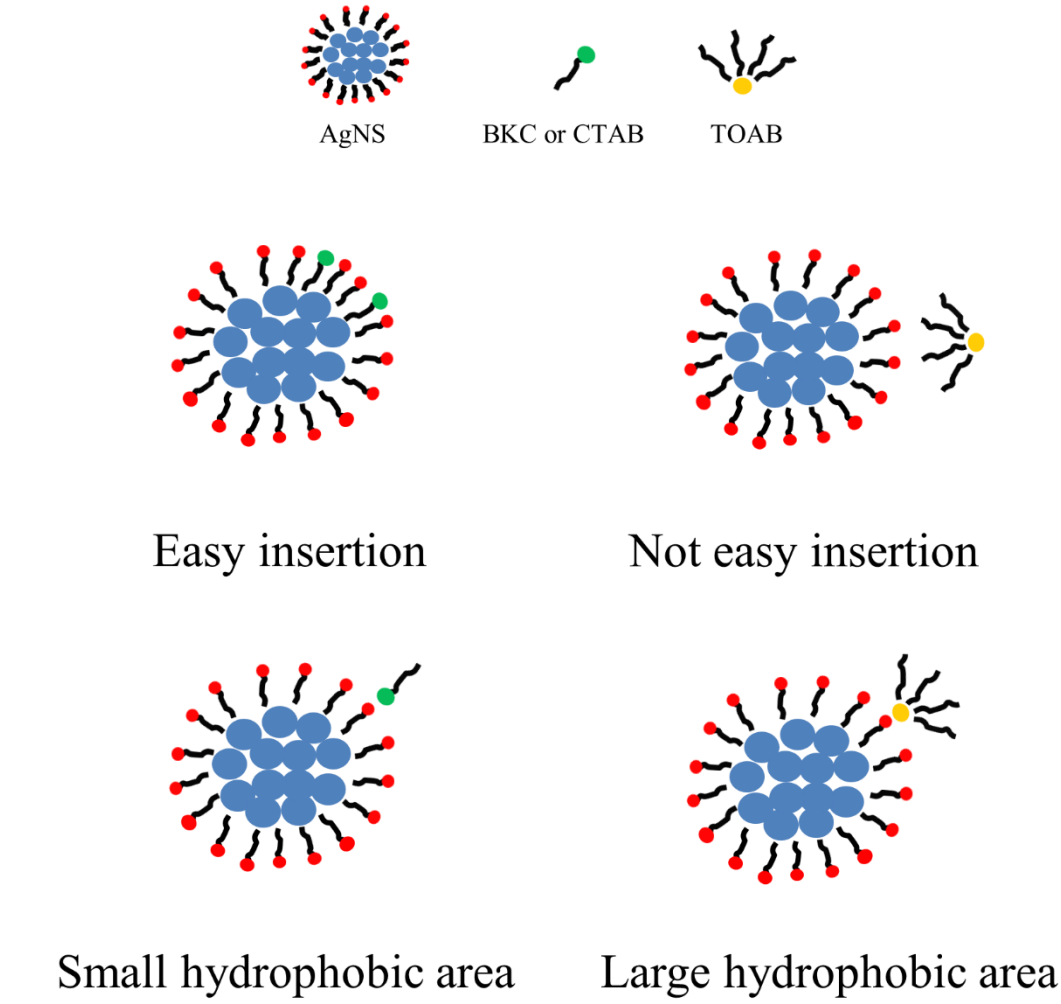

Figure B 1 Effect of hydrophobic tail area according to the surfactants

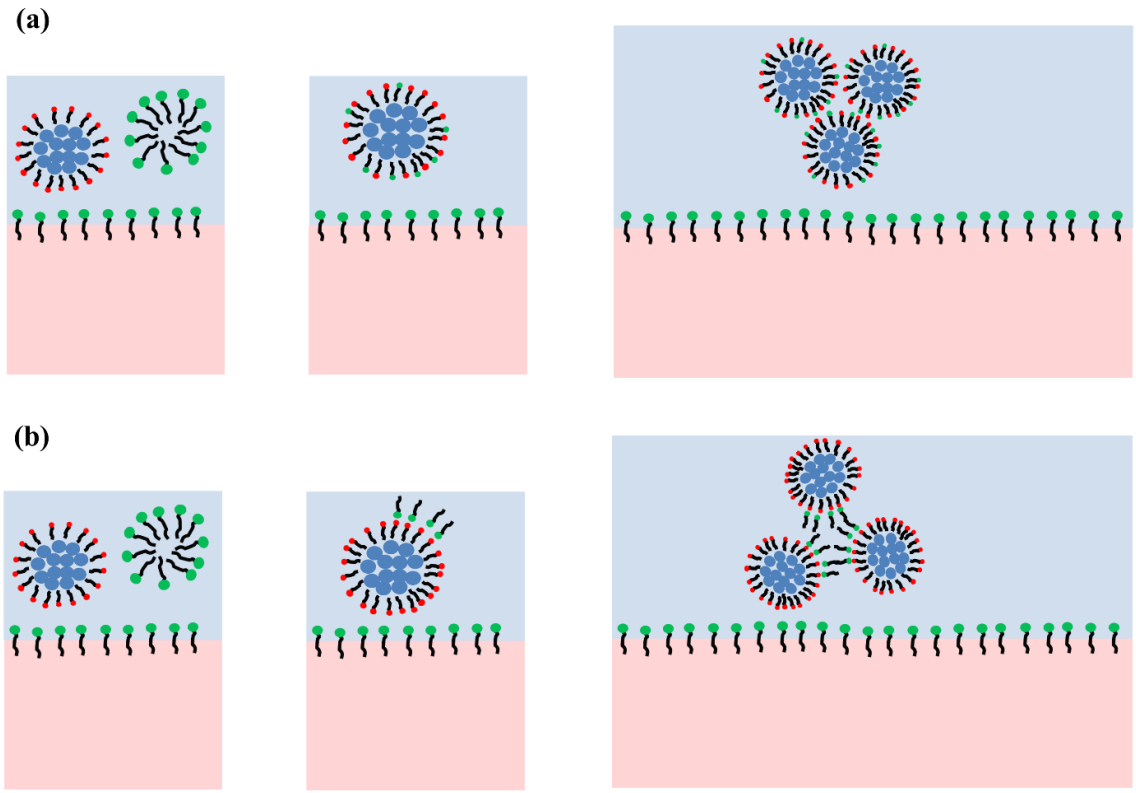

Figure B 2 Scheme of possible interaction between AgNS and added surfactant with small hydrophobic tail (BKC, CTAB) in water phase (Blue: water, Pink: dichloromethane) (a) surfactant insertion into AgNS (b) surfactant attraction to AgNS

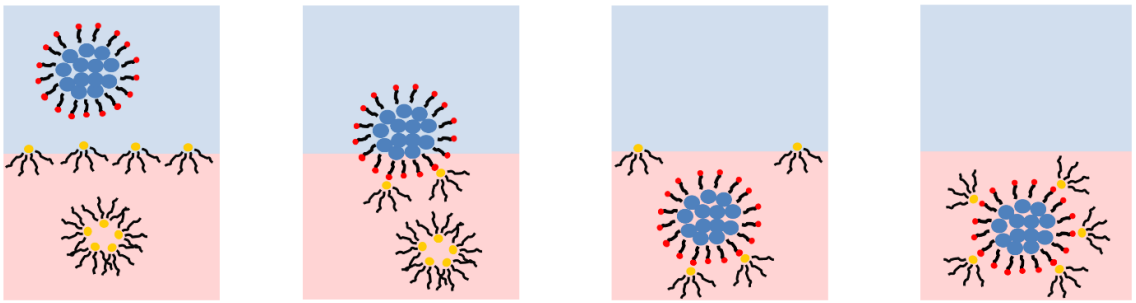

Figure B 3 Scheme of phase transfer of AgNS by added TOAB dissolved in dichloromethane (Blue: water, Pink: dichloromethane)

APPENDIX C

SUPPLEMENT FOR CHAPTER 5

C. 1 Gas concentration approximation

a. Maximum limit based on the assumption that the vapor was generated due to its o wn vapor pressure

$$\therefore\ C_{VOC,max}[ppmv] = \frac{V_{VOC}}{V_{Total}} \times 10^6 = \frac{P_{VOC}}{P_{atm}} \times 10^6$$

$V_{VOC} = volume\ of\ VOC\ [L]$,

$V_{Total} = total\ volume\ of\ the\ chamber = 120 \times 10^{-3}[L]$

$P_{atm} = standard\ atmosphere = 1\ [atm]$, P_{VOC}

$= vapor\ pressure\ of\ VOC\ [atm]$,

R = Ideal gas constant = $0.0821\ \left[\frac{L\ atm}{K\ mole}\right]$, T = Absolute temperature

= 298 [K] at 25 °C

Table C 1 Concentration approximation for three VOCs

VOC	Vapor pressure (atm)	$C_{VOC,min}[ppmv]$
Linalool	0.00022	220
Cis-3-hexen-1-ol	0.0012	1200
Methyl salicylate	0.000045	45

C. 2 Headspace static VOC collection set-up

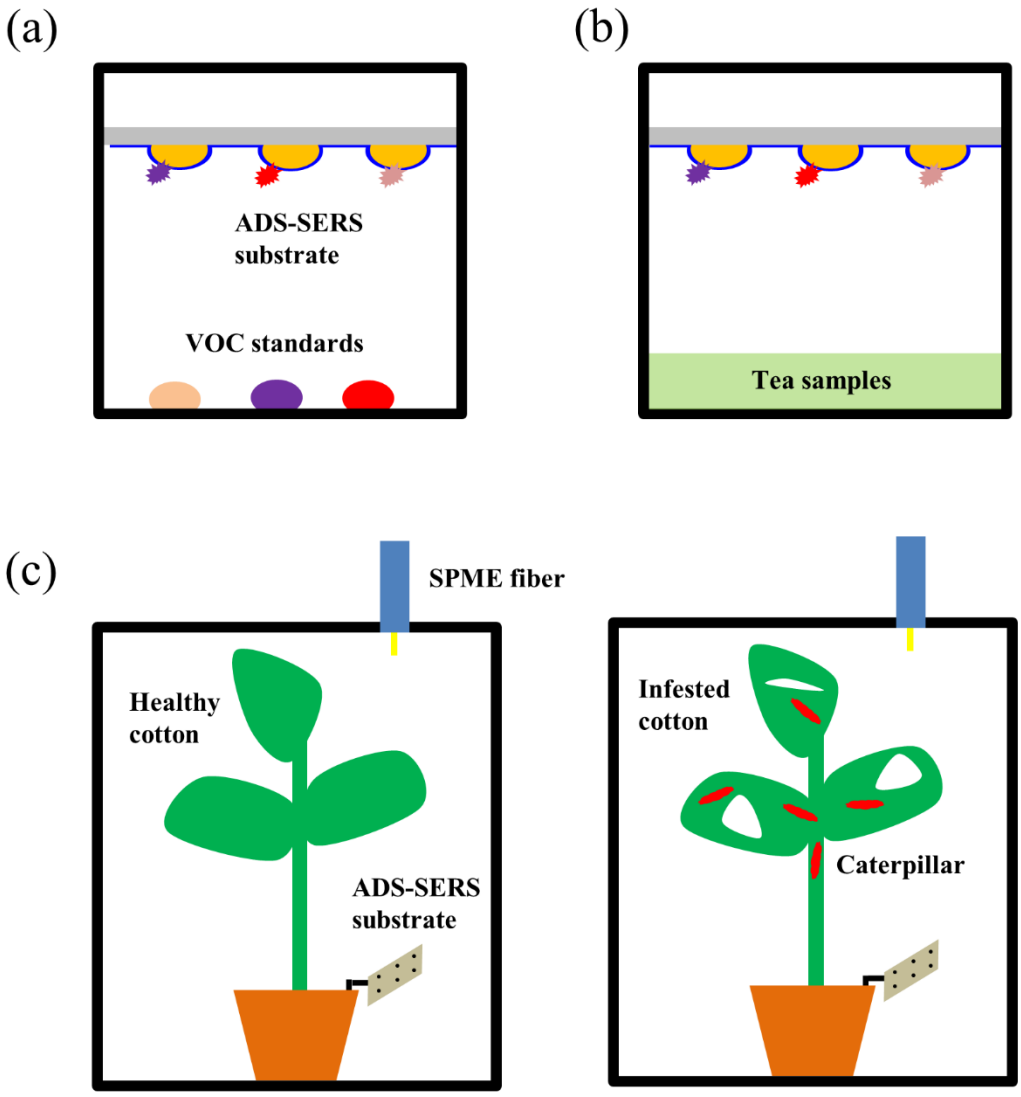

Figure C 1 Headspace static VOCs collection set-up (a) VOC standards (b) Tea samples (c) Cotton-caterpillar

C. 3 Possible molecular groups

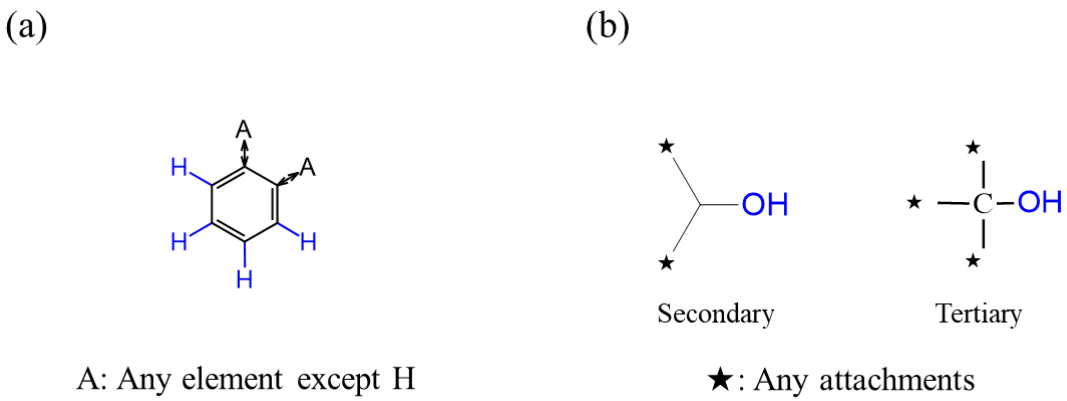

Figure C 2 Possible molecular groups (a) Aromatic component with ortho-disubstituted (b) any secondary or tertiary alcohol

APPENDIX D

GRAPHICAL ABSTRACTS

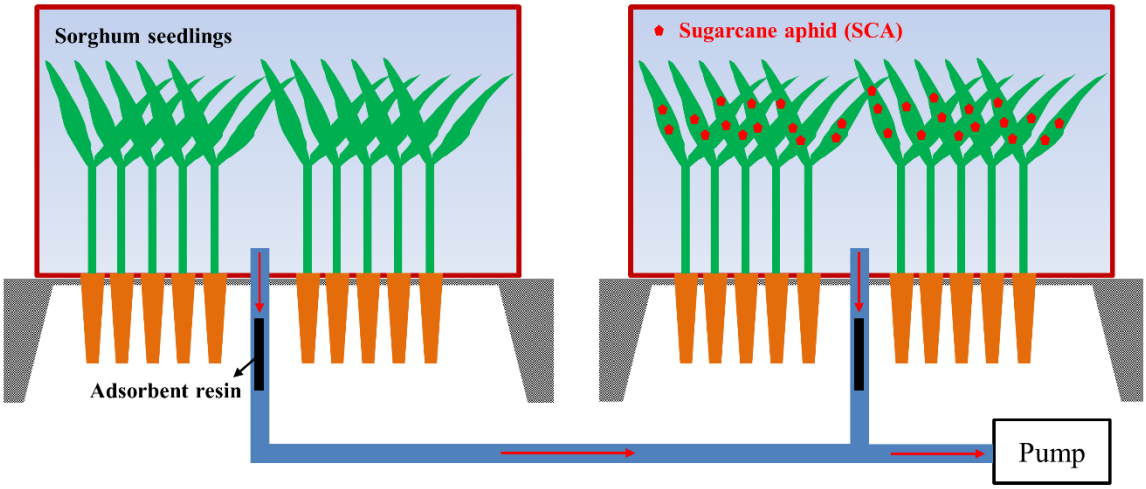

VOCs collection set-up for one replication

	Healthy	Infested
Terpene	32%	41%
Alcohol	36%	30%
Aromatic	8%	6%

VOCs compositional changes after herbivore

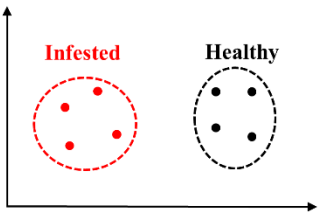

Multivariate statistical analysis

Figure D 1 Graphical abstract for chapter 2

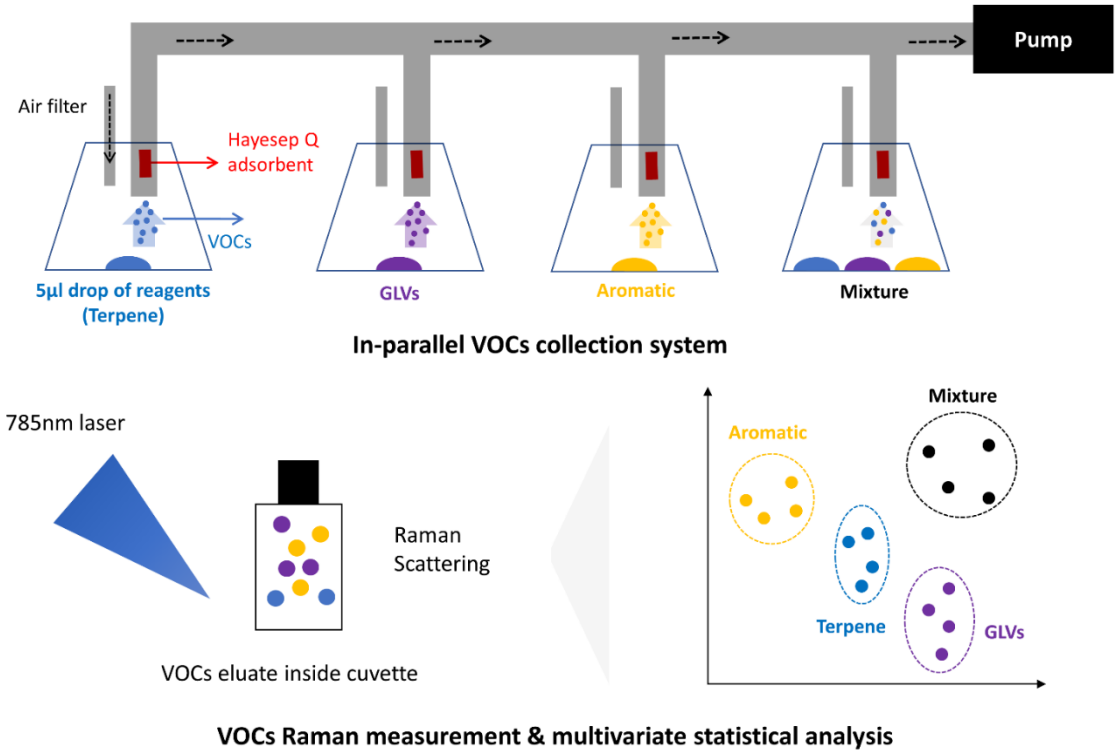

Figure D 2 Graphical abstract for chapter 3

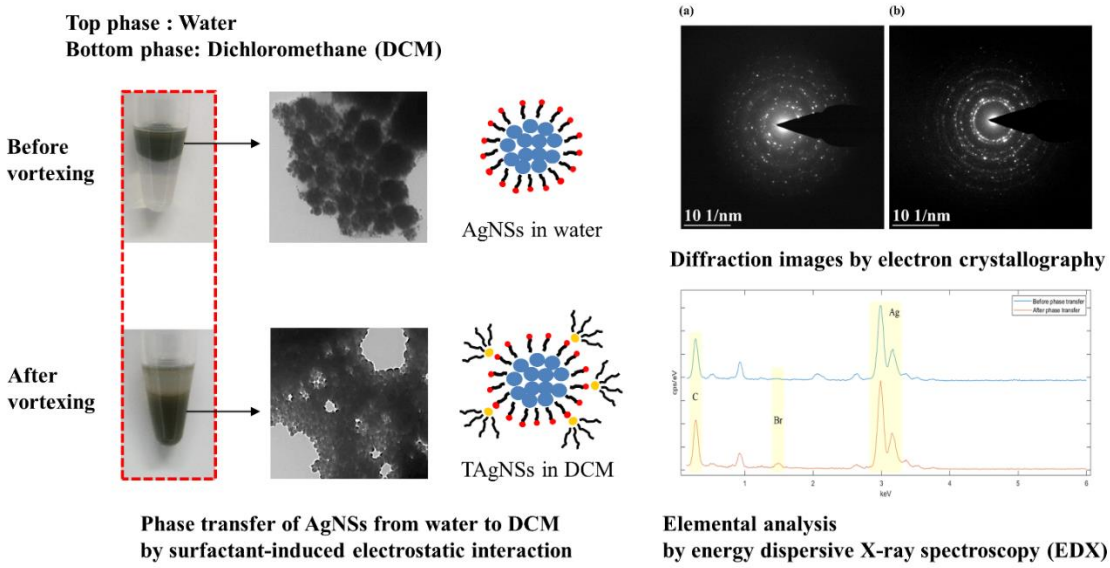

Figure D 3 Graphical abstract for chapter 4